ROMA TRE UNIVERSITY

DOCTOR OF PHILOSOPHY
IN
MECHANICAL AND INDUSTRIAL ENGINEERING
Ph.D. Thesis

CONTROL METHODOLOGIES FOR HORIZONTAL AXIS WIND TURBINE LOADS ALLEVIATION

By

Fratini Riccardo

Supervisor

Prof. Massimo Gennaretti

Co-Supervisors

Prof. Stefano Panzieri

Jacopo Serafini

Coordinator

Prof. Edoardo Bemporad

Riccardo Santini

Academic year 2018/2019

To my beloved ones

Contents

List of Figures

Chapter 1

Introduction

One of the fundamental goals of the wind energy industry is the reduction of the cost of the energy production, in order to make it competitive with respect to other sources, such as fossil fuels. In the last few years, several companies have entered the global market, introducing price competitive and high performances wind turbines, thus resulting in a downward pressure on energy prices. These trends, combined with the overcapacity of the wind turbine manufacturers, drive the price per installed MW power down drastically (2). Even though the customers benefit from this aspect, the manufacturers experienced increasing competition to retain their market share. As a result, the need of increasingly performing Horizontal Axis Wind Turbine (HAWT) is one of the crucial aspects that have led to a closer collaboration between academia and industry. Nowadays, two trends can be identified in turbine design: turbines are getting larger in terms of extracted power and rotor diameter, leading to a shift towards offshore wind turbines. As the turbines become larger, the rotor area increases and the wake vorticity gains strength.Furthermore, the tower shadow becomes larger due to the larger tower and the wind shear increases, giving stronger vibratory loads (3; 4; 5; 6; 7). Another important aspect related to the increasing dimension of the rotor disc is the weight of the disc itself. This effect can be determined by observing some basic scaling laws: the output power raises with the square of the scale factor, whereas the weight generally increases with the third power.

Having wind turbines to operate over a life design of 20 years or more, the analysis

of the effects of the loads acting on the structure in different operating conditions is mandatory. The mechanical loads can be divided into two categories: the static ones, which are the result of the interaction between the turbine and mean wind velocity, and the dynamic ones. The latter are induced by the spatial and temporal non-uniform distribution of wind velocity within the area swept by the rotor. Dynamic loads are also present in the form of transient loads (low frequency), caused by turbulence and gusts, or cyclic loads that are related to the interaction between asymmetric loads or external disturbances with the wind turbine structure. In addition to unsteady wind effects (wind shear, gust, turbulence), the HAWT experiences several negative effects as a result of a pitch change imposed by the controller to match the optimal operational point: blade vibrations, material fatigue, peak forces and blade stall are the most important ones (8). At the same time, the vibratory loads, affecting the mechanical parts, can be reduced by controlling the pitch angle in order to extend their life time.

For wind turbines control, three actuation strategies are usually applicable: blade pitch, generator torque, and machine yaw (9; 10; 11; 12) that can be used in different operational conditions, depending on wind speed magnitude. Usually, the turbine starts producing electricity at a wind velocity of 3-5 m/s, also called the cut-in wind speed, shuts down at approximately 25 m/s, also called the cut-out wind speed and reaches its nominal, or rated wind speed, at around 11-14 m/s. We can divide wind speed range into two main parts: the region between the cut-in wind speed and nominal wind speed is called region 1. Here, the blades are set at an optimal pitch angle, whereas the region up to cut-out wind speed is called region 3. Advanced control techniques have been extensively studied for energy capture in region 1 and load reduction for region 3 operations, in order to reduce the cost of energy. The generator torque is most often used in region 1 to maintain turbine operation at a maximum power coefficient, C_p. It can also be used to add damping to the drive-train torsion modes of the turbine in region 3. In addition, the turbine power output can be limited by yawing the machine out of the wind, thereby decreasing the projected rotor area and reducing power. Most often, yaw control is only used to respond to changes in wind direction in the attempt to reduce the yaw error (the angle between the mean wind direction and the direction of orientation of the turbine) and thereby maximize power. The blade pitch controller,

instead, is the most effective device to control aerodynamic loads. There are two types of this controller: Collective Pitch Control (CPC) and Individual Pitch Control (IPC). The main differences lie on the control commands: for the CPC the blades are pitched using a common (collective) signal, whereas for the IPC each blade is independently pitched from the others. A major drawback of CPC is the inability of dealing with asymmetric loads (13). Several IPC schemes have been developed to deal with the asymmetric loads of turbine (14; 15; 16; 17; 18; 19; 20), considering different measurement setups: strain gauge sensors installed at the blade root, the measurement of the nacelle tilt and yawing moments, of the drive-train shaft bending moments or of acceleration of the rotor blade tips and local blade wind inflow measurements. Individual pitch control and field tests to assess the viability of such strategy are studied, for instance, in (21; 13). In (22) a multiple model robust control strategy is considered, and a fault tolerant pitch control is proposed to reject faults in a turbine pitch actuator. Moreover, model predictive control (MPC) techniques are active research topics in this field and recent studies have shown promising results (23; 24; 25). Finally, repetitive control strategies for wind turbines have been proposed in (25; 26; 27; 28)when the reference command to be tracked and/or the disturbance to be rejected are periodic signals with a fixed period.

1.1 Aim of the thesis

The thesis has two main objectives. The first main point is the design and simulation of nonlinear differential model, for a three-bladed horizontal axis wind turbine suited for control applications. The second point is related to the different control strategies applied for reducing loads on both rotating and fixed-frame components. The controller structures will consist in collective and individual pitch actuations, one based on a Repetitive approach and the other one on parallel single-input single-output loops. The goal of these designs is to increase the performance of a wind turbine, in terms of quantity and quality of power harvested, and to avoid the excessive stress of structural components. Different effects are taken into account:

- Wind shear
- Tower shadow
- Turbulence
- Wake inflow

1.2 Outline of the thesis

This thesis is divided into six chapters. A short overview of the chapters, excluding the introduction, is reported down below:

- Chapter 2 introduces an overview of the different wind turbine operative conditions. The aerodynamic effects a wind turbine experiences are introduced, also a classification of structural loads on different elements is reported as well as their interactions. On a wind turbine different effects can be found: the wind variation with the altitude (wind shear), the presence of the pylon on the wind field (tower shadow), aerodynamic variations such as turbulence, gusts and induced velocity are important factors for a correct wind turbine modeling. Then, it is essential to know which kind of loads act on fixed and moving wind turbine elements and how they propagate through them.

- Chapter 3 introduces a new non-linear differential-equation aero-elastic model related to a up-to-wind Horizontal Axis Wind Turbine (HAWT). Different frames of reference are introduced together with their application points. The center of mass position and velocity vectors related to the wind turbine parts (nacelle, blade) are obtained too. Furthermore, kinetic and potential energies are defined as a function of the model degrees of freedom.

- In chapter 4, an outline of different control strategies applied to variable speed wind turbines, is summarized. It is reported the objectives and the different control loops used. The Repetitive and Individual approaches are here introduced: the first consists in learning a behaviour (external disturbance or internal dynamic) and rejecting it, the second one concerns the decomposition of a signal in harmonic contributions through the passage between the rotating frame of reference and the fixed one.

- Chapter 5 shows the results of the implementation of various controllers to the proposed model. It is reported the wind turbine features chosen (rated parameters, structural properties, configuration). Therefore, the proposed controllers are validated in different configurations (collective-individual pitch control) with various effects (wind shear, tower shadow).

- Chapter 6 summarizes the conclusions drawn from the illustrated work and provides recommendations for future researches.

Chapter 2

Wind turbine operative conditions

During operations, the horizontal axis wind turbine receives an interaction with the wind that does not only result in desired energy production, but also in stresses throughout the material of the turbine (hub, low and high-speed shafts, electrical generator). In order to survive the conditions a turbine is exposed to, engineers must carefully consider the wind turbine loads during the design process. The variability of the wind sites and the uncertainty in modelling and simulation of turbines, introduce the need of safety margins on all aspects of designing a structurally sound turbine. These margins have been defined in several certification guidelines, and it is an engineers task to make a turbine as cost effective as possible, while adhering to the guidelines themselves. By applying Collective and Individual Pitch Control, we are able to reduce loads and thus create opportunities to design a more cost effective turbine. This requires knowledge of different load types and sources, which are discussed in this chapter. A first division between loads is made between external and internal ones. A few examples of external loads are:

- Aerodynamic
- Gravitational
- Earthquake

And the main internal loads are:

- Structural

- Dynamic, such as inertial or gyroscopic loads

The most important loads for the controller design and for the cost-optimization are the aerodynamic and structural loads. Next section will explain the aerodynamic and structural loads respectively.

2.1 Aerodynamic effects

Aerodynamic forces are at the basis of energy production and they are the cause of most of the structural loads. There are many different types of aerodynamic loads, which are most easily distinguished by their frequency behaviour. A summary of these types, including a brief description, is given below:

- Steady loads

Rotational loads which do not vary in time and direction, for instance a uniform axial-symmetric wind speed blowing on a operating wind turbine.

- Cyclic loads

Cyclic loads are loads that vary in a periodic manner or in a non axial-symmetric direction, which in the case of a wind turbine is often a result of the rotation of the rotor. There are several sources of cyclic loads, such as wind shear, yaw error and tower shadow. In this report cyclic loads are indicated by the P notation, where P is an abbreviation for per revolution. Following this convention, the rotor rotational frequency is called 1P, and it can have harmonics on multiples of the frequency such as 2P, 3P etc...

- Stochastic loads

Stochastic loads are time varying loads that change in a seemingly random manner. Turbulence is an example of such a load, which can be described in a statistical manner as a force with a zero mean value.

- Transient loads

During its lifetime, a wind turbine can experience transient loads. Such loads result from an external event of temporary duration. Whilst being short lived, these loads can induce significant peaks in structural loads which make them important for extreme load analysis.

In this work different aerodynamic effects are implemented such as wind shear, tower shadow and wake inflow. Next a description of these aerodynamic load sources is reported in more detail.

2.1.1 Wind shear

Wind shear is the term used to describe the vertical profile of wind speed. Generally, it is assumed that the wind speed is low at the Earth's surface and increases with increasing height. The amount of wind shear is an important factor for the amount of energy available for extraction at a wind site and for the design of the wind turbine. The level of wind shear influences the optimal hub height as well as the fatigue loading of the turbine. Wind shear is dependent on the surface roughness of the Earth's surface, the terrain, and atmospheric stability. This paragraph will focus on the influence of surface roughness on wind shear. There are two main approaches in wind energy to describe wind shear, colloquially known as the log- law and power-law. The log-law describes the wind shear through a logarithmic relation with the surface roughness length that is dependent on the wind site, and values for this parameter have been established empirically. Some examples of typical values of are provided in table (2.1).

Type of terrain	Roughness length z_o(m)
Cities, forests	0.7
Suburbs, wooded countryside	0.3
Villages, countryside with trees and hedges	0.1
Open farmland, few trees and buildings	0.03
Flat grassy plains	0.01
Flat desert, rough sea	0.001

Figure 2.1: Wind shear roughness lengths

The log-law can be used to calculate the mean wind speed at any height from knowledge of the wind speed at a reference height (for instance the wind speed at the

anemometer height). The log-law, as presented in (29) reads:

$$U(z) = U(z_r)\frac{\ln(\frac{z}{z_0})}{\ln(\frac{z_r}{z_0})} \tag{2.1}$$

where $U(z)$ is the average wind speed in the fore-aft direction at the height z, $U(z_r)$ is the reference height z_r and z_0 is the surface roughness length. The other equation that is the power-law is defined by:

$$U(z) = U(z_r)(\frac{z}{z_r})^{\alpha} \tag{2.2}$$

Where α is the power-law exponent, which can be estimated through empirical fit of wind data. The value of α should also be adjusted to the height interval over which the power-law is applied. This is a point of critique, concerning the usefulness of the power-law compared to the log-law (30; 31). Both wind profile laws are used in the industry and in certification guidelines.

2.1.2 Turbulence

For wind turbine engineers, turbulence is a major factor in the design process and it is a highly complex topic. This is recognized in the standards, which specify wind classes based on the turbulence intensity. This section is confined to the explanation of some basic characteristics of turbulence and how they apply to wind energy. A turbulent wind can be described as the sum of a short-term mean wind, U, and a fluctuation component with zero mean, $\widetilde{u}$ (32):

$$u = U + \widetilde{u} \tag{2.3}$$

Due to the chaotic nature of the process, turbulence is best described statistically. A simple statistical qualifier of turbulence is the previously mentioned turbulence intensity:

$$I = \frac{\sigma}{U} \tag{2.4}$$

Where σ is the standard deviation of wind speed variations about the mean wind speed U. As with wind shear, turbulence is dependent on surface roughness, terrain type and thermal effects. This in turn, results in a negative correlation between turbulence intensity and height, due to reduced surface effects. The frequency spectrum of turbulence can be described by several models, the von Karman and Kaimal are used most frequently in the industry. In the work of Petersen et *al.*, the von Karman spectrum is defined as being accurate in describing turbulence in wind tunnels while the Kaimal spectrum provides an accurate empirical description of the frequency distribution of atmospheric turbulence (29). Therefore, in this research, the simulations are based on the wind distributions generated according to the Kaimal spectrum.

2.1.3 Tower shadow

The wind speed is altered by the presence of the tower. For a upwind turbine, it means that the wind directed in front of the pylon decelerates, whereas the wind in a lateral region of the tower accelerates. Each blade experiences a minimum wind, leading to a reduction of the aerodynamic torque and consequentially an alteration of the power generated. The torque pulsations, due to the tower shadow, are most

significant when a turbine has the blades downwind of the tower: for this reason the majority of modern large scale wind turbines present upwind rotors. This work will deal with the tower shadow wind oscillations for three-bladed horizontal axis upwind rotor. Each of the three blades is affected by the tower shadow effect, causing a 3P incident wind alteration. The rotor rotational frequency is called 1P, and it can have harmonics on multiples of the frequency such as 2P, 3P etc... The wind field that only takes into account the tower shadow is reported in equation (3.43), where V_h represents the hub height wind speed and the term v_{tower} is the disturbance in the incident wind speed due to tower shadow contribute.

Several representations have been formulated to describe tower effect. Sorensen (33) started from a potential flow representation for wind movement around the pylon.

Figure (2.2) shows an aerial view of the tower immersed in a uniform wind flow. When the wind is incident to the tower, it tries to overcome the obstacle by bending around the curvature. At the point marked "Source", the wind streamlines, moving to the stagnation point, decrease their magnitude and radiate outwards and later converge at the point called "Sink". Both this points are very close, separated by the tower diameter and form a doublet (34). Hence, by following the potential theory, the wind field can be described by superimposing a doublet on uniform flow, see equation (2.5).

$$\begin{aligned} \psi &= \psi_{uniform} + \psi_{doublet} \\ &= V_h y \left(1 - \frac{a^2}{x^2 + y^2}\right) \end{aligned} \tag{2.5}$$

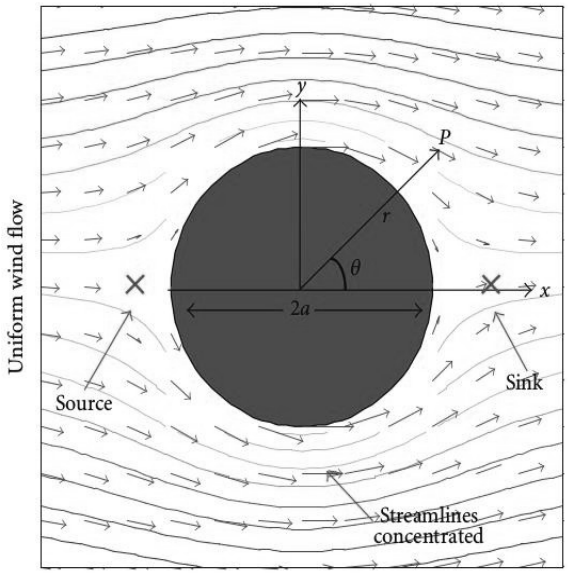

Figure 2.2: Wind flow around the tower obtained by superposing a doublet in uniform wind.

2.1.4 Extreme Operating gust

Besides surviving fatigue damage, a turbine must also be able to handle situations of extreme loading. There are several ultimate load cases, which enable the designer to evaluate a turbine's response to extreme situations the turbine would likely encounter during its lifetime. An example of an important extreme transient load is the extreme operating gust (EOG). The EOG follows a shape which is colloquially known as the "Mexican hat" gust. Starting from a constant non-turbulent wind, the wind speed drops for a short period after which a steep increase raises the speed to a maximum. After reaching the maximum the wind speed follows a path symmetrical to the rise of the gust. The magnitude of a gust at hub height with a period N is calculated by the follow equation:

$$V_{gustN} = \beta\Big(\frac{\sigma_1}{1 + 0.1(\frac{D}{\Lambda_1})}\Big) \tag{2.6}$$

Where σ_1 represents the standard deviation of the longitudinal wind speed at the hub height, D is the rotor diameter, Λ_1 is the turbulence scale parameter and β is related to the period N (29).

2.1.5 Wake inflow

Wind turbines operate for most of their time in an unsteady flow environment (35; 36). The air loads on each blade element vary in time because the turbine is usually yawed with respect to the oncoming wind. Furthermore, this also happens because of shear in the ambient wind, ambient turbulence, blade flapping and vibratory displacements, and other factors such as "tower shadow". While unsteady effects are important on many different types of rotating machinery, the issues associated with wind turbines are particularly acute because large amplitude flow perturbations and high effective reduced frequencies may be involved. For example, because of the relatively low rotational velocity of wind turbines (about one-second per rotor revolution), changes in wind speed or atmospheric fluctuations can result in significant changes in angle of attack at the blade elements. Also, when the turbine is yawed with respect to the wind, there are large fluctuations in the relative velocity at the leading-edge blade element compared to the velocity induced by blade rotation alone. These large amplitude displacements in local angle of attack and onset velocity contribute significantly to the unsteady flow environment on the blades. A particularly interesting aspect of the wind turbine aerodynamics problem is a quantification of the unsteadiness associated with the flow field and the turbine operating state. It is convenient to characterize the significance of unsteady problems, in general, in terms of an effective reduced frequency k. This parameter can be written as $k = \omega c/2V$, where ω is some characteristic physical frequency of the flow, c is a characteristic length such as blade chord, and V is an average flow velocity. Because of the typically low rotational velocities of wind turbines, the perturbations at the blade elements may have high effective values of reduced frequency, and especially so on moving inward along the blade from its tip because V becomes smaller. Thus, it is important to consider the unsteady aerodynamic in wind turbine operating conditions: for example, under yawed conditions, the 1P fluctuations in the component of flow velocity normal to the blade can occur at reduced frequencies greater than 0.1, and considerably higher inboard on the blade. Also, the passage of the blade through the tower shadow results in transient changes in angle of attack that may involve effective values of k that exceed 0.2 (only for $k < \mathrm{o}(0.01)$ the flow can be assumed steady or quasi-steady).

2.2 Frames of reference

In this section, the frames of reference (FOR) used to obtain the structural part of the wind turbine model are introduced. In particular, their application point will be outlined and its rotational matrices will be introduced.

2.2.1 Inertial frame of reference

The inertial FOR consists in any system for which is valid the Newton law. Its origin is externally placed with regard to the turbine. The y_0, z_0 axes are directed along the pylon and out-of-plane respectively, forming a right-hand-side with the x_0 axis.

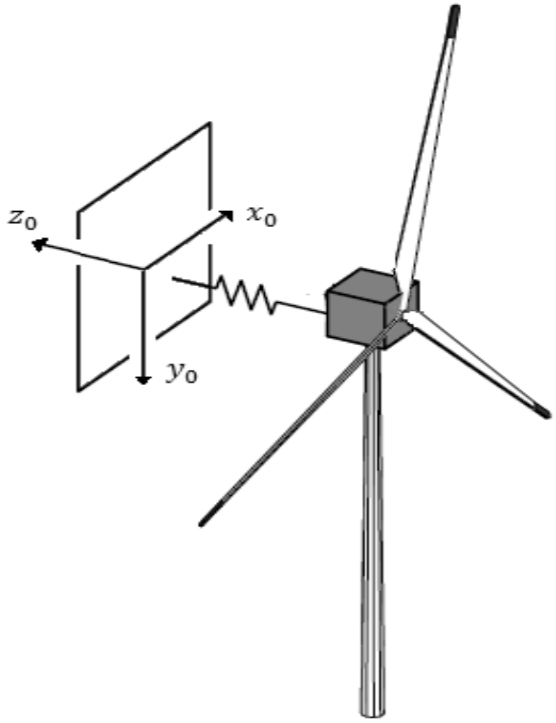

Figure 2.3: Inertial frame of reference

2.2.2 Non-rotating hub system frame of reference

The non-rotating hub system FOR is fixed with the top of the tower and can translate along the z_1 direction. The origin is placed in the nacelle center of mass. For small

rotation of the pylon, the directions of this frame remain parallel to the previous FOR (2.2.1), it means that only the translation of the pylon it is considered. Furthermore, this frame is not influenced by the disc rotation, so that, the y_1 and z_1 have the same direction during the rotation.

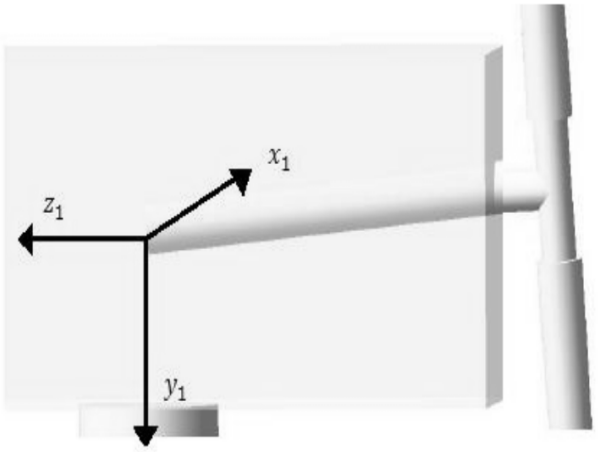

Figure 2.4: Non-rotating hub system frame of reference

2.2.3 Rotating hub system frame of reference

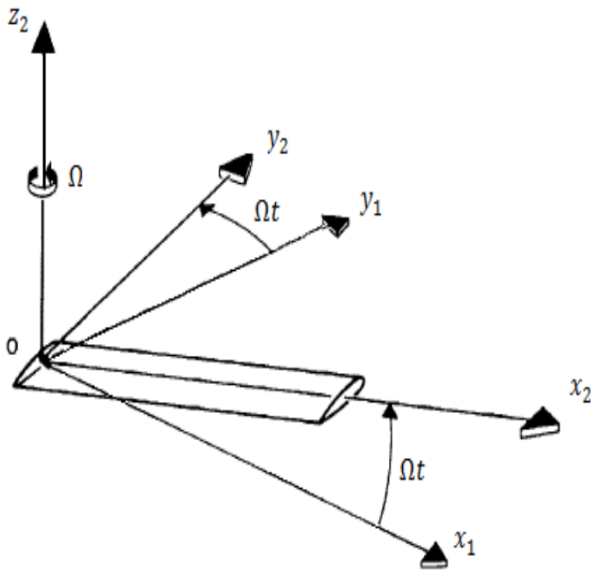

Figure 2.5: Rotating hub system frame of reference

The rotating hub system FOR has the origin in the airfoil root geometric center (the elastic center and the center of mass lie in the same point). The x_2 axis is parallel to the the blade length and passes through each airfoil center. y_2 is lied along the chord-wise direction and with z_2 axis form a right-hand-side. This reference system is moved along the x_2 direction of the offset f, that is the distance between the hub of the rotor disc and the blade flap hinge.

2.2.4 Blade fixed frame of references

The blade fixed FOR follows the blade deformation during a rotation in out-of-plane flap-wise direction and in pitching motion. The first motion is identified by β angle in figure (2.6), where the rotation is considered positive with the axis $y_2 = y_3$. The reference system origin is placed on the elastic airfoil center line (for hypothesis, it coincides to the geometric center and to the center of airfoil mass). The axis x_3 is located along the deformed span-wise direction, and with z_3, it forms a right-hand-side. The second motion is obtained by the previous FOR through a pitch θ rotation along the $x_3 = x_4$ axis , figure (2.7). In this way, the new y_4 and z_4 axes lie on the parallel and orthogonal directions of the airfoil, forming a right-hand-side with x_4 axis.

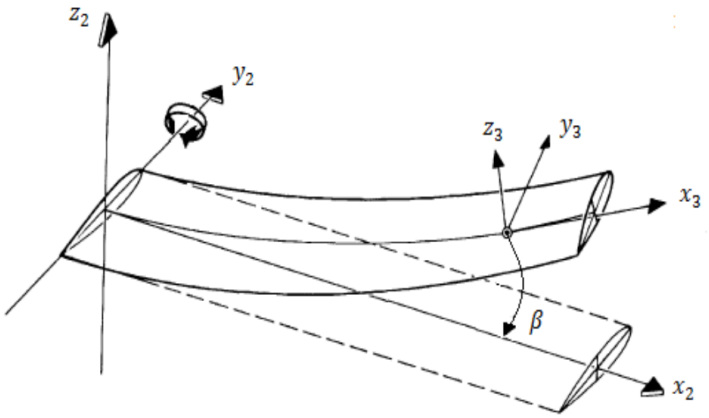

Figure 2.6: Blade flapping reference system

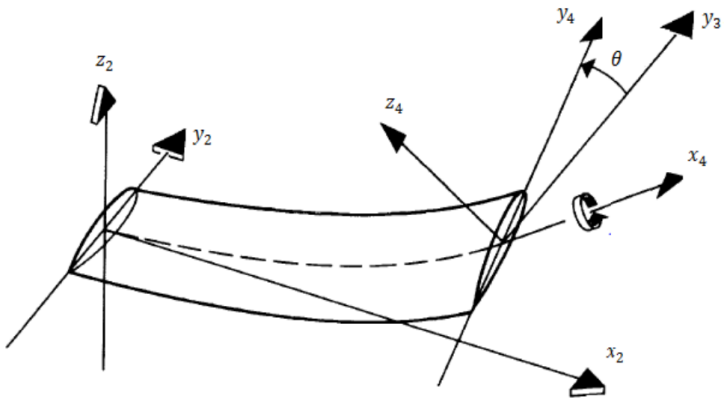

Figure 2.7: Blade pitch reference system

2.3 Blade and rotor loads

The group of loads which are of concern for this research are the hub loads. Hub loads are caused by the interaction between the external loads and the structure. For the group of structural loads, we choose a subdivision between loads in the rotating and the non-rotating frame of reference.

2.3.1 Rotating frame of reference loads

In the rotating reference system the blade bending moments are the most important factor for the redesign of the blades, based on fatigue reduction and also for the design and implementation of different control strategies as Collective and Individual Pitch Control (CPC,IPC). There are three different blade bending moments defined: the flap-wise, edge-wise and torsional bending moments. The orientation of these bending moments is shown in figure (2.8). For what concern the wind turbine, the main source for the

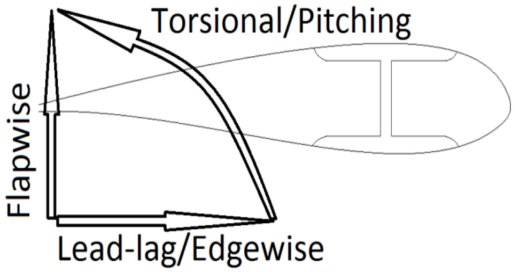

Figure 2.8: Blade bending moments

flap-wise bending moment is the aerodynamic load applied to the blades while the edge-wise load (or lead-lag load) is related to the gravitational loading. Furthermore, the torsional load (or pitching one) is caused by coupling with the other two bending moments, as well as the load generated by blade pitching movement. For control purposes, the flap-wise blade bending moment is the most important structural load to examine. By influencing this load, fatigue reductions for the blades and the fixed structure can be realized. Since flap-wise loading is mainly caused by aerodynamic load, its frequency spectrum is strongly coupled to the frequency spectrum of the aerodynamics. Therefore, the dominant frequencies in the effective wind speed on a blade should also be

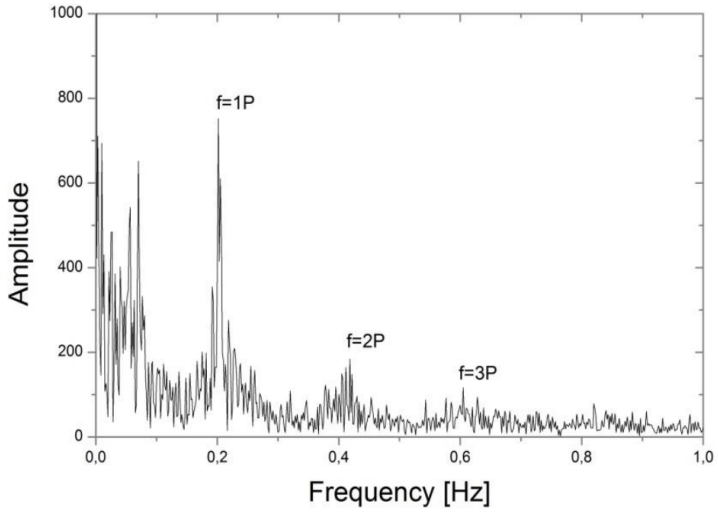

Figure 2.9: Frequency spectrum of flap-wise blade root bending moment

present in the blade flap-wise bending moment. Figure (2.9) shows a power spectral density plot of the flap-wise blade root bending moment of an operating wind turbine, experiencing a turbulent wind with average speed of 15.0 m/s. The spectrum of figure (2.9) shows that the load signal has a strong low frequent component between 0-0.1 Hz. This can be thought of as the slowly varying average wind causing lift and drag on the blade, thus resulting in a bending moment. Then, at 0.2 Hz, a peak can be found in the spectrum; this peak is situated around the first rotational frequency of the blade which is $f_{1p} = 12.1\ rpm$. Harmonic multiples of this frequency 2P and 3P can be found around 0.4 and 0.6 Hz respectively. The cyclic component of the load signal (1P) is a consequence of the presence of the 1P fluctuation in the aerodynamic load. The turbulence in the wind does not result in distinguishable peaks, due to the stochastic nature of the phenomenon. Besides flap-wise loads, edge-wise loads are also investigated in some of the redesign steps because, for the controller design, the edgewise loads are of less importance than the flap-wise loads. As stated previously, edge-wise loads are dominated by gravitational loads, which are cyclic with the rotational frequency (or in other words, 1P). For completeness, a final note on the rotor FOR is reported. It is important to distinguish the blade FOR and the rotor FOR. In fact different naming conventions for the bending moments are used: whilst talking about the rotor FOR,

one uses out-of-plane and in-plane bending moments; and while talking about the blade FOR, one specifies flap-wise and edge-wise bending moments.

2.3.2 Non-rotating frame of reference loads

Components such as the drive-train, nacelle and tower experience loads in a fixed FOR. For the fixed frame components the principal moments are described here below.

- Low-speed shaft tip tilt and yawing moment: moving from the rotor towards the drive-train, the first important component to consider is the main rotor bearing. The bending of the low-speed shaft at the location of the rotor bearing will be determining in the fatigue accumulation of the rotor bearing. Since bearings are not easily redesigned, it is important to see how the fatigue damage in this component changes in every turbine design case.

-Yaw bearing/Tower top tilt and yawing moment: continuing down the nacelle, the next component of interest is the connection between the nacelle and the tower; the yaw bearing. The loading at this point is also sometimes referred to as the tower-top.

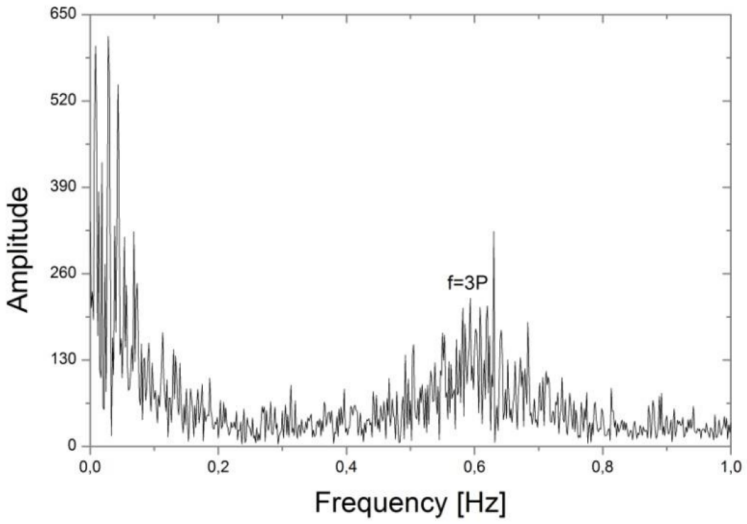

Figure 2.10: Frequency spectrum of the bending moment of the low-speed shaft at main bearing position

To provide insight into the load spectra of the non-rotating loads, the frequency spectrum of the low-speed shaft tip bending moment is plotted in figure (2.10). One can observe that the yawing bending moment in the low-speed shaft tip is dominated

by slow varying, near steady state loads and another peak around the 3P frequency. This is in contrast to the spectrum of the blade root flap-wise bending moment, figure (2.9), which has also peaks at 1P and 2P. The next paragraph will show how the loads in the rotating FOR are transferred to the fixed FOR, which will explain the difference in the location of the dominant load peaks. Furthermore, figure (2.11) depicts the fixed components of a wind turbine.

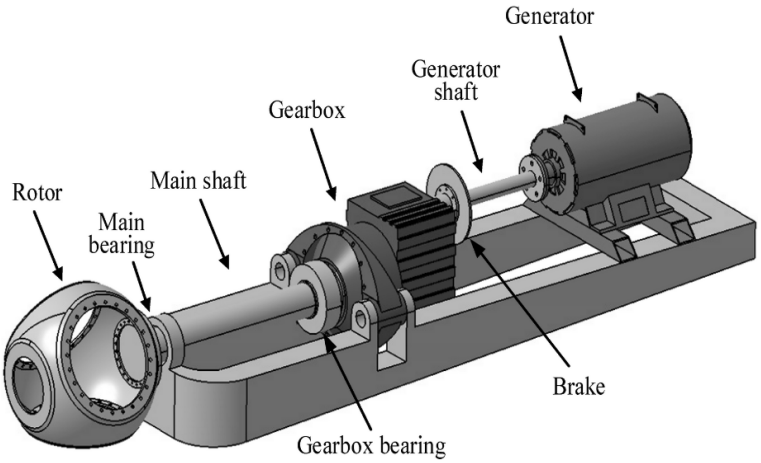

Figure 2.11: Shaft Component

2.3.3 Load transfer between the rotating and the fixed frame of reference

There is a clear difference between the frequency spectra of loads in the rotating FOR respect to fixed FOR. The reason for this is that the rotating components experience loads which are the resultant of the loads on a single blade, while components in the fixed FOR experience loads which are the resultant of the loads on all three blades combined. Due to the asymmetry of the loads on the blade, as well as the phase shift between them, the composition of the FOR loads is not a simple summation of the blade loads. Instead, the blade loads are decomposed into a new, fixed frame of reference, by means of a transformation.

Generally, any rotating degree of freedom can be transformed into a fixed frame of reference. This is done through a Coleman transformation, which can also be referred to as Fourier Coordinate Transform (helicopter community) or d-q axes transform (elec-

tronics field). In case of a three blade rotor, the following set of equations is used to transform the rotating degree of freedom into the same but fixed frame (37).

$$\begin{aligned}\epsilon_0 &= \frac{1}{3}\sum_{i=1}^{3}\epsilon^i \\ \epsilon_{Nd} &= \frac{2}{3}\sum_{i=1}^{3}\epsilon^i\cos(N\psi_i) \\ \epsilon_{Nq} &= \frac{2}{3}\sum_{i=1}^{3}\epsilon^i\sin(N\psi_i)\end{aligned} \tag{2.7}$$

Where i superscript indicates which blade is examined and ϵ^i represents a certain degree of freedom in the rotating FOR and ψ refers to the angular position in a revolution. In a general formulation, exist N Coleman transformations. The first (1P) Coleman transformation represents the projection from rotating to non-rotating FOR, the higher transformations (2P,3P,etc...) are not related to physical FOR, but are only used for control purpose, and will be discussed in following chapters.

If the 1P Coleman transformation of the out-of-plane blade bending moment for a generic blade is considered $M_{b,i}$, it results (eq. 2.7):

$$\begin{pmatrix} M_{avg} \\ M_{tilt} \\ M_{yaw} \end{pmatrix} = \begin{pmatrix} \frac{1}{3} & \frac{1}{3} & \frac{1}{3} \\ \frac{2}{3}\cos(\psi) & \frac{2}{3}\cos(\psi+\frac{2\psi}{3}) & \frac{2}{3}\cos(\psi+\frac{4\psi}{3}) \\ \frac{2}{3}\sin(\psi) & \frac{2}{3}\sin(\psi+\frac{2\psi}{3}) & \frac{2}{3}\sin(\psi+\frac{4\psi}{3}) \end{pmatrix} \begin{pmatrix} M_{b,1} \\ M_{b,2} \\ M_{b,3} \end{pmatrix} \tag{2.8}$$

where the first moment M_{avg} represents the average bending moment of the blades, M_{tilt} and M_{yaw} are the tilting and yawing moments on the fixed rotor plane, which are depicted in figure (2.12). For what concern the transfer of loads, in the following sections, the different harmonics of the blade root moment are examined to see how they will be reflected in the fixed structure of the turbine. For instance, the 1P signal in the blade root moment transposes into a 0P component when 1P Coleman transformation is applied. This implies that blade moments fluctuating with a constant amplitude at 1P frequency will result in 0P moments around the tilt and yawing axes for the fixed structure. Appendix A contains several transfers written out analytically.

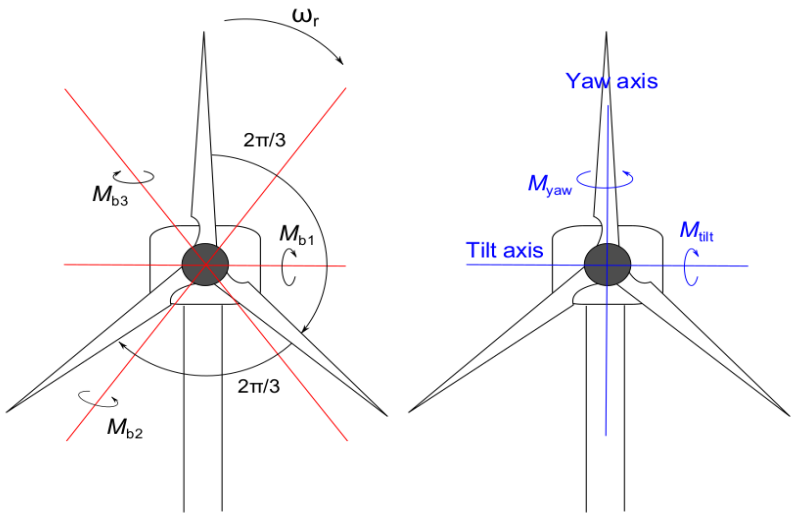

Figure 2.12: Rotating blade moment axes (—) and fixed yaw and tilt axis (—)

2.3.4 Coleman Transformation

In this section, the behaviour of different harmonics of a generic signal is reported by using the Coleman transformation. The Coleman approach is a transformation from one reference system (rotating) to another (fixed) by using the component of rotating angle ψ. Now, it will be shown how the different harmonics combine with each other and which of them remains in the transformation.

In a generic periodic rotational motion, the disc acts like a filter: it means that the hub only receives the steady loads and the harmonics that are multiple of the blades number.

The loads are in-plane and out-of-plane components: the former is the result of the previous and the following harmonics, the latter has a direct transmission. Therefore, we suppose that the rotating loads are harmonic signals and identically phase-shifted, so that it is possible to rewrite them by using the Fourier transformation (where b is the blade number, j is the blade considered and n is the number of the harmonic):

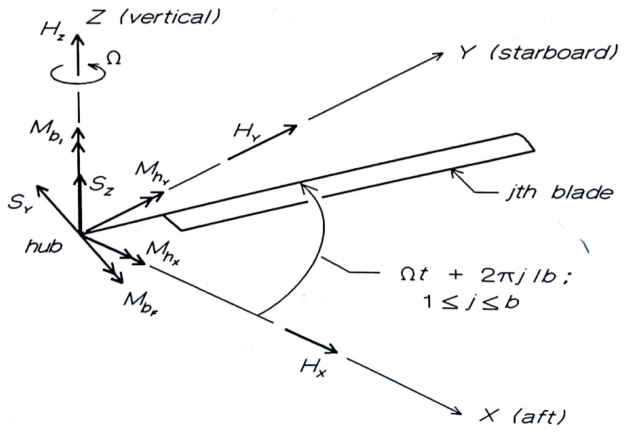

Figure 2.13: Hub loads

$$
\begin{aligned}
S_{y_j} &= S_{y0} + \sum_{n=1}^{\infty}\left[S_{y_{nc}} cosn\left(\Omega t + \frac{2\pi j}{b}\right) + S_{y_{ns}} sinn\left(\Omega t + \frac{2\pi j}{b}\right)\right] \\
S_{z_j} &= S_{z0} + \sum_{n=1}^{\infty}\left[S_{z_{nc}} cosn\left(\Omega t + \frac{2\pi j}{b}\right) + S_{z_{ns}} sinn\left(\Omega t + \frac{2\pi j}{b}\right)\right]
\end{aligned}
\tag{2.9}
$$

The orthogonal resulting component is

$$H_z = bS_{z_0} + \sum_{j=1}^{\infty}\left\{\sum_{n=1}^{\infty}\left[S_{z_{nc}}cosn\left(\Omega t + \frac{2\pi j}{b}\right) + S_{z_{ns}}sinn\left(\Omega t + \frac{2\pi j}{b}\right)\right]\right\} \tag{2.10}$$

By using trigonometric rules results:

$$H_z = b\left\{S_{z_0} + \sum_{n=1}^{\infty}\delta_{nj}\left[S_{z_{nc}}\ cosn\Omega t + S_{z_{ns}}\ sinn\Omega t\right]\right\} \tag{2.11}$$

with δ_{nj} is the Kronecker delta:

$$\delta_{nj} \equiv \begin{cases} 1; & n = j \\ 0; & n \neq j \end{cases} \tag{2.12}$$

furthermore, the fixed loads components result in

$$\begin{pmatrix} H_x \\ H_y \end{pmatrix} = \sum_{j=1}^{b}\left\{S_{y_0} + \sum_{n=1}^{\infty}\left[S_{y_{nc}}cosn\left(\Omega t + \frac{2\pi j}{b}\right) + S_{y_{ns}}sinn\left(\Omega t + \frac{2\pi j}{b}\right)\right]\right\}\begin{pmatrix} -\sin(\Omega t + \frac{2\pi j}{b}) \\ \cos(\Omega t + \frac{2\pi j}{b}) \end{pmatrix} \tag{2.13}$$

and by using appropriate simplifications:

$$\begin{pmatrix} H_x \\ H_y \end{pmatrix} = \frac{b}{2}\left\{\begin{pmatrix} -S_{y_{1s}} \\ S_{y_{1c}} \end{pmatrix} + \sum_{n=1}^{\infty}\delta_{nj}\left[\begin{pmatrix} S_{y_{(n-1)s}} - S_{y_{(n+1)s}} \\ S_{y_{(n-1)c}} - S_{y_{(n+1)c}} \end{pmatrix}\ cosn\Omega t + \right.\right. \\ \left.\left. + \begin{pmatrix} -S_{y_{(n-1)c}} + S_{y_{(n+1)c}} \\ S_{y_{(n-1)s}} + S_{y_{(n+1)s}} \end{pmatrix}\ sinn\Omega t\right]\right\} \tag{2.14}$$

All is valid for the in-plane and out-of-plane forces. For what concerns the orthogonal moment components, it results in

$$-Q = bM_{b_{I_0}} + \sum_{j=1}^{\infty}\left\{\sum_{n=1}^{\infty}\left[M_{I_{nc}}cosn\left(\Omega t + \frac{2\pi j}{b}\right) + M_{I_{ns}}sinn\left(\Omega t + \frac{2\pi j}{b}\right)\right]\right\} \tag{2.15}$$

The in-plane moment components are

$$\begin{pmatrix} M_{h_x} \\ M_{h_y} \end{pmatrix} = \frac{b}{2}\left\{\begin{pmatrix} M_{b_{F_{1s}}} \\ -M_{b_{F_{1c}}} \end{pmatrix} + \sum_{n=1}^{\infty}\delta_{n(kb)}\left[\begin{pmatrix} -M_{b_{F_{(n-1)s}}} + M_{b_{F_{(n+1)s}}} \\ -M_{b_{F_{(n-1)c}}} - M_{b_{F_{(n+1)c}}} \end{pmatrix}\ cosn\Omega t + \right.\right. \\ \left.\left. + \begin{pmatrix} +M_{b_{F_{(n-1)c}}} - M_{b_{F_{(n+1)c}}} \\ -M_{b_{F_{(n-1)s}}} - M_{b_{F_{(n+1)s}}} \end{pmatrix}\ sinn\Omega t\right]\right\} \tag{2.16}$$

where b and h are referred to the blade and hub respectively and $(\ )_F$ e $(\ )_I$ are related to in-plane and out-of-plane components. Thus, we have :

1. The disc acts like a filter, it means that only remains the harmonics that are multiple of the blades number (b).

2. The orthogonal loads have the same harmonics to the hub ($k \times b$), whereas the in-plane harmonic loads are strictly dependent to the previous (-1) and the following ($+1$) harmonics.

An example of the aforementioned transformation is reported. A generic periodic function (*e.g.* $\sin(\omega t + \phi)$) is defined, where ω is the pulsation related to the frequency $f = \omega/2\pi$ and ϕ is the phase.

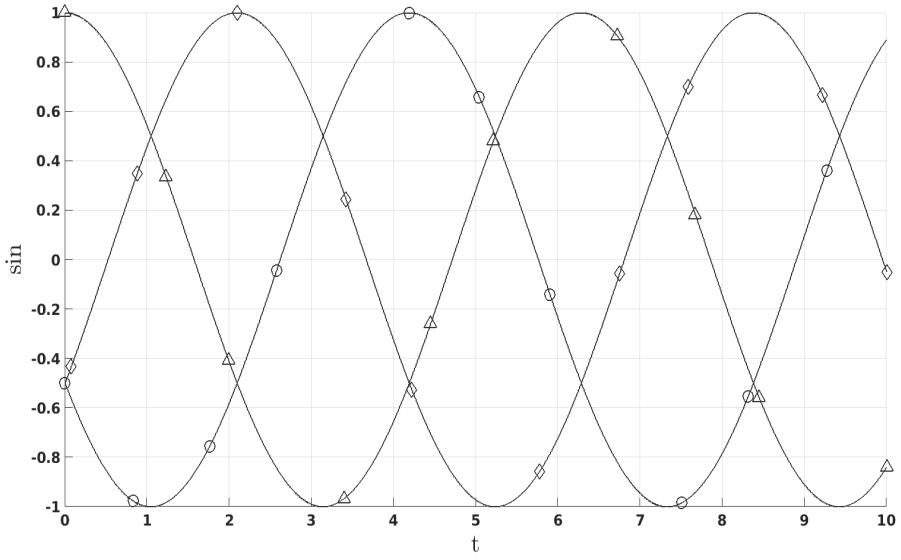

Figure 2.14: Different signals: $\sin(\omega t)(\triangle)$, $\sin(\omega t + \frac{2\pi}{3})$ $(\circ)$, $\sin(\omega t + \frac{4\pi}{3})$ $(\diamond)$

Figure (2.14) shows three phase-shifted signals having just the first harmonic component ($\omega = 1$ rad/sec and $f = 0.159$ Hz). Also, figure (2.15) depicts the sum of the first two harmonics. Figure (2.16) depicts the transition of the 1P harmonic component of a signal by using 1P Coleman transformation. It is shown the fast Fourier transform of a signal in the rotating FOR (dashed line) that only has the 1P contribute ($f = 0.159$

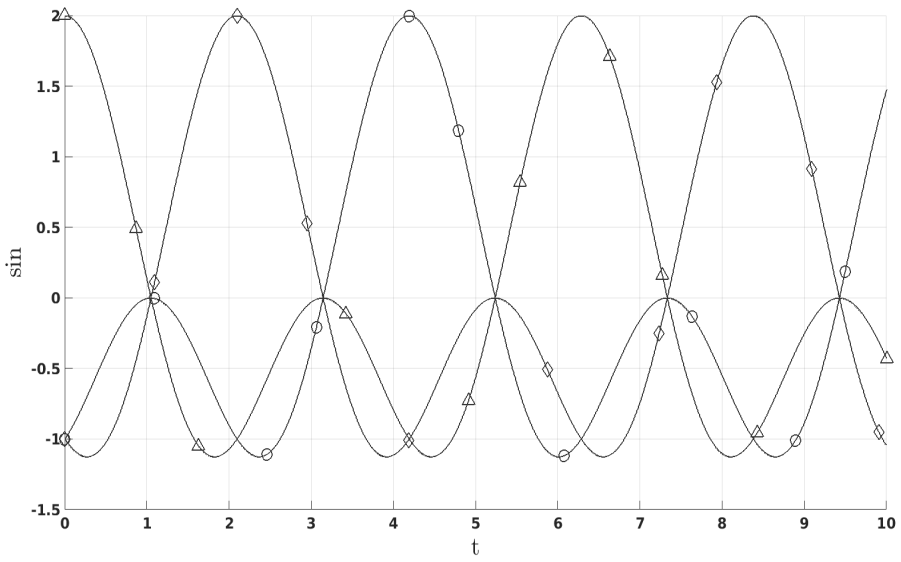

Figure 2.15: Different signals: $\sin(\omega t) + \sin 2(\omega t)(\triangle)$, $\sin(\omega t + \frac{2\pi}{3}) + \sin 2(\omega t + \frac{2\pi}{3})$ $(\bigcirc)$, $\sin(\omega t + \frac{4\pi}{3}) + \sin 2(\omega t + \frac{4\pi}{3})$ $(\diamond)$

Hz). Therefore, the 1P transformation is made, only the 0P value is reached in the fixed FOR (continue line), as shown in equation (A.11).

In figure (2.17) is reported the transformation of a 2P ($f = 0.3$ Hz) harmonic with 1P Coleman, as it is reported in equation (A.7). It only survives the 3P contribute in the fixed FOR (about $f = 0.5$ Hz). The harmonics that are multiple of blades number do not result in the fixed FOR, figure (2.18), even if there are two negligible contributes in the 2P and 4P. Also, the 4P contribute will result in the 3P one, figure (2.19). In the same way, the higher harmonic behaviors up to the seventh are reported in figures (2.20-2.22).

The total behaviour of all harmonics is reported in figure (2.23): in the fixed FOR only the harmonics that are multiple of the blades number are visible depicted by the continuous line ($f = 0$ Hz , about $f = 0.5$ Hz , about$f = 0.1$ Hz)

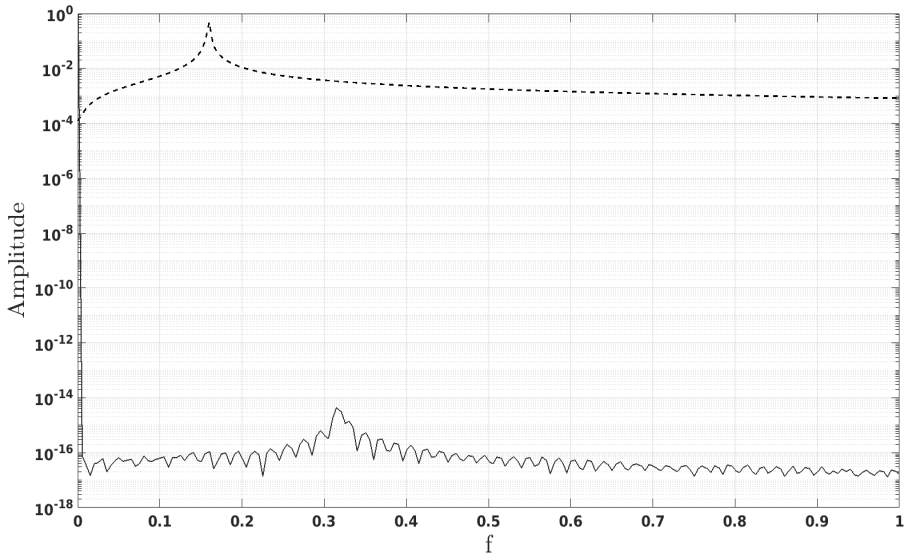

Figure 2.16: Transformation of the 1P harmonic by using 1P Coleman.

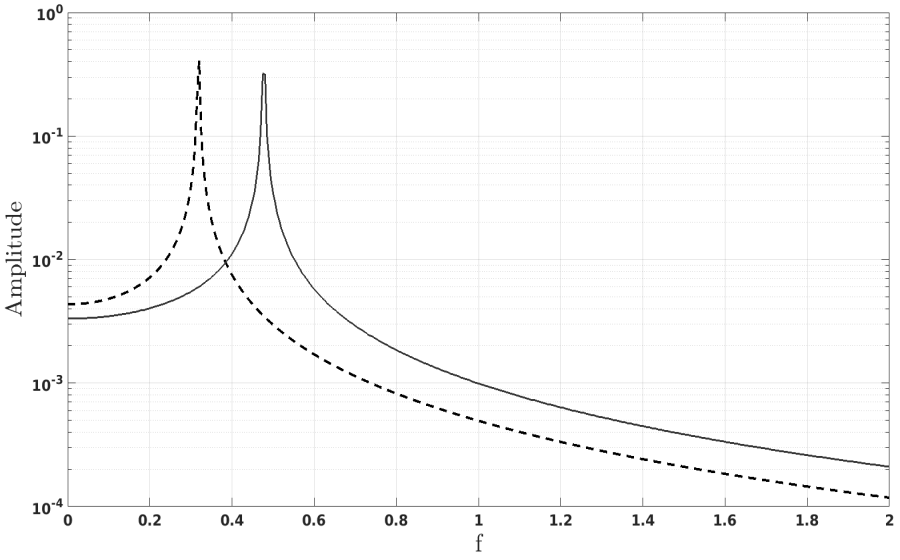

Figure 2.17: Transformation of the 2P harmonic by using 1P Coleman.

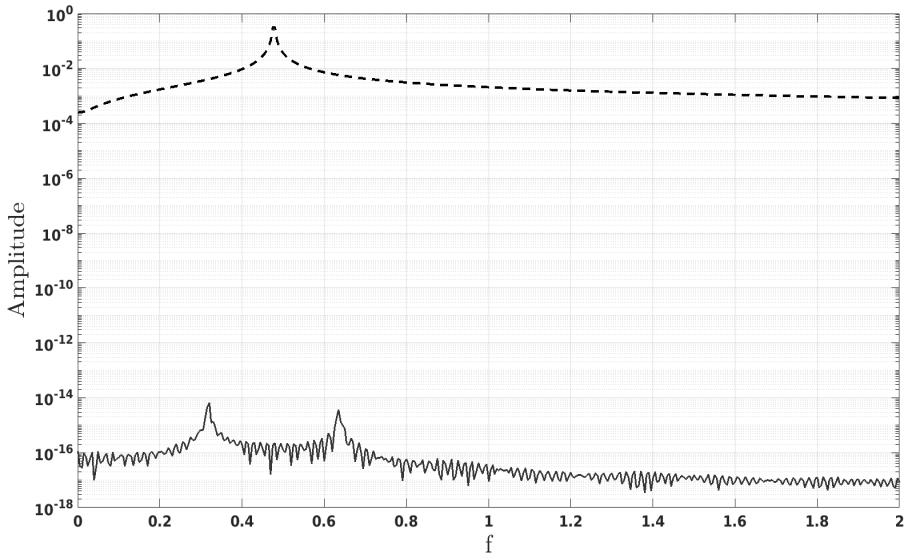

Figure 2.18: Transformation of the 3P harmonic by using 1P Coleman.

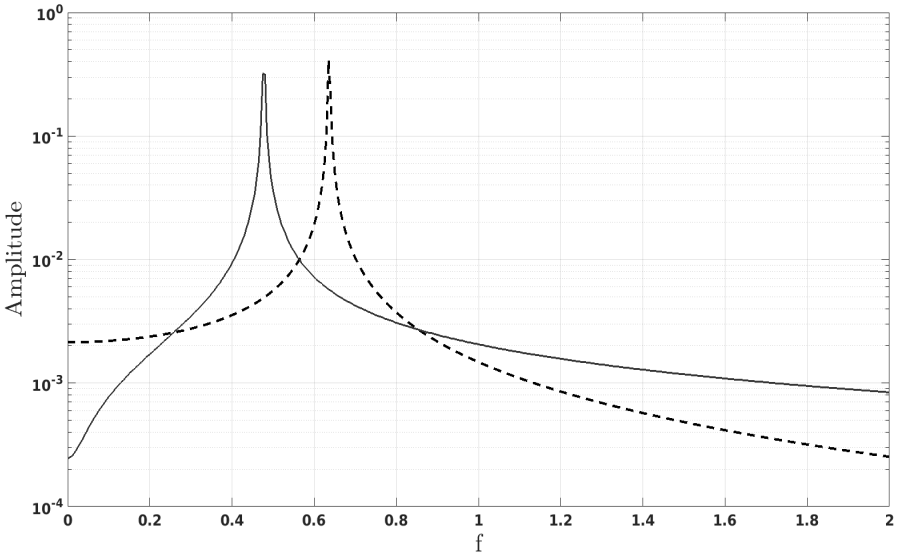

Figure 2.19: Transformation of the 4P harmonic by using 1P Coleman.

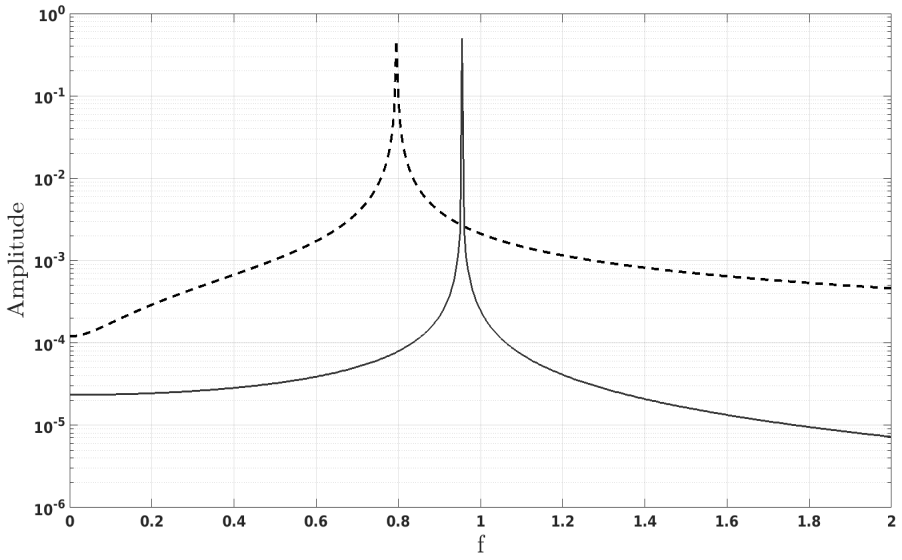

Figure 2.20: Transformation of the 5P harmonic by using 1P Coleman.

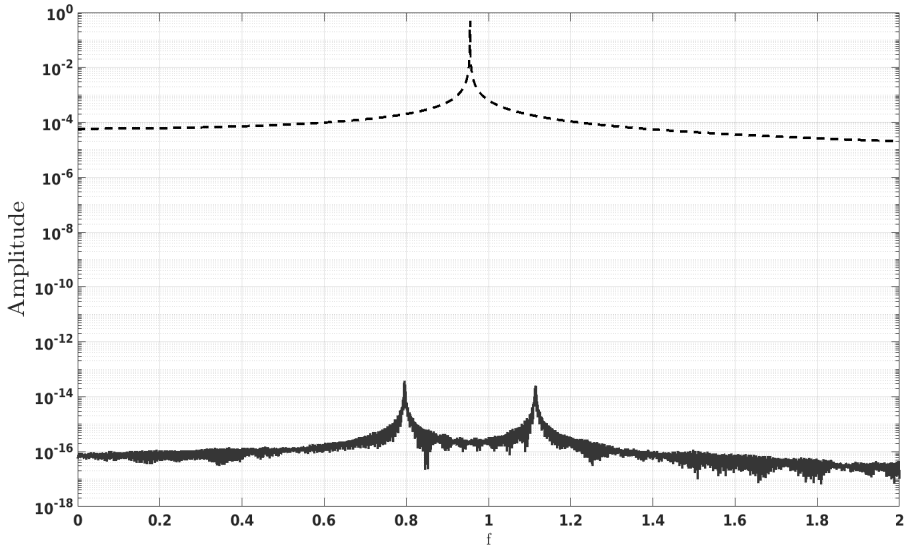

Figure 2.21: Transformation of the 6P harmonic by using 1P Coleman.

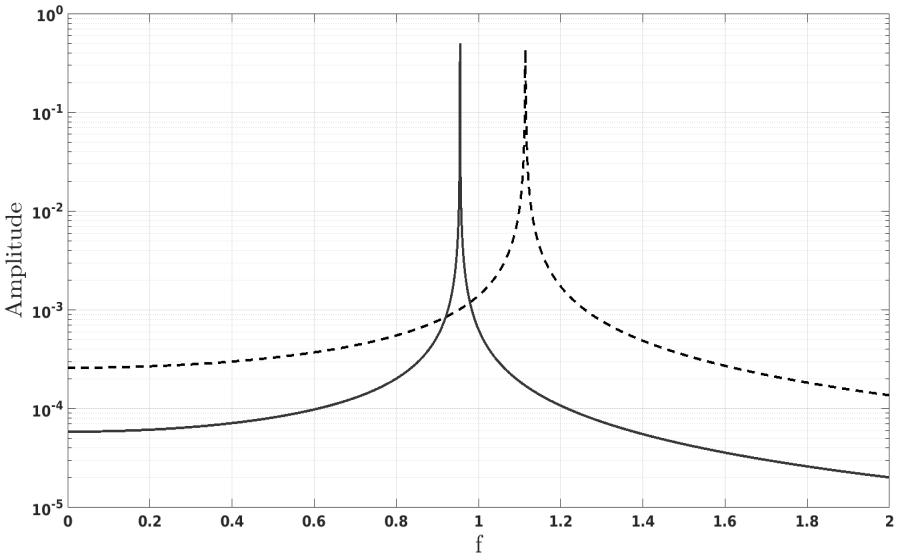

Figure 2.22: Transformation of the 7P harmonic by using 1P Coleman.

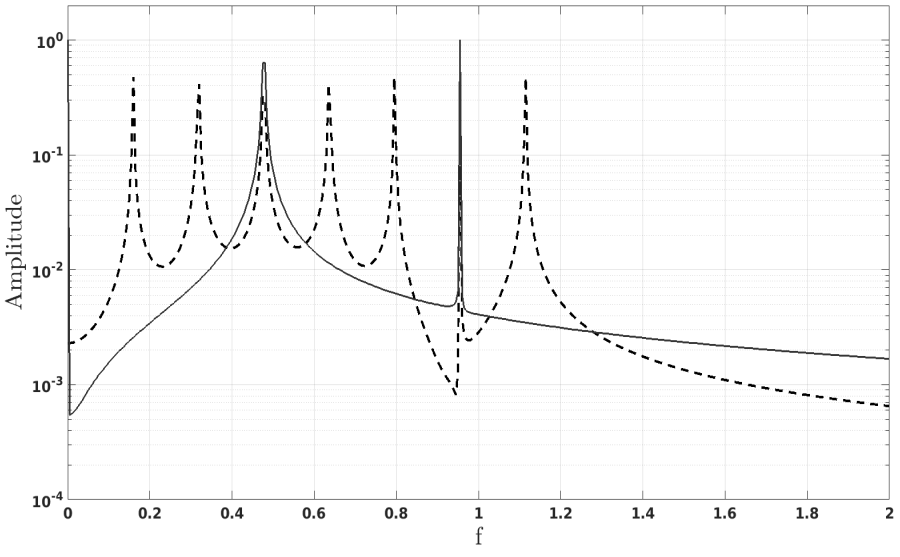

Figure 2.23: Total Transformation by using 1P Coleman.

Chapter 3

Aeroelastic model

Mathematical model of a tower-rotor-blade wind turbine system

This section presents a non-linear differential-equations for horizontal axis wind turbine suited for control applications. It is based on 8-dofs, lumped parameters structural dynamics coupled with a quasi-steady aerodynamic theory. In particular, using Euler-Lagrange Equation, this model is derived and then validated. Developing the model, the attention has been focused in finding the correct balance between analytical complexity and computational efficiency. The proposed model includes translation of the pylon, rotor disc rotation, flapping out-of-plane deformation and Pitch motion specifically. Also, inflow velocity and three degrees of freedom (one for each blade) for Pitch and flap motions are taken into account.

Both translations and rotations are to be considered "rigid": this does not mean that in the model the elasticity is not taken into account, rather, it will be considered trough appropriate elastic parameters. For what concerns the aerodynamic model, the Greenberg theory, an extension of the theory proposed by Theodorsen to the case of thin airfoils undergoing pulsating flows, is used. Specifically, in this work, that theory is restricted under the hypothesis of low perturbation reduced frequency k, which causes the lift deficiency function $C(k)$ to be real and equal to 1. Furthermore, the expressions of the aerodynamic loads are obtained, using the quasi-steady strip theory (Hodges and

Ormiston), as a function of the chord-wise and normal components of relative velocity between flow and airfoil U_t, U_p, their derivatives, and section angular velocity $\dot{\epsilon}$. A schematic representation of the wind turbine's degrees of freedom is depicted in Fig. 3.1

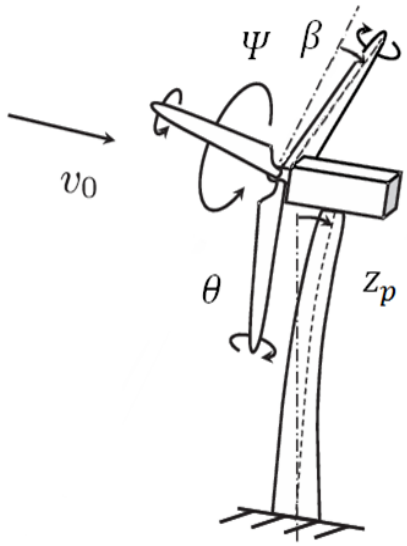

Figure 3.1: Wind turbine's degrees of freedom.

3.1 Structural dynamic model

Developing the aero-elastic model of an horizontal-axis wind turbine, the authors moved from Euler-Lagrange differential equation

$$\frac{d}{dt}\left(\frac{\partial \mathcal{T}}{\partial \dot{q}_i}\right) - \frac{\partial(\mathcal{T}-U)}{\partial q_i} = F_i \quad \forall i = 1, \cdots, n. \tag{3.1}$$

where $\mathcal{T} = \mathcal{T}(\dot{\mathbf{q}}, \mathbf{q})$ and $\mathcal{U} = \mathcal{U}(\mathbf{q})$ are the kinetic and potential energy, respectively, $F_i = F_i(\ddot{\mathbf{q}}, \dot{\mathbf{q}}, \mathbf{q})$ are the generalized forces and $\mathbf{q}$ is the vector collecting the generalized coordinates q_i, which include rigid dofs. In this work, eight degrees of freedom, providing a semi-rigid (lumped parameters) model for the aero-elasticity of rotor-pylon system of a three-bladed HAWT, are considered. In particular, the elastic degrees of freedom are represented with a 'rigid' motions, coupled with stiffness springs concentrated in the bond that simulates the elasticity of the components. The generalized coordinates are:

- $q_1 = z_p$
- $q_{2,3,4} = \beta_{1,2,3}$
- $q_{5,6,7} = \theta_{1,2,3}$
- $q_8 = \psi$

where z_p represents the tower top fore-aft elastic displacement, β_i and θ_i are, respectively, flap and pitch angles of each blade, and Ψ is the azimuthal position of reference blade. The total kinetic energy $\mathcal{T}$ may be expressed as:

$$\mathcal{T} = \frac{1}{2}\bar{v}_{g_n}^T(\dot{\mathbf{q}},\mathbf{q})M_{tot}\bar{v}_{g_n}(\dot{\mathbf{q}},\mathbf{q}) + \frac{1}{2}\sum_{i=1}^{3}\bar{v}_{g_{b_i}}^T(\dot{\mathbf{q}},\mathbf{q})M_b\bar{v}_{g_{b_i}}(\dot{\mathbf{q}},\mathbf{q}) + \frac{1}{2}\sum_{i=1}^{3}\bar{\omega}_{b_i}^T(\dot{\mathbf{q}},\mathbf{q})J_{g_b}\bar{\omega}_{b_i}(\dot{\mathbf{q}},\mathbf{q}) \tag{3.2}$$

where $\bar{v}_{g_n}$ represents the velocity of the nacelle center of gravity, M_{tot} is the sum of the nacelle and pylon mass. $\bar{v}_{g_{b_i}}$ and $\bar{\omega}_{b_i}$ are the i-th blade velocities, whereas M_b and J_{g_b} represent, respectively, blade mass and matrix of inertia with respect to center of gravity. Note that $\bar{v}_{g_n}$, $\bar{v}_{g_{b_i}}$ and $\bar{\omega}_{b_i}$ may be easily expressed as function of $\mathbf{q}, \dot{\mathbf{q}}$ exploiting rigid body motion relations. The total potential energy $\mathcal{U}$ is the sum of gravitational and elastic contributions ($\mathcal{U}_g$ and $\mathcal{U}_e$, respectively), *i.e.*

$$\mathcal{U} = \mathcal{U}_g + \mathcal{U}_e, \tag{3.3}$$

In particular, the elastic energy is associated to the springs acting on z_p, β_i and θ_i dofs. These terms read as

$$\begin{aligned} \mathcal{U}_g &= \sum_{i=1}^{3} U_{b_i} = \sum_{i=1}^{3} -M_b g \sin\Psi(x_{g_b}\cos\beta_i + f + H_n), \\ \mathcal{U}_e &= \frac{1}{2}k_p z_p^2 + \frac{1}{2}\sum_{i=1}^{3} k_{\beta_i}\beta_i^2 + \frac{1}{2}\sum_{i=1}^{3} k_{\theta_i}\theta_i^2, \end{aligned} \tag{3.4}$$

where M_b is the mass of the rotor blade and x_{g_b} is the radial position of the blade center of mass with respect to the flapping hinge, f is the offset respect to the rotor center and H_n is the height of the tower. Subsequently, the previous elements are expressed in the different reference systems by introducing appropriate rotation matrices.

3.1.1 Nacelle center of mass position and velocity vectors

The position of the nacelle center of mass is a pure translation for hypothesis. So, the $\bar{x}_{g_n}$ and $\bar{v}_{g_n}$ vectors can be expressed respect to the inertial FOR as

$$\bar{x}_{g_n}|_0 = \left\{0, 0, z_p\right\} \ , \ \bar{v}_{g_n}|_0 = \left\{0, 0, \dot{z_p}\right\}$$

3.1.2 Blade center of mass position and velocity vectors in the rotating frame of reference

The position of the center of mass, related to a generic blade, is the sum of the vector flap hinge position and the projection of the center of mass in the rotating reference system, starting from the "rigid" deformation. Also, this position is not affected by the pitch motion because of the hypothesis that the center of mass line and the elastic one are the same.

$$\bar{x}_{g_b}|_2 = \bar{x}_f|_2 + R_{3-2}\bar{x}_{g_b}|_3 \tag{3.5}$$

where $\bar{x}_f|_2 = \left\{f, 0, 0\right\}$ and $\bar{x}_{g_b}|_3 = \left\{x_{g_b}, 0, 0\right\}$ are the flap hinge position in rotating hub FOR and the blade center of mass defined in blade fixed FOR respectively. Also, the transformation matrix between (2.2.4) and (2.2.3) is:

$$R_{3-2} = \begin{bmatrix} \cos(\beta) & 0 & \sin(\beta) \\ 0 & 1 & 0 \\ -\sin(\beta) & 0 & \cos(\beta) \end{bmatrix} \tag{3.6}$$

Thus, the position of the center of mass in the rotating reference system results in:

$$\bar{x}_{g_b}|_2 = \left\{f + x_{g_b}\cos(\beta), 0, -x_{g_b}\sin(\beta)\right\} \tag{3.7}$$

With flap angle (β) defined in Fig. (2.6).

3.1.3 Blade center of mass position and velocity vectors in the inertial frame of reference

The position of the center of mass in non-rotating reference system is defined as:

$$\bar{x}_{g_b}|_1 = R_{2-1}\bar{x}_{g_b}|_2 \tag{3.8}$$

where the transformation matrix between non-rotating hub system and the rotating one is:

$$R_{2-1} = \begin{bmatrix} \cos(\psi) & -\sin(\psi) & 0 \\ \sin(\psi) & \cos(\psi) & 0 \\ 0 & 0 & 1 \end{bmatrix} \tag{3.9}$$

by using equation (3.7), it results:

$$\bar{x}_{g_b}|_1 = \Big\{\cos(\psi)(f + x_{g_b}\cos(\beta)), \sin(\psi)(f + x_{g_b}\cos(\beta)), -x_{g_b}\sin(\beta)\Big\} \tag{3.10}$$

In the inertial reference system the translation refers to the blade center of mass will be:

$$\bar{x}_{g_b}|_0 = \bar{x}_{g_b}|_1 + \bar{x}_{g_n}|_0 = \Big\{\cos(\psi)(f + x_{g_b}\cos(\beta)), \sin(\psi)(f + x_{g_b}\cos(\beta)), -x_{g_b}\sin(\beta) + z_p\Big\} \tag{3.11}$$

Furthermore, by performing the time derivative

$$\bar{v}_{g_b}|_0 = \frac{d}{dt}(\bar{x}_{g_b}|_0) = -\frac{d}{dt}(R_{2-1}(\bar{x}_f|_2 + R_{3-2}\bar{x}_{g_b}|_3) + \bar{x}_{g_n}|_0) \tag{3.12}$$

$$\bar{v}_{g_b}|_0 = \dot{R}_{2-1}(\bar{x}_f|_2 + R_{3-2}\bar{x}_{g_b}|_3) + R_{2-1}\dot{R}_{3-2}\bar{x}_{g_b}|_3 + \bar{v}_{g_n}|_0 \tag{3.13}$$

with

$$\dot{R}_{2-1} = \Big\{0, 0, \Omega\Big\} \times R_{2-1} \tag{3.14}$$

$$\dot{R}_{3-2} = \Big\{0, \dot{\beta}, 0\Big\} \times R_{3-2} \tag{3.15}$$

yielding to

$$\bar{v}_{g_b}|_0 = \Big\{0, 0, \Omega\Big\} \times R_{2-1}(\bar{x}_f|_2 + R_{3-2}\bar{x}_{g_b}|_3) + R_{2-1}(\Big\{0, \dot{\beta}, 0\Big\} \times R_{3-2}\bar{x}_{g_b}|_3) + \bar{v}_{n_b}|_3 \tag{3.16}$$

by performing $A \times B \cdot C = B \cdot A \times C$, it results:

$$\bar{v}_{g_b}|_0 = R_{2-1}[\Big\{0, 0, \Omega\Big\} \times (\bar{x}_f|_2 + R_{3-2}\bar{x}_{g_b}|_3) + R_{3-2}\Big\{0, \dot{\beta}, 0\Big\} \times \bar{x}_{g_b}|_3\,] + \bar{v}_{n_b}|_3 \tag{3.17}$$

Once, the inertial variables are found, by using the inverse matrix transformation, it is possible to write the velocity vector in the rotating reference system as it follows:

$$\bar{v}_{g_b}|_2 = R_{2-1}^T\bar{v}_{g_b}|_0 = \Big\{-x_{g_b}\dot{\beta}\sin(\beta), \Omega(f + x_{g_b}\cos(\beta)), -x_{g_b}\dot{\beta}\cos(\beta) + \dot{z_p}\Big\} \tag{3.18}$$

3.1.4 Blade angular velocity in the blade frame of reference

We can define the angular velocity vector related to a generic blade section in the (2.2.4) reference system as it follows:

$$\bar{\omega}_b|_4 = R_{4-3}^T R_{3-2}^T R_{2-1}^T \left\{0, 0, \Omega\right\} + R_{4-3}^T \left\{0, \dot{\beta}, 0\right\} + \left\{\dot{\theta}, 0, 0\right\} \tag{3.19}$$

where the transformation matrix between blade flapping and Pitch reference system is:

$$R_{4-3} = \begin{bmatrix} 1 & 0 & 0 \\ 0 & \cos(\theta) & -\sin(\theta) \\ 0 & \sin(\theta) & \cos(\theta) \end{bmatrix} \tag{3.20}$$

where θ is defined in fixed FOR resulting in:

$$\bar{\omega}_b|_4 = \left\{\Omega \sin(\beta) + \dot{\theta}, \Omega \cos(\beta) \sin(\theta) + \dot{\beta} \cos(\theta), \Omega \cos(\beta) \cos(\theta) - \dot{\beta} \sin(\theta)\right\} \tag{3.21}$$

.

3.1.5 Kinetic and Potential energy contributions

The kinetic components related to (3.2) are:

$$\frac{1}{2} \bar{v}_{g_n}^T (M_p + M_n) \bar{v}_{g_n} = \frac{1}{2} M_{tot} \dot{z_p}^2 \tag{3.22}$$

$$\frac{1}{2} \bar{v}_{g_b}^T M_b \bar{v}_{g_b} = \frac{1}{2} M_b \{x_{g_b}^2 \dot{\beta}^2 + f^2 \Omega^2 + 2 f x_{g_b} \Omega^2 \cos(\beta) + x_{g_b}^2 \dot{\Omega}^2 \cos^2(\beta) + \dot{z_p}^2 - 2 x_{g_b} \dot{\beta}^2 \dot{z_p} \cos(\beta)\} \tag{3.23}$$

$$\begin{aligned} \frac{1}{2} \bar{\omega}_b^T J_{g_b} \bar{\omega}_b = \frac{1}{2} \{ & J_{g_x} (\Omega^2 \sin^2(\beta) + \dot{\theta}^2 - 2\Omega\dot{\theta} \sin(\beta) + \Omega^2 \cos^2(\beta) \cos^2(\theta) + \dot{\beta}^2 \sin^2(\theta) \\ & - 2\Omega\dot{\beta} \cos(\beta) cos(\theta) \sin(\theta)) + J_{g_y} (\Omega^2 \cos^2(\beta) + \dot{\beta}^2)\} \end{aligned} \tag{3.24}$$

where the moments of inertia are related to the airfoil principal axes system as it follows:

$$J_{g_b}|_4 = \begin{bmatrix} J_{g_x} & 0 & 0 \\ 0 & J_{g_y} & 0 \\ 0 & 0 & J_{g_z} \end{bmatrix}$$

Furthermore, by considering one blade section dimension lower than the other two, it yields to $J_{g_z} = J_{g_x} + J_{g_y}$. Also, the moments of inertia are defined as:

$$\begin{aligned} J_{g_x} &= \iiint \rho(y^2 + z^2)\, dV \\ J_{g_y} &= \iiint \rho(x^2 + z^2)\, dV \\ J_{g_z} &= \iiint \rho(x^2 + y^2)\, dV. \end{aligned} \tag{3.25}$$

But with the airfoil thickness dimension lower than the chord and span dimensions (it means $z << y << x$), it results:

$$\begin{aligned} J_{g_x} &\tilde{=} \iiint \rho y^2\, dV \\ J_{g_y} &\tilde{=} \iiint \rho x^2\, dV \\ J_{g_z} &= \iiint \rho(x^2 + y^2)\, dV. \end{aligned} \tag{3.26}$$

Now, under the assumption of small pitching and flapping angles, *i.e.* $\sin(\beta_i, \theta_i) \approx \beta_i, \theta_i$ and $\cos(\beta_i, \theta_i) \approx 1$, and substituting (3.2) and (3.4) in (3.1), the following

nonlinear system is obtained:

$$
\begin{aligned}
&M_{tot}\ddot{z}_p - \sum_{i=1}^{3} M_b x_{g_b}\ddot{\beta}_i^2 + k_p z_p \;= \sum_{i=1}^{3}\int_0^L L_{w_i} dr \\
&J_{o_y}\ddot{\beta}_1 - M_b x_{g_b}\ddot{z}_p + \left(J_{o_y}\Omega^2 + M_b x_{g_b} f\Omega^2 + k_{\beta_1}\right)\beta_1 - M_b x_{g_b} g\sin\Psi_1 - J_{g_x}\dot{\Omega}\theta_1 = \int_0^L L_{w_1} r dr \\
&J_{o_y}\ddot{\beta}_2 - M_b x_{g_b}\ddot{z}_p + \left(J_{o_y}\Omega^2 + M_b x_{g_b} f\Omega^2 + k_{\beta_2}\right)\beta_2 - M_b x_{g_b} g\sin\Psi_2 - J_{g_x}\dot{\Omega}\theta_2 = \int_0^L L_{w_2} r dr \\
&J_{o_y}\ddot{\beta}_3 - M_b x_{g_b}\ddot{z}_p + \left(J_{o_y}\Omega^2 + M_b x_{g_b} f\Omega^2 + k_{\beta_3}\right)\beta_3 - M_b x_{g_b} g\sin\Psi_3 - J_{g_x}\dot{\Omega}\theta_3 = \int_0^L L_{w_3} r dr \\
&\sum_{i=1}^{3}\left[M_b f^2 + J_{o_z} + 2M_b x_{g_b} f\right]\dot{\Omega} - 2\sum_{i=1}^{3} J_{o_y}\Omega\dot{\beta}_i\beta_i = \sum_{i=1}^{3}\int_0^L L_{v_i}(r+f)dr + C_{res} \\
&J_{g_x}\ddot{\theta}_1 + J_{g_x}\Omega^2\theta_1 - J_{g_x}\beta_1\dot{\Omega} = \int_0^L M_{\phi_2} dr + C_{\tau_1} \\
&J_{g_x}\ddot{\theta}_2 + J_{g_x}\Omega^2\theta_2 - J_{g_x}\beta_2\dot{\Omega} = \int_0^L M_{\phi_2} dr + C_{\tau_2} \\
&J_{g_x}\ddot{\theta}_3 + J_{g_x}\Omega^2\theta_3 - J_{g_x}\beta_3\dot{\Omega} = \int_0^L M_{\phi_3} dr + C_{\tau_3}
\end{aligned}
\tag{3.27}
$$

where $\Omega = \dot{\Psi}$ is the rotor angular velocity, f is the distance between flapping hinge and rotation axis, and g is the gravitational acceleration that, although small compared with the other inputs, is one of the sources of system periodicity. Thus, eight differential second-order time dependent non-linear equations are found, lumped parameters (k) can be observed and obtained from the first mode frequency of different structural parts (e.g. $k_p = \omega^2 M_{pylon}$ or $k_\beta = \omega_\beta^2 J_{0_y}$).

The first equation describes the fore-aft motion of the top of the pylon, forced by the sum of out-of-plane (L_w) sectional forces. From the second to the firth equations are reported the flap-wise deflections. The dynamic of the rotor disc is reported in the fifth equation in which the right side is the sum of the moments generated from the in-plane (L_v) forces respect to the rotor center and the resistant rotor torque. The last three equations are related to the pitch dynamics forced by aerodynamic moments (M) and torque control actions (C_τ). Moreover C_{res} represents the control action related to the rotor disc. In order to take into account the effect of wake vorticity dynamics, the mean wake inflow ($\dot{\lambda_0}$) is included as an additional, aerodynamic state, through the classical

dynamic inflow model proposed by Leishman (38; 39) as an adaptation of Pitt-Peters model to wind turbines. Thus, an additional dynamic equation, reading

$$m_a\dot{\lambda_0} = \sum_{i=1}^{3}\int_0^L L_{w_i}dr + \rho A\lambda_0(\lambda_0 - V_w + \frac{2}{3}\dot{\beta}R) \tag{3.28}$$

is added to the system.

In the equations (3.27) it has been taken into account this ordering scheme and the terms above the second one have been neglected:

$$\left\{\begin{array}{c} M_b = o(1) \\ z_p = \dot{z_p} = \ddot{z_p} = o(\epsilon) \\ \beta = \dot{\beta} = \ddot{\beta} = o(\epsilon) \\ \Omega = \dot{\Omega} = o(1) \\ \theta = \dot{\theta} = \ddot{\theta} = o(\epsilon) \\ x_{g_b} = o(1) \\ f = o(\epsilon) \\ J_{g_y} = J_{g_z} = o(1) \\ J_{g_x} = o(\epsilon) \end{array}\right\} \tag{3.29}$$

3.2 Aerodynamic model

The aerodynamic model chosen for this study is derived from the Greenberg's theory (40), an extension of Theodorsen's theory (41) to the case of thin airfoils undergoing pulsating flows. The rotor blade aerodynamic forces are formulated from strip theory in which only the velocity components perpendicular and tangent to the blade spanwise axis influence the turbine forces. A quasi-steady approximation of the unsteady theory is employed in which low perturbation reduced frequency k is considered, which causes the *lift deficiency function* $C(k)$ (41) to be real and equal to 1 (*i.e.*, no delay between boundary conditions and resulting load is present). The sectional aerodynamic lift force and moment are then sum of two contributions: the former is the circulatory component due to the circulation around the airfoil and the latter is the non-circulatory part, also present on non-lifting bodies. It is worth noting that, while circulatory lift and moment exist also in steady flows, non-circulatory contribution is only due to

unsteadiness. Furthermore, a simple expression for skin friction and form drag is added through the inclusion of drag coefficient, C_{d0}. Following the approach proposed by Hodges and Ormiston (1), the authors expressed aerodynamic loads as a function of the chord-wise and normal components of relative velocity between flow and airfoil U_t, U_p, their derivatives , and section angular velocity $\dot{\varepsilon}$ (see Fig. 3.2). The circulatory and

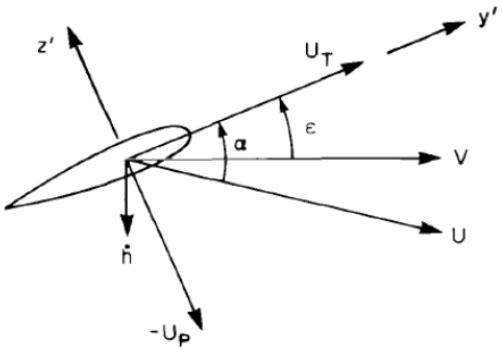

Figure 3.2: Section velocity, from (1).

non-circulatory components are calculated as follow:

$$\begin{aligned} L_c &= \frac{2\pi\rho c}{2} U(-U_p + \frac{c}{2}\dot{\epsilon}) \\ L_{nc} &= \frac{2\pi\rho c}{2}\frac{c}{4}(-\dot{U}_p + \frac{c}{4}\ddot{\epsilon}) \end{aligned} \tag{3.30}$$

Where U is the magnitude incident wind, c is the chord dimension and $\ddot{\epsilon}$ represents the angular acceleration. Furthermore the expressions of the aerodynamic moments and drag force result:

$$\begin{aligned} M_c &= -\frac{2\pi\rho c}{2}(\frac{c}{4})^2 U_t\dot{\epsilon} \\ M_{nc} &= -\frac{2\pi\rho c}{2}(\frac{c}{4})^2(-\dot{U}_p + \frac{3c}{8}\ddot{\epsilon}) \\ D &= -\frac{2\pi\rho c}{2}\frac{C_{d_0}}{2\pi}(U_t^2 + U_p^2) \end{aligned} \tag{3.31}$$

Where C_{d_0} is the drag aerodynamic coefficient. Also the angle of incidence is related to the wind velocity as follow:

$$\cos(\alpha) = \frac{U_t}{U} = \frac{U_t}{\sqrt{U_t^2 + U_p^2}}\ ,\ \sin(\alpha) = -\frac{U_p}{U} = \frac{U_p}{\sqrt{U_t^2 + U_p^2}} \tag{3.32}$$

The projection of the forces is shown in figure (3.3) where T and S represents orthogonal

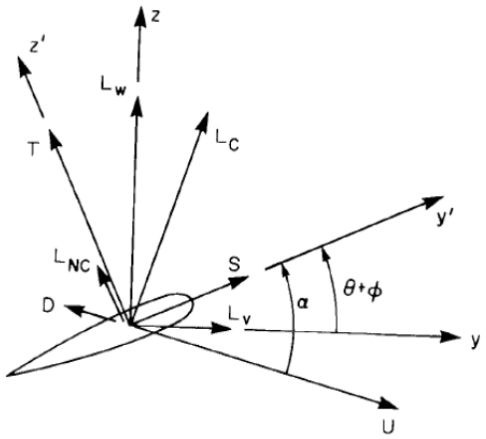

Figure 3.3: Section forces, from (1).

and parallel component respect to chord-wise direction whereas L_v and L_w are in plane and out of plane components respectively. Also α represents the angle of attack between chord and incident wind directions, and $(\Theta + \phi)$ takes into account the pitch and twist angles. Then results:

$$\begin{aligned} T &= L_c \cos\alpha + L_{nc} + D \sin\alpha \\ S &= -L_c \sin\alpha - D \cos\alpha \end{aligned} \tag{3.33}$$

Substituting equations (3.30), (3.31) and (3.32) into (3.33) one obtains

$$\begin{aligned} T &= \frac{2\pi\rho c}{2}\Big[- U_p U_t + \frac{c}{2} U_t \dot{\epsilon} - \frac{c}{4}\dot{U}_p + (\frac{c}{4})^2 \ddot{\epsilon} + \frac{C_{d_0}}{2\pi}(U_t^2 + U_p^2)\frac{U_p}{\sqrt{U_t^2 + U_p^2}}\Big] \\ S &= \frac{2\pi\rho c}{2}\Big[U_p^2 - \frac{c}{2} U_p \dot{\epsilon} - \frac{C_{d_0}}{2\pi} U_t^2\Big] \end{aligned} \tag{3.34}$$

where has been considered $U_p << U_t$ and $\frac{C_{d_0}}{2\pi}$ to be neglected respect to unity. Therefore, to obtain the forces in the rotating reference system, (3.33) are projected through

pitch and twist angles [1] such that:

$$\begin{aligned}
L_v \approx & \frac{2\pi\rho c}{2}\Big[U_p^2 - \frac{c}{2}U_p\dot{\epsilon} - \frac{C_{d_0}}{2\pi}U_t^2\Big]\,(C\phi - \Theta S\phi) + \\
& - \frac{2\pi\rho c}{2}\Big[-U_pU_t + \frac{c}{2}U_t\dot{\epsilon} - \frac{c}{4}\dot{U}_p + (\frac{c}{4})^2\ddot{\epsilon}\Big]\,(\Theta C\phi + S\phi) \\
L_w \approx & \frac{2\pi\rho c}{2}\Big[U_p^2 - \frac{c}{2}U_p\dot{\epsilon} - \frac{C_{d_0}}{2\pi}U_t^2\Big]\,(\Theta C\phi + S\phi) + \\
& + \frac{2\pi\rho c}{2}\Big[-U_pU_t + \frac{c}{2}U_t\dot{\epsilon} - \frac{c}{4}\dot{U}_p + (\frac{c}{4})^2\ddot{\epsilon}\Big]\,(C\phi - \Theta S\phi) \\
M_\phi \approx & -\frac{2\pi\rho c}{2}(\frac{c}{4})^2\Big[-U_t\dot{\epsilon} - \dot{U}_p + \frac{3c}{8}\ddot{\epsilon}\Big]
\end{aligned} \tag{3.35}$$

To obtain the aerodynamic sectional forces, it is essential to define the velocity components related to the quarter of chord and the angular velocity (with its temporal derivatives) in terms of system dofs (exploiting rigid body motion relations). Thus, the velocity of the aerodynamic center results in:

$$\bar{v}_a = \bar{v}_o + \bar{\Omega} \times \bar{f} + \bar{\omega} \times (\bar{x}_a - \bar{x}_h) \tag{3.36}$$

where $\bar{v}_a$ is the velocity of the aerodynamic center (quarter of chord) of the airfoil, $\bar{v}|_o$ is the velocity of rotor disc center, Ω is the rotor disc angular velocity, ω is the blade angular velocity, f is the offset hinge position and $(\bar{x}_a - \bar{x}_h)$ is the distance between the quarter of chord and flap-hinge position. Therefore, by projecting the vectors in the reference system (2.2.4), the following velocity components are obtained:

$$\bar{v}|_4 = \begin{Bmatrix} U_r \\ U_t \\ U_p \end{Bmatrix} = \begin{Bmatrix} -\dot{z_p}\beta \\ (\dot{z_p} + V_w + \lambda_0 - \dot{\beta}r)(C(\phi) - \theta S(\phi)) + (\Omega(f+r)(S(\phi) + \theta C(\phi)) \\ (\dot{z_p} + V_w - \lambda_0 - \dot{\beta}r)(C(\phi) - \theta S(\phi)) - (\Omega(f+r)(S(\phi) + \theta C(\phi)) \end{Bmatrix} \tag{3.37}$$

[1] $L_v = S\cos(\epsilon) - T\sin(\epsilon), L_w = S\sin(\epsilon) + T\cos(\epsilon)$, with $\epsilon = \theta + \phi$

in which U_r, U_t, U_p are , respectively, radial, orthogonal and parallel components to the airfoil chord

$$\left\{\begin{array}{c} z_p = \dot{z_p} = o(\epsilon) \\ \beta = \dot{\beta} = o(\epsilon) \\ \Omega = o(1) \\ \theta = \dot{\theta} = o(\epsilon) \\ r = o(1) \\ f = o(\epsilon) \\ c = o(\epsilon) \\ \frac{C_{d_0}}{2\pi} = o(\epsilon^2) \end{array}\right\} \tag{3.38}$$

In this way, only the U_t, U_p components with also $\dot{\epsilon} = \dot{\theta} + \Omega\beta$ and $\ddot{\epsilon} = \ddot{\theta} + \dot{\Omega}\beta + \dot{\beta}\Omega$ are used in equation (3.35) to obtain the following expressions for aerodynamic in-plane (L_v) and out-of-plane (L_w) sectional forces and moment (M_ϕ), see figure (3.3), appearing in equations (3.27):

$$\begin{aligned} L_v \approx & \frac{2\pi\rho c}{2}\Big[(V_w^2 + \Omega r\theta(V_w + \lambda_0))(S^2\phi\, C\phi + C^3\phi) + \lambda_0(C^3\phi - S^2\phi\, C\phi) \\ & - \frac{C_{d_0}\Omega^2 r^2 C^3\phi}{2\pi} - \Omega r\big(r\dot{\beta} + V_w + \lambda_0 - \dot{z}_p\big)(S\phi\, C^2\phi + S^3\phi) - \frac{c}{4}\dot{\Omega} r\, S^2\phi\Big] \\ L_w \approx & \frac{2\pi\rho c}{2}\Big[\Omega(\Omega(r + 2f) - V_w r\theta - \lambda_0 r\theta)(S\phi\, C^2\phi + S^3\phi) - \frac{C_{d_0}\Omega^2 r^2\, S\phi\, C^2\phi}{2\pi} + \\ & + \Omega r(\dot{z}_p + \Omega r\theta - V_w - r\dot{\beta})(S^2\phi C\phi + C^3\phi) + \frac{c}{4}\dot{\Omega} r S\phi C\phi + 2(\Omega r f + \lambda_0^2)\, S\phi\, C^2\phi\Big] \\ M_\phi \approx & -\frac{2\pi\rho c}{2}(\frac{c}{4})^2\Big[\dot{\Omega}(r + f)S\phi + (\Omega^2 r\beta + \ddot{z}_p + \dot{\Omega} r\theta + 2\Omega r\dot{\theta} - \ddot{\beta} r - V_w C\phi)\Big] \end{aligned} \tag{3.39}$$

where c is blade chord, r is a span-wise distance from the center of the rotor disc, ρ is the air density, V_w is the wind velocity, ϕ is the blade structural twist, whereas S and C are abbreviation for sin() and cos().

3.2.1 Dynamic Wake inflow modeling

The principles of the dynamic inflow approach can be attributed to Carpenter & Friedovich (38), where the idea is to consider the unsteady aerodynamic lag of the inflow development over the rotor disk in response to changes in blade pitch inputs or

changes in rotor thrust. The mathematics of the approach formally embody the concepts of the BEM theory. The equations describing the distribution of inflow are written in the form of ordinary differential equations, with a time constant (or constants) representing the dynamic lag in the build-up of the inflow. One attraction of dynamic inflow models for use in wind turbine work is their mathematical form and relative numerical efficiency, and also the prior predictive success in using these methods for various applications in the helicopter field. The main advantage of representing the aerodynamic model as ordinary differential equations is that it is appealing for many forms of structural dynamic and aero-elastic analysis of the rotor, so that the entire coupled problem can be solved simultaneously using the same numerical methods. Crews et al. (42), Ormiston (43), Peters (44) and Curtiss (45) have shown that using dynamic inflow models can have a significant influence on predictions made in helicopter flight dynamics and rotor aero-elasticity. The most popular model of dynamic inflow for both helicopter and wind turbine work is that of Pitt & Peters (46), which has seen several further developments for helicopter applications. For a discussion and background of dynamic inflow models in regard to their possible application to wind turbine problems, see Hansen & Butterfield (47) Bierbooms (48). The principle of the dynamic inflow approach can be illustrated as it follows. Using the blade element momentum theory, the rotor thrust can be related to the inflow using

$$T = m_a\dot{\lambda_0} + \rho A\lambda_0(\lambda_0 - V_w + \frac{2}{3}\dot{\beta}R) \tag{3.40}$$

where m_a is associated by Carpenter & Friedovich with the "apparent mass" of an impermeable circular disk accelerating in a stagnant fluid. They suggest this to be 63.7% the mass of a sphere of fluid with radius equal to the rotor one (i.e. $m_a 0.637\rho(\frac{4\pi R^3}{3})$). The $m_a\dot{\lambda_0}$ therm, therefore, represents the additional force on the rotor disk because of the accelerating inflow, V_w is the wind velocity and the term $\frac{2}{3}\dot{\beta}R$ represents the flap motion.

3.2.2 Wind shear modeling

Writing equation (2.2) as a function of radial distance from the center of the rotor axis (R) and blade azimuth angle (ψ), it becomes:

$$U(z) = U(z_r)(\frac{R\cos(\psi)}{z_r})^{\alpha}. \tag{3.41}$$

The disturbance in wind due to wind shear is dependent on $U(z_r)$, z_r, α and R.

Figure (3.4) shows the variation of the wind shear with the average wind speed at the top of the pylon. For $U(z_r) = 11.4m/s$, the maximum wind speed experienced by the blades of a wind turbine is $12.00m/s$ while the minimum value is $10.18m/s$. Hence, the variation in wind speed, that is the difference between maximum and minimum wind speed for one complete rotation, is $1.82m/s$. Similarly, for $U(z_r) = 14m/s$, the variation in wind speed is $2.24m/s$. Thus, wind shear increases with the increase in $U(z_r)$. Also, note that the minimum wind speed occurs in $\psi = 180°$, that is, when the blade is pointed downwards and the maximum value is experienced in $\psi = 0°$, that is, blade is pointed upwards. Figure (3.5) shows that wind shear decreases with increase in hub height. For example, at $z = 120m$, the variation in wind speed is $1.26m/s$ while at $z = 80m$ the wind variation is $2.78m/s$. Figure (3.6) reports the impact of α on the wind shear. The values are chosen depending on the terrain, as shown in table (2.1). As α increases, wind shear increases. Figure (3.7) reports the wind shear experienced from different sections along the span of the blade: minimum wind shear is experienced by the blade elements closest to the center of the rotor disc ($R = 5m$).

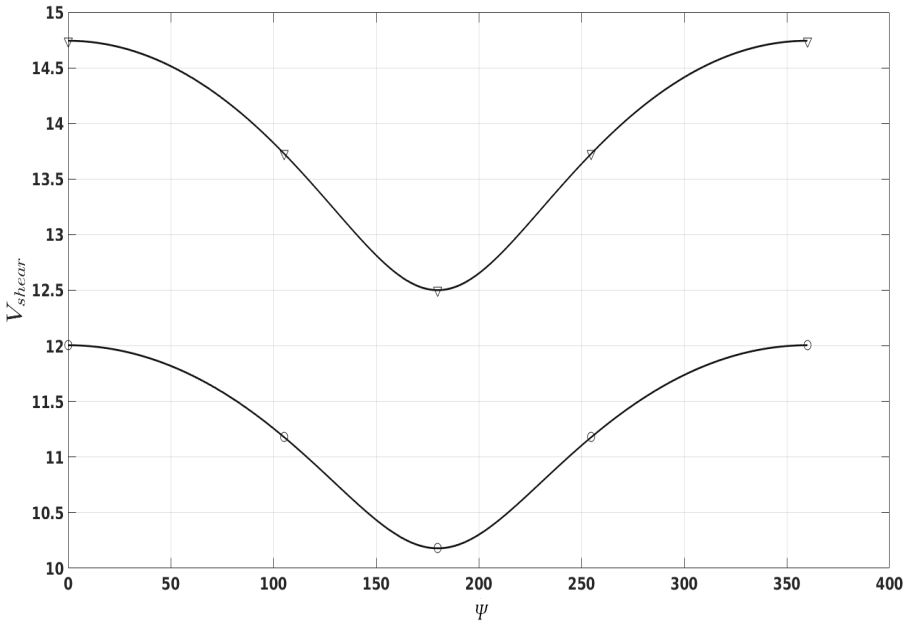

Figure 3.4: Effect of wind speed on wind shear $(U(z_r) = 14m/s, \triangle), (U(z_r) = 11.4m/s, \circ)$

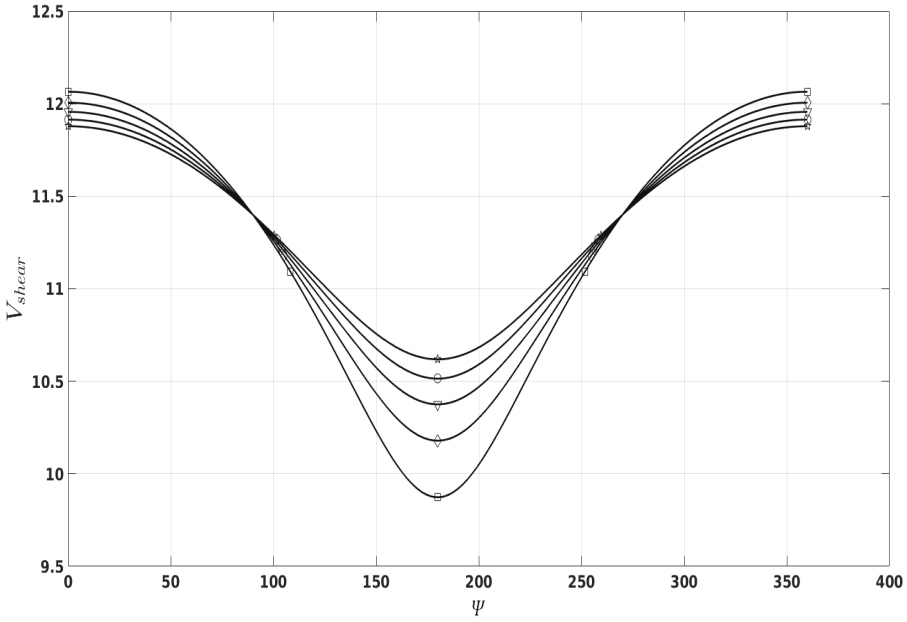

Figure 3.5: Effect of hub height on wind shear $(z = 80m, \square), (z = 90m, \diamond), (z = 100m, \triangle), (z = 110m, \circ), (z = 120m, \star)$

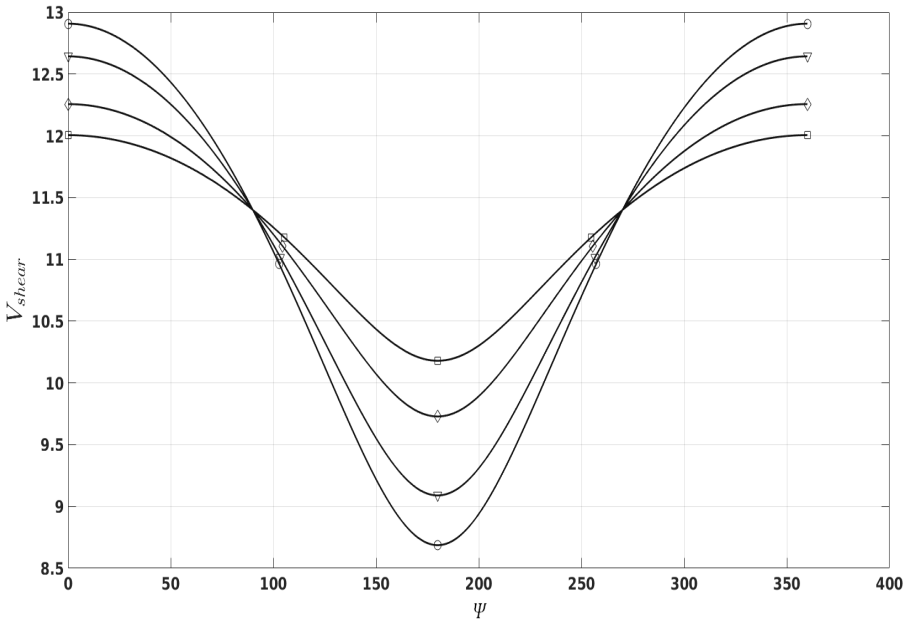

Figure 3.6: Effect of terrain on wind shear $(\alpha = 0.1, \square), (\alpha = 0.14, \diamond), (\alpha = 0.2, \triangle), (\alpha = 0.24, \circ)$

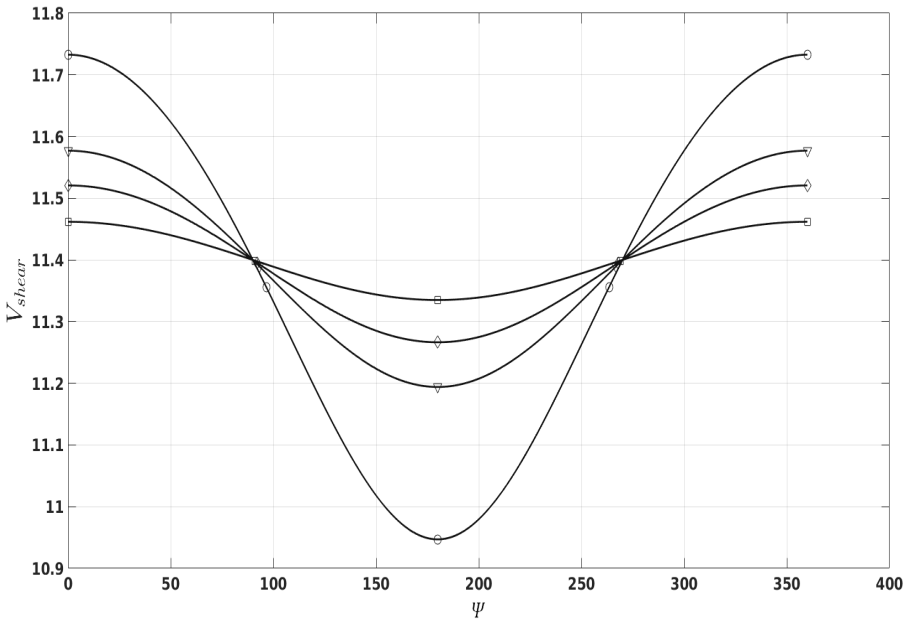

Figure 3.7: Effect of radial distance on wind shear $(R = 5m, \square), (R = 10m, \diamond), (R = 15m, \triangle), (R = 30m, \circ)$

3.2.3 Tower shadow modeling

The tower shadow aerodynamic effect can be represented as equation (2.5). Hence, differentiating stream function ψ with respect to y yields the total wind velocity $V(x, y)$ in x-direction as:

$$\begin{aligned} V(x,y) = \frac{\partial \psi}{\partial y} &= V_h \left[1 + \frac{a^2(y^2 - x^2)}{(x^2 + y^2)^2}\right] \\ &= V_h + v_{tower}(y, x). \end{aligned} \tag{3.42}$$

where the second term in the right-hand side is the disturbance in wind due to the presence of the pylon:

$$v_{tower}(y, x) = V_h \frac{a^2(y^2 - x^2)}{(x^2 + y^2)^2}. \tag{3.43}$$

In equation (3.43) V_h is the spatial mean wind speed, a is the tower radius, y is the lateral distance from the blade to the tower mid-line, and x represents the distance between blade origin and tower mid-line as it is reported in figure (3.8). Writing the equation

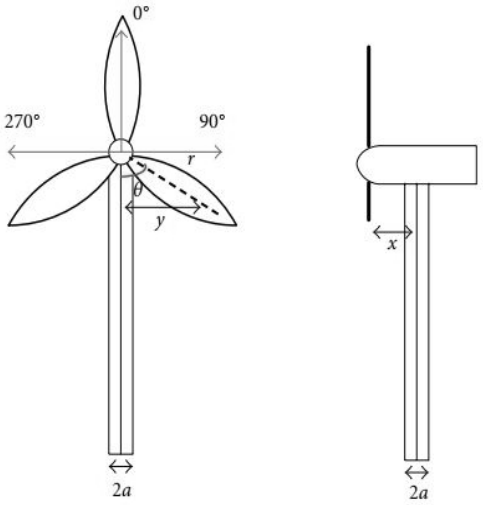

Figure 3.8: Dimensions used in equation (3.43).

(3.43) as a function of r (radial distance from rotor axis) and ψ (blade azimuthal angle), it yields to:

$$v_{tower}(r, \psi, x) = V_h \frac{a^2(r^2 sin^2\psi - x^2)}{(r^2 sin^2\psi + x^2)^2} \tag{3.44}$$

It should be noted that equation (3.44) depends from three factors (a, r, x) and is valid only for an azimuthal angle $90° < \psi < 270°$ because the generic blade only receives the wind variation crossing in the lower part of the disc calling this area tower-shadow zone. In figure (3.9) r is varied from $5m$ to $20m$. It is observed that blade elements closer to the hub ($r = 5m$) experience a longer duration of the disturbance, also for an azimuthal angle value of 180°, that is blade directly in front of the tower; the same wind deficit is seen for all radial value considered. Next, maintaining constant the radial value, figure

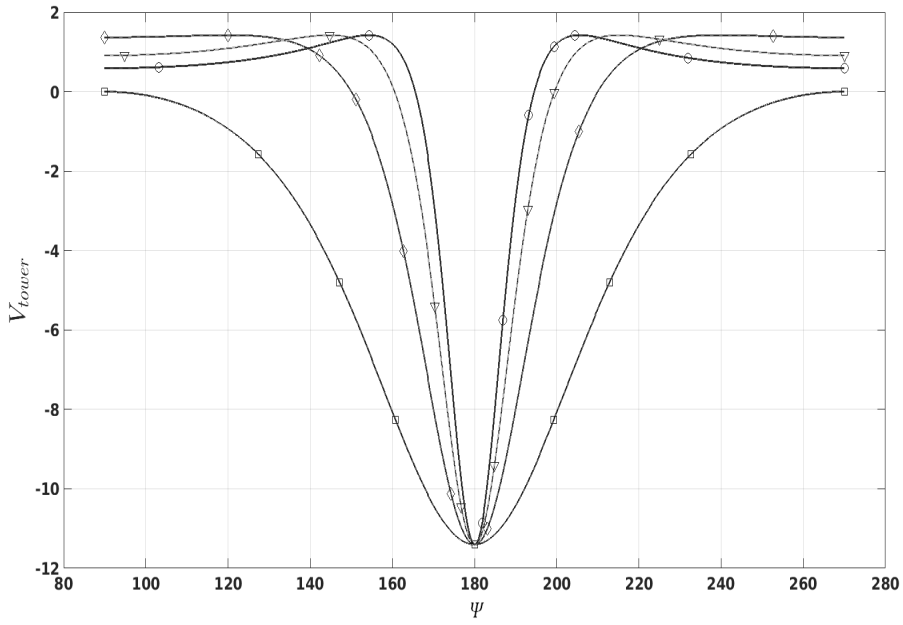

Figure 3.9: Effect of the radial distance from rotor axis $(r = 5m, \square), (r = 10m, \diamond), (r = 15m, \triangle), (r = 20m, \circ)$

(3.10) shows the influence of the distance between blade origin and the tower mid-line, that is x. This parameter is varied starting from $2m$ to $5m$, as shown as the distance decreases, the tower shadow deficit is remarkable ($x = 2m$). Hence, mounting the blades away from the pylon minimizes tower shadow effect. Figure (3.11) depicts the effect of tower's radius on the incident wind. As the radius increases, the characteristic inverted cone shape becomes bigger. The space can be divided into three regions according to the different effects of the tower shadow on the wind. For $0° < \psi < 90°$ or $270° < \psi < 360°$, the tower shadow does not exist , that is $v_{tower} = 0$. When $\psi = 180°$, that is directly

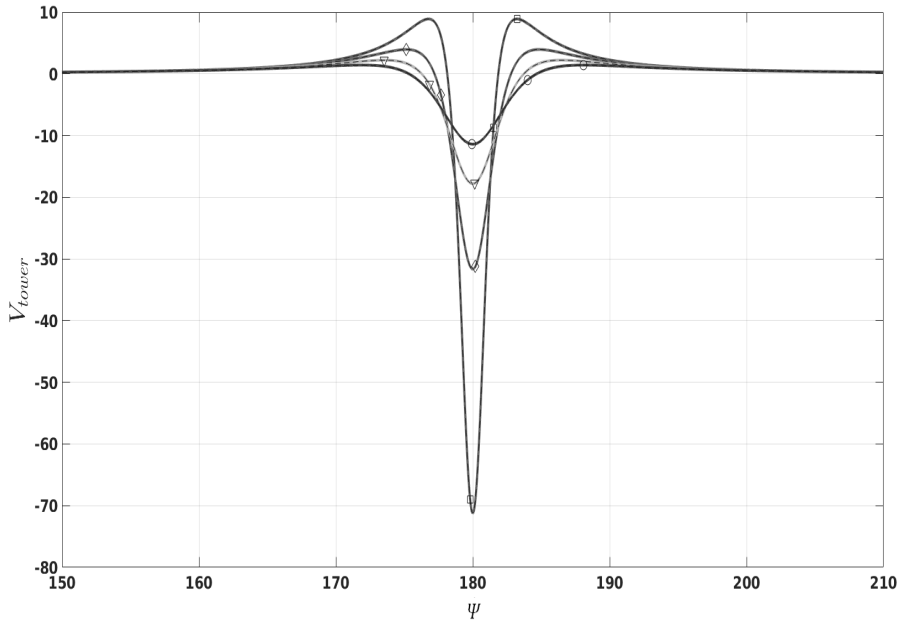

Figure 3.10: Effect of the distance between blade origin and tower mid-line ($x = 2m, \square$), ($x = 3m, \diamond$), ($x = 4m, \triangle$), ($x = 5m, \circ$)

in front of the tower, the wind speed is significantly decreased, accelerating before and decelerating after. The maximum and minimum v_{tower} are $v_{tower_{max}} = 0.0444$ and $v_{tower_{min}} = -0.36$ respectively; thus the variation is $\Delta v_{tower} = 0.4044$.

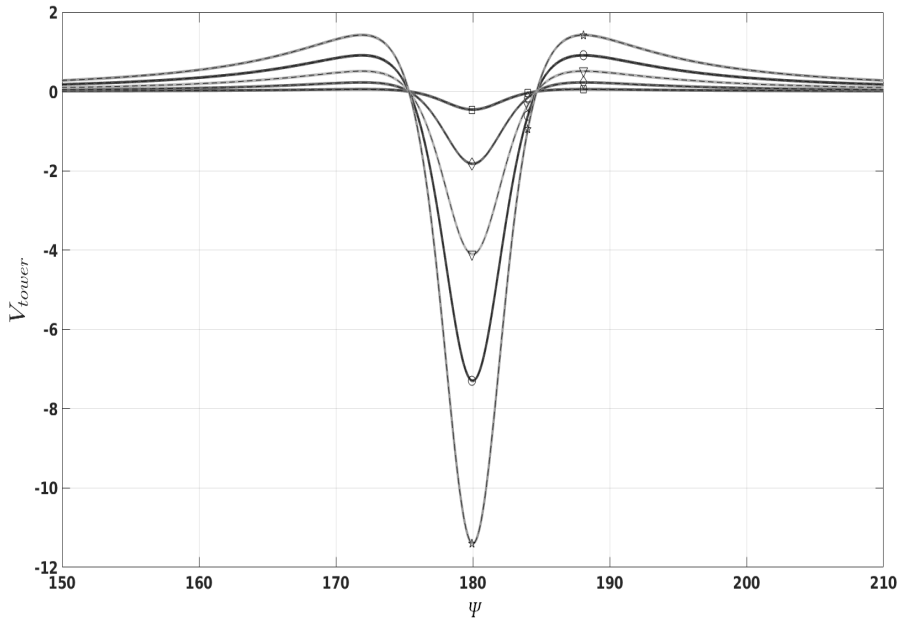

Figure 3.11: Effect the tower radius $(a = 1m, \square), (a = 2m, \diamond), (a = 3m, \triangle), (a = 4m, \bigcirc), (a = 5m, \star)$

Chapter 4

Control objectives and strategies

In this section, the control objective and strategies for the wind turbines are outlined. In particular, the Repetitive and Multi-Harmonic control strategies are introduced.

4.1 Control Objectives

This chapter describes the classic control objectives associated to wind turbine. This machine is essentially a device that captures part of the wind energy and converts it into useful work. To achieve this goal, several factors can be taken into account: Reaching this target there are some many factors that can be arranged in the following topics:

- *Energy capture*: Energy maximization with safe operation restrictions (*e.g.*, rated power, rated speed and cut-off wind speed);
- *Mechanical loads*: Protect the wind turbine against excessive dynamic mechanical loads;
- *Power quality*: Provide good Power Quality to comply with the standards of grid connected wind turbines.

In addition, different working condition are possible for a wind turbine, such as fixed-speed/variable-speed or fixed-pitch/variable-pitch. These strategies are usually combined together in order to achieve the control objectives over the full range of operational wind speeds. With the introduction of variable speed generators, variable rotor

speed was suddenly possible. Since the power gained from the wind is dependent of the wind speed and rotor speed, the power gain can be optimized by changing the speed of the rotor. This new kind of generator meant that a high quality of power, in regard to phase, frequency and amplitude could be maintained, while running at variable speed. Nowadays, variable speed generators are the most common type used.

Power quality is another control objective. Control of power quality is mainly about controlling the voltage and frequency. A wind turbine operated at variable speed works by rectifying the AC generated into DC and then inverting it back into AC delivered on the grid. Power control is typically also an issue, when controlling wind farms of multiple wind turbines, where the supply and demand also need to be matched. Control of the power quality is within the scope of this project and will be investigated further in this thesis.

Most variable speed wind turbines has three main actuators, which can be used for control. The first is a yaw actuator (10; 11; 12), which can be used to turn the nacelle and rotors to be pointing into the wind. This actuator is usually controlled very slowly to avoid undesired loads. Most often, yaw control is only used to respond to changes in wind direction in an attempt to reduce the yaw error (the angle between the mean wind direction and the direction of orientation of the turbine) and thereby maximize power.

Next, the angle of the blades can be controlled by pitch actuators that is the most effective one in the control of the aerodynamic loads. These actuators turn the whole or parts of the blade to change the aerodynamic load on the rotor. Pitch can be controlled either collectively or individually. In the first configuration the angle of each blade is adjusted identically, whereas for the second pitch control the angle is adjusted independently of the other blades. An advantage of individual pitch control is better load compensation with regard to non-homogeneous wind fields.

The last main actuator is generator torque, which can be used to optimize the angular velocity of the rotor and is most often used in region 2 to maintain turbine operation at maximum power coefficient C_p, it can also be used to add damping to the drive-train torsion modes.

Creating control to compensate for both non-homogeneous and homogeneous wind fields is a focus of this thesis, so a collective pitch and individual pitch schemes are used,

whereas control of the yaw and the generator are omitted. A classic control strategy is to divide the area of operation into different control regions. These regions are here described and can be seen in figure (4.1). Control Regions:

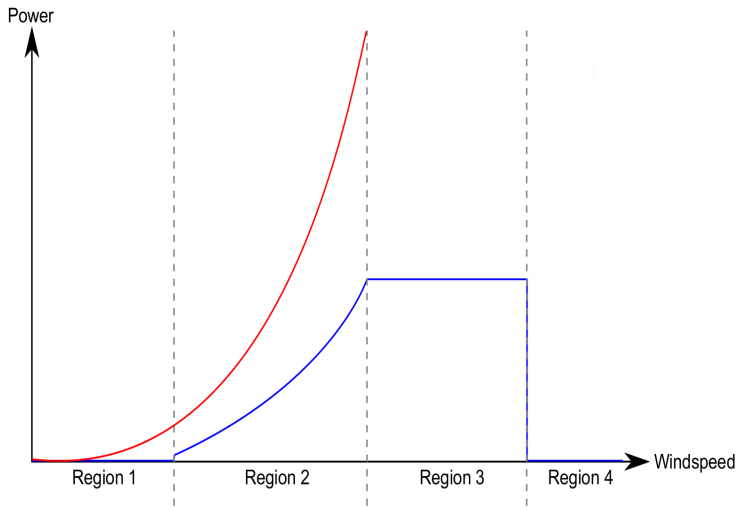

Figure 4.1: Illustration of power generated in the different control regions.Wind power (—), Wind Turbine Power(—).

- In Region 1, the wind turbine is stopped or just starting up due to low wind speeds. Below the cut-in speed the operation cost of the wind turbine is higher than what can be gained.
- In Region 2, the objective is to maximize wind power extracted from the wind. Variable speed control is usually used in this region, where pitch is kept constant and torque on the generator is controlled. This region is typically called partial load region due to the wind turbine operating at lower than rated load.
- In Region 3, the power extracted is limited and kept constant to avoid loads larger, than what the wind turbine is rated to. Constant speed control is often used in this region, where pitch is controlled (either collectively or separately) and generator torque is kept constant. This region is referred to as full load region since the wind turbine is operated at the rated power. The objective of the control in this region is the minimize the variance in power generation. Too little power is less profitable and too much power increases fatigue on the wind turbine.

- Region 4 starts when hitting wind speed larger, than the cut-out threshold and the wind turbine is brought to a stop. Here, the blades are pitched out to minimize the resulting aerodynamic torque and the brakes are enabled to stop movement of the rotor.

Region 1 and 4 which involve start up and shut down of the wind turbine are out of the scope of this project and will not be analyzed in this thesis. The focus will be on control at the beginning of region 3, where dynamic inflow has the largest influence. In figure (4.1) the different control regions are depicted with an illustration of total energy contained in the wind and extracted power of the wind turbine as a function of the wind speed. A multitude of different control schemes exists dealing with the weighing between fatigue and power generated. Since these control schemes consist of different individual controller, it can be hard to ensure optimally of the control actions. In this work, it has been chosen to work with a fixed-speed/variable-speed mode such that the wind turbine can reach the maximum power conversion only at a specific wind speed. In particular, the power has been limited, above the rated wind speed, using the well known pitch-to-feather approach. With this method, it is possible to stop the rotor when the wind exceeds the maximum rated speed. Specifically, the controller acts increasing the pitch angle while the trim angle decreases.

4.2 Repetitive Control

Tracking reference commands without a steady state error and reject disturbances acting on the control variables, are well known basic requirements in controls systems. In addition, in many practical applications (such as high accuracy trajectory control in servomechanisms, robot control, altitude stabilization of satellites, current compensation in active filters and control of rotation mechanisms), the control tasks are often of a repetitive nature. Due to the increasingly high demand on the productivity and quality, one of the most challenging tasks in the last years, has become the high precision control of such kind of systems. Hence, instead the classical tuning of general servo controllers such as PID or state feedback controllers, a special class of techniques may be considered to handle with these periodic signals. In particular, when the reference

command to be tracked and/or the disturbance to be rejected are periodic signals with a fixed period, the *repetitive control* strategy can be applied (49; 50). Indeed, since its introduction to the control community, this technique has distinguished itself by its high precision, simple implementation and little performance dependency on system parameters. Furthermore, thanks to a great effort to its theoretical development and to various algorithms that have been proposed in the last years, a lot of engineering problems (e.g., wind turbines control) are now treated with a repetitive control model (51; 52; 53). In figure (4.2) the functional scheme of a repetitive controller approach is

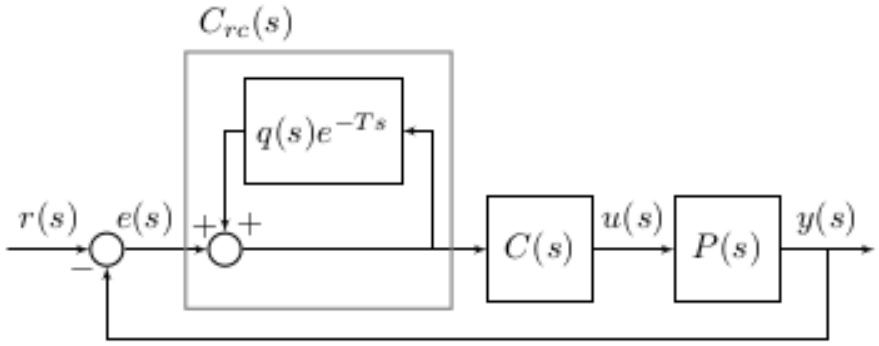

Figure 4.2: Repetitive control scheme

shown. The blocks $C(s)$ and $P(s)$ represent, in a schematic view, the control and plant respectively. The block $C_{rc}(s)$ is usually added to an existing feedback control system and is composed of a free time-delay system e^{-Ts} in a positive feed-back loop, and a low-pass filter $q(s)$. It should be noticed that, while the time-delay term is well known for decreasing the stability margin, on the other hand the low pass filter is added to ensure stability. In particular, the repetitive control loop in figure (4.2) is equivalent to the modified version proposed by Hara in (54), with $a(s) = 1$, which sacrifices tracking performances at high frequencies for system stability.

4.2.1 The proposed repetitive controller

The idea we followed for the controller design, derives from the procedure detailed in (55; 56; 57) where a phase shifting is considered. To this aim, the free time delay system in figure (4.2) has been modified as

$$e^{-(T-\gamma_k)}, \tag{4.1}$$

where T is the period of the signal and γ_k is a phase shifting of k samples of the same periodic signal. It should be noticed that, the phase shifting technique is particularly useful in non-minimum phase systems, such as flexible structures. In fact, using the phase shifting, the iterative algorithm could reach the convergence also at high frequencies. Moreover, in (58) it has been shown that iterative learning algorithms are sub-optimal, converging with a small error, for quasi-linear systems with smalls non-linearity.

For the tuning of the proposed controller, we followed the approach deriving from the linear iterative learning control theory. To this aim, let $y_j(k)$ be the output of the considered system, such that:

$$y_j(k) = P(q)\, u_j(k) + d_j(k) \tag{4.2}$$

where $k \in \{0, 1, ..., N-1\}$ is the time index[1], j is the iteration index, q is the forward time-shift operator such that $qx(k) = x(k+1)$, u_j is the control input, and d_j is an exogenous signal. We indicate the plant as $P(q)$.

The desired output and the system error read as:

$$y_d(k), \quad e_j(k) = y_d(k) - y_j(k). \tag{4.3}$$

It is worth noting that, the N-sample sequence is proportional to the simulation sample time Δt and the total simulation time can be indicated as $T = N\Delta t$.

A widely used ILC learning algorithm is:

$$u_{j+1}(k) = Q(q)\, u_j(k) + L(q)\, e_j(k+1) \tag{4.4}$$

[1] N represents the sample sequence.

where the LTI dynamics $Q(q)$ and $L(q)$ are defined as the Q-filter and the Learning Function, respectively. Specifically, the command input $u_{j+1}(k)$ (related to $j+1$ iteration at sample time k) is proportionally through Q filter to the previous control action $u_j(k)$. Also, the error signal $e_j(k+1)$ is modulated and shifted through L action. From

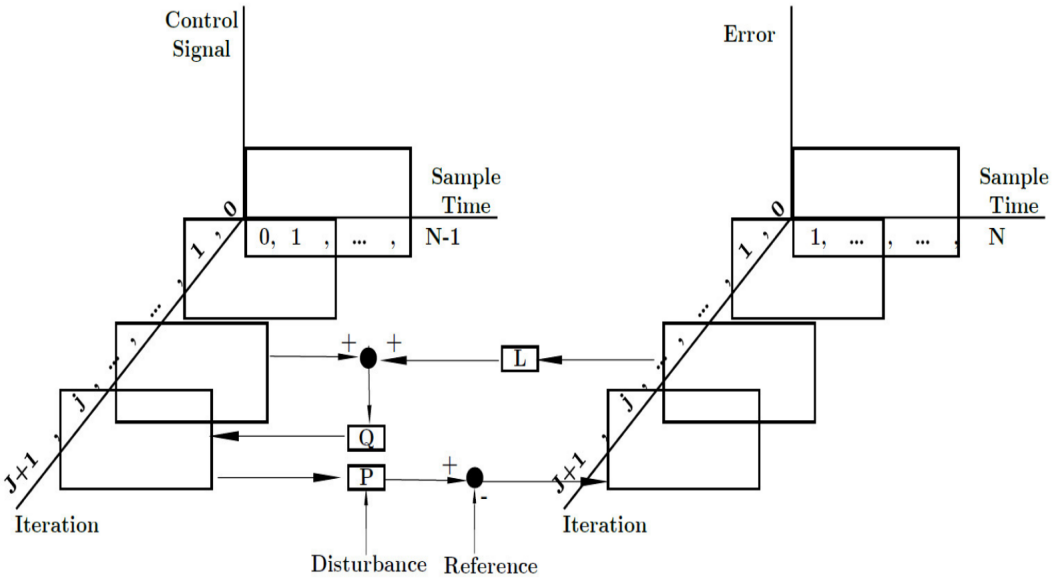

Figure 4.3: Repetitive control scheme

a practical point of view the control attempts to improve the response of the system by adjusting the input to the plant based on the errors observed during past operations. Figure (4.3) shows the action of the command input designed through the repetitive approach. In particular, the control core, consists in acquiring signals related to all the controls and errors of the system at the previous iterations, $u_j(k)$ and $e_j(k)$. For each time step, the control acts by using the error at the previous iteration and related to the successive sample, namely $e_j(k+1)$, to update the control command, $u_j(k)$, yielding to the actual control action $u_{j+1}(k)$ that will determine the relative error $e_{j+1}(k)$. Thus, the convergence is achieved when the error is within a fixed tolerance, which is, from a mathematical point of view, described by the following condition:

$$\lim_{j\to\infty} \|e_j\| = 0 \tag{4.5}$$

where e_j is defined in equation (4.3) and $\|\cdot\|$ denotes an appropriate norm.

In application, only a finite number of iterations is completed, thus $j \to \infty$ is only a mathematical writing giving us the amount of iterations required. Also a frequently used form of Q filter (also known as forgetting factor or feedforward part) is:

$$Q(u_j(k)) = \alpha_1 u_j(k-1) + \alpha_0 u_j(k) + \alpha_1 u_j(k+1) \tag{4.6}$$

where $2\alpha_1 + \alpha_0 = 1$. In general, the Q filter can improve the robustness of Repetitive strategy to high frequency uncertainties but it results in non-zero final tracking error. In this work, a value of $\alpha_0 = 1$ is considered for all simulations performed yielding to $Q(u_j(k)) = u_j(k)$. The second part of equation (4.4) is called updating law of the Repetitive control, where L is a filter that can be applied as proportionally filter to the error, $L(e_j(k+1))$, or as a derivative filter, $L(e_{j+1}(k+1) - e_j(k+1))$. In this work, the first strategy is applied and the value of the L filter, in terms of modulation and shifting, varies with the simulations. The Q-filter and the learning function can be written respectively:

$$Q(\mathrm{q}) = ... + q_{-2}\mathrm{q}^2 + q_{-1}\mathrm{q}^1 + q_0 + q_1\mathrm{q}^{-1} + q_2\mathrm{q}^{-2} + ...$$

$$L(\mathrm{q}) = ... + l_{-2}\mathrm{q}^2 + l_{-1}\mathrm{q}^1 + l_0 + l_1\mathrm{q}^{-1} + l_2\mathrm{q}^{-2} + ...$$

Thus, equation (4.4) becomes:

$$\begin{bmatrix} u_{j+1}(0) \\ u_{j+1}(1) \\ \vdots \\ u_{j+1}(N-1) \end{bmatrix} = \begin{bmatrix} q_0 & q_{-1} & ... & q_{N-1} \\ q_1 & q_0 & ... & q_{N-2} \\ \vdots & & & \vdots \\ q_{N-1} & q_{N-2} & ... & q_0 \end{bmatrix} \begin{bmatrix} u_j(0) \\ u_j(1) \\ \vdots \\ u_j(N-1) \end{bmatrix} + \tag{4.7}$$

$$\begin{bmatrix} l_0 & l_{-1} & ... & l_{N-1} \\ l_1 & l_0 & ... & l_{N-2} \\ \vdots & & & \vdots \\ l_{N-1} & l_{N-2} & ... & l_0 \end{bmatrix} \begin{bmatrix} e_j(0) \\ e_j(1) \\ \vdots \\ e_j(N-1) \end{bmatrix} \tag{4.8}$$

When $Q(q)$ and $L(q)$ are causal functions, it follows that $q1 = q2 = \ = 0$ and $l1 = l2 = \ = 0$, and thus the matrices are lower triangular and have all of the entries along each diagonal identical.

In this work, a modified repetitive control strategy is applied on the model proposed in Chapter 3. During the validation steps of the model (open loop approach), the authors observed a periodic trend of the pitch angle due to the effects of the wind and of gravitational force. To counterbalance this periodic trend, we design a repetitive controller with a *spatial* action: the term *spatial* refers to the azimuth angle on which the controller acts. Recent studies (59; 60; 61; 62), have shown that a spatial-based repetitive controller can be used, without degrading its performances, in combination with systems operating at varying speed such as the wind turbine model presented in Chapter 3.

4.3 Individual Pitch Control

Torque and power generated by a wind turbine is much more variable than that produced by more conventional generators. The reason of these power fluctuations is due both to stochastic and periodic processes (wind shear and tower shadow).

Wind shear describes the variation of wind speed with the vertical elevation, whereas tower shadow describes the modification of the wind speed due the presence of the tower. Both of these aspects affect the aerodynamics of wind turbines inducing unsteady loads and thus vibration on the entire structure that can lead to fatigue loads and fluctuating power output that can cause problems on the electric grid management.

Various strategies have been proposed to mitigate fluctuations in aerodynamic loads and power output due to wind shear and tower shadow and, most of these, use an individual pitch control strategy (14; 15; 17; 18; 19; 20). However these methods are only focused on load reduction around one time the rotational frequency (IPC 1P) and a drawback is the still existing blade load components around multiples of the rotational speed (2P, 3P, ...). In three-bladed turbines the most common and largest periodic pulsation occurs at a 3p frequency, that is three times the rotor frequency or the same frequency at which a generic blade pass by the tower. Thus, even for a constant wind speed, a turbine blade would encounter variable wind as it rotates: torque pulsation and power fluctuation are observed due to the periodic variations of the wind speed experienced at different locations. The 3P oscillations must be considered in the wind turbine model, due to the wide ranging effects they can produce on both the control

system and to the power quality. This section presents a control strategy based on the individual and collective action on the pitch angle, to reach steady state angular velocity while reducing loads on the blades.

4.3.1 Individual Pitch Control based on blade root measurements

The out-of-plane bending moment at the blade roots can be determined by the implementation of strain gauge sensors in the blade manufacturing process. Previously such sensors consisted of wire strain gauges, which have a varying resistance depending on the elastic deformation of the blade on which it is mounted. These types of sensors experience calibration drift and are sensitive to lightning strikes. Due to these characteristics these sensors could be considered unfit for wind turbine applications. Advances in fiber-optic strain gauges resulted in an affordable and more reliable alternative to resistance gauges (63). Fiber-optic strain gauges do not suffer from either electrical interference or calibration drift (64). The possibility of using IPC must be evaluated before blade fabrication. There are blade manufacturers such as LM Wind power and Vestas who have started to incorporate strain gauges in their larger blades series.

The global functioning of the IPC strategy is as followed. First, the blade root moments are measured and the out-of-plane component is determined. These out-of-plane bending moments are then converted to a fixed frame of reference, using the Coleman transformation (equation (2.8)). The fixed frame of reference is the same frame as described in paragraph (2.2.2). Conversion of the 1P signal present in the rotating blade bending moment results in a near steady (or 0P) signal in the non-rotating FOR. The decomposed signals are approximates of the yawing and tilting moment. This signal passes through a low-pass filter, which is designed to filter out the components with frequencies of $f \geq 3P$. The signal is then multiplied by a gain which is scheduled according to the control operating condition of the wind turbine, which yields us to a virtual tilting and yawing angles. Optionally, this angle can be passed through a limiting saturator, in order to constrain the demanded pitch angles. The fictitious tilt and yawing angles determine the amplitudes of the sinusoidal pitch variations of the blades while rotating. In order to convert the tilt and yawing angle to 'real' blade pitch

variations we need to perform an inverse Coleman transformation to move from the fixed FOR back to the rotating one. The inverse Coleman transformation in case of the pitch angles has the following structure:

$$\begin{pmatrix} \theta_1 \\ \theta_2 \\ \theta_3 \end{pmatrix} = \begin{pmatrix} \cos(\psi) & \sin(\psi) \\ \cos(\psi + \frac{2\psi}{3}) & \sin(\psi + \frac{2\psi}{3}) \\ \cos(\psi + \frac{4\psi}{3}) & \sin(\psi + \frac{4\psi}{3}) \end{pmatrix} \begin{pmatrix} \theta_{tilt} \\ \theta_{yaw} \end{pmatrix} \tag{4.9}$$

Note that the angles θ_i only refer to the IPC part of the total pitch angle; the final demanded angles for the pitch actuators are the sum of the IPC and the CPC ones depicted as in figure (4.5). Where, $M_{y,i}$ is the out-of-plane bending moment of the

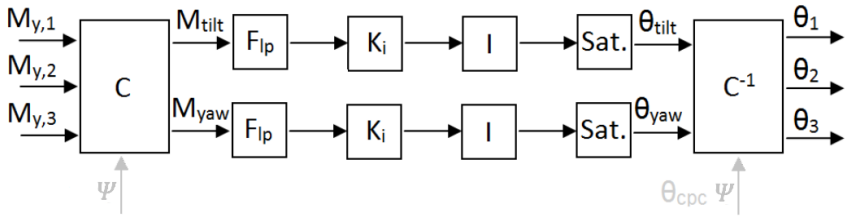

Figure 4.4: Schematic of the 1P Individual Pitch Controller structure

i-th blade, ψ is the rotor azimuth angle, M_{tilt} and M_{yaw} are the tilting and yawing moments, C is the Coleman transformation matrix as specified in paragraph (2.3.3), F_{Ip} denotes the low-pass filter, K_i is the scheduled gain, I denotes the integrator, $Sat.$ is the saturation block, θ_{tilt} and θ_{yaw} are the virtual demanded tilting and yawing angles, C^{-1} denotes the inverse Coleman transformation and θ_i denotes the demanded angle for the i-th blade.

The controller is designed to only compensate at the frequency assigned by the Coleman transfer matrix. In this case, equation (4.9), is related only for the rotational (or 1P) frequency. As previously mentioned, there is a large 1P component present in the blade root signal, which can be caused by any combination of wind shear, tower shadow and periodically sampled turbulence. It should be noted that periodically sampled turbulence will not be a 'pure 1P' signal, but rather form a band around the frequency due to the time dependency of the turbulent structures. The 1P load is converted to a near steady state 0P load in the fixed frame of reference and it is valid for both the controller signals. Therefore, by setting the tilting and yawing moment in the control

loop to zero, the actual nacelle/tower loading will experience a reduction in the 0P loading for both axes, this will provide reduction in fatigue damage on fixed frame components but the actuation must be performed at a different frequency than 1P in order to reduce all the fatigue damage of fixed components. Inspection of the load spectrum of the yawing bending moment of the low-speed shaft, figure (2.11), showed a large peak at the 3P frequency. From the conversion between the rotating and fixed-FOR we know that the 2P peak is converted to a 3P peak. Thus, an approach to reducing fixed frame fatigue damage can be to reduce the 2P peak in the rotating blade loads. This concept is explored in the next paragraph.

4.3.2 The proposed Individual Pitch Control

An extension of classical 1P Individual Pitch Control can be found in Higher Harmonic IPC, sometimes referred to as multi-rotational modes IPC. The basic concept is to use several IPC loops in parallel which all target a different cyclic load. The structure of each of the loops is nearly the same as the structure depicted in figure (4.4); the only difference is in the formulation of the Coleman transformations, because are modified to a transformation on a different frequency; specifically the frequency of the load that the loop will be reducing. The Coleman transformation on the frequency is defined as (in which the average moment signal is omitted):

$$\begin{pmatrix} M_{N,tilt} \\ M_{N,yaw} \end{pmatrix} = \frac{2}{3} \begin{pmatrix} \cos N(\psi) & \cos N(\psi + \frac{2\psi}{3}) & \cos N(\psi + \frac{4\psi}{3}) \\ \sin N(\psi) & \sin N(\psi + \frac{2\psi}{3}) & \sin N(\psi + \frac{4\psi}{3}) \end{pmatrix} \begin{pmatrix} M_{y,1} \\ M_{y,2} \\ M_{y,3} \end{pmatrix} \tag{4.10}$$

and the inverse Coleman transformation results in:

$$\begin{pmatrix} \theta_{N,1} \\ \theta_{N,2} \\ \theta_{N,3} \end{pmatrix} = \begin{pmatrix} \cos N(\psi) & \sin N(\psi) \\ \cos N(\psi + \frac{2\psi}{3}) & \sin N(\psi + \frac{2\psi}{3}) \\ \cos N(\psi + \frac{4\psi}{3}) & \sin N(\psi + \frac{4\psi}{3}) \end{pmatrix} \begin{pmatrix} \theta_{N,tilt} \\ \theta_{N,yaw} \end{pmatrix} \tag{4.11}$$

Where, N is the harmonic of the cyclic load (NP) which is being reduced. The parallel loops work independently, which can only be assumed if proper filtering in the controller is employed. Each of the loops will generate three blade pitch periodic signals at their

respective frequencies. A schematic of the total parallel operating pitch control strategy is shown in figure (4.5). The control designer now has the choice of which harmonic cyclic loads to include in the control strategy.

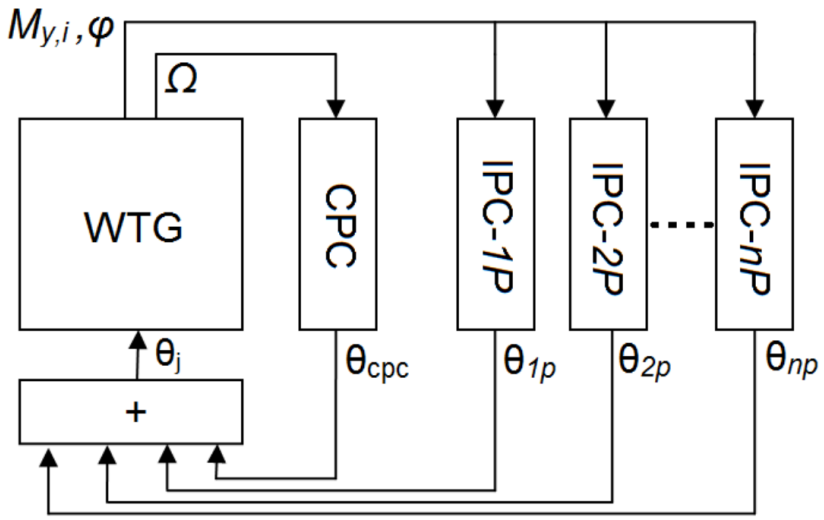

Figure 4.5: Structure of the pitch control parallel loops

Chapter 5

Validation of proposed controllers on a 5.0 MW wind turbine model

In this work, a 5 MW, three-bladed HAWT is examined (65). It has radius $R = 61.5$ m, mean chord $c = 3$ m, up-wind rotor orientation, hub height from terrain $h = 90$ m, nominal angular speed $\Omega = 1.26$ rad/s, nominal wind speed $V_{wind} = 11.4$ m/s. The general properties of the turbine can be found in table (5.1).

After defining the aero-elastic model, the numerical implementation is reported here. The real time simulations have been done through MATLAB software by using SIMULINK environment. Specifically a S-FUNCTION is created that contains the eight differential second order non-linear lumped parameters model. The differential set of equations can be summarized as follow:

The differential set of equations can be summarized as follow:

$$M\ddot{q} + C\dot{q} + Kq = f_{nl}^{in} + f_{aer} \tag{5.1}$$

in which $q = q_1, ...q_N$ are the aforementioned dofs, M,C and K are inertia, damping and stiffness matrices respectively, f_{nl}^{in} represents non-linear inertial vector and f_{aer} is the aerodynamic vector.

Table 5.1: Wind Turbine Parameters

$M_{nacelle}$	240000 $[Kg]$
M_{pylon}	347460 $[Kg]$
M_b	17740 $[Kg]$
x_{g_b}	20.475 $[m]$
k_p	2649654 $[Kg/sec^2]$
k_{β_i}	208392825 $[Kgm^2\ sec^2]$
J_{o_y}	11804647 $[Kgm^2]$
J_{o_y}	11804647 $[Kgm^2]$
J_{o_y}	28600 $[Kgm^2]$
f	1.5 $[m]$
g	9.81 $[m/sec^2]$
ρ	1.22 $[Kg/m^3]$
c	3 $[m]$
C_{d_0}	0.01
$Power\ rating$	5 $[MW]$
$Rotor\ orientation$	$Up-wind, 3\ blades$
$Control$	$Variable\ speed, variable\ \ pitch$
$Rotor, Hub\ diameter$	126 $[m]$, 3 $[m]$
$Blade\ length$	61.5 $[m]$
$Hub\ height$	90 $[m]$
$Cut-in, rated, cut-out\ \ wind\ speed$	3 $[m]$, 11.4 $[m]$, 25 $[m]$
$Cut-in, rated\ rotor\ speed$	6.9 $[rpm]$, 12.1 $[rpm]$
$Rated\ Tip\ Speed$	80 $[m/sec]$

5.1 Investigation on rotating blade loads and numerical results with the application of the Repetitive control strategy

In this section, the validation of the proposed model (open-loop results) is presented along with the assessment of the controller efficiency (closed loop simulations). The first analysis performed is the steady state solution (with no wind effects taken into account), considering a uniform wind $V_w = 11.4$ m/s and imposing collective pitch angle $\theta = -0.88°$. In the open-loop simulation the C_{res} and θ are the nominal values and they are near to that reported in FAST documentation (66) for the same turbine. Moreover, in this work, the C_{res} is modeled by knowing nominal condition

$$C_{res}(t) = \frac{C_{res_n}}{\Omega_n^2}\Omega^2(t) \tag{5.2}$$

where $C_{res}(t)$ is the torque in a condition different from the nominal one, $\Omega(t)$ is the angular value as the output of simulation, C_{res_n} and Ω_n are the nominal values.

In particular, Figure (5.1) shows the time-history of the angular velocity Ω and its equilibrium value (1.6 rad/s) over 200 s of simulation. Figure (5.2) shows the almost-

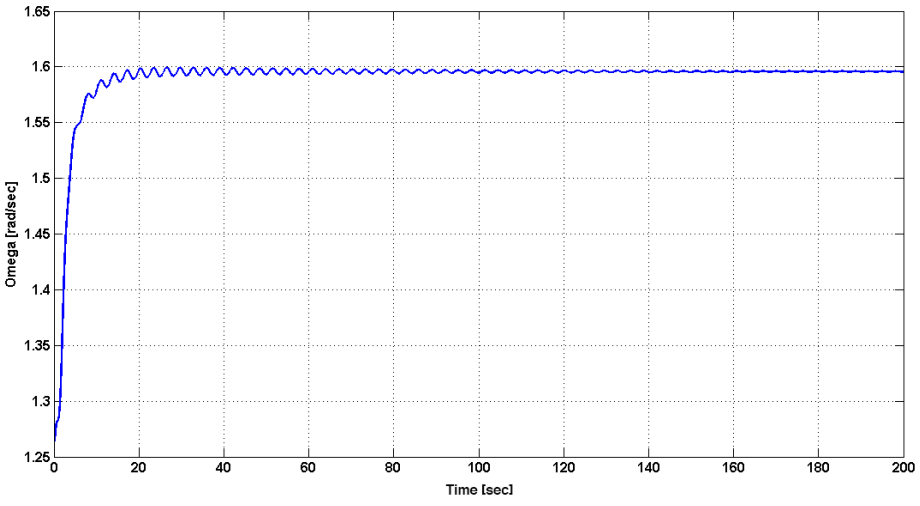

Figure 5.1: Open-Loop convergence of angular velocity.

periodic solution of the pitch angle, when the blade rotation is constrained with a rotational spring about $\theta = -0.88°$ (instead of being clamped). The periodicity of the system is clearly dominated by the Ω frequency and the phases between consecutive blades solutions are all equal to 1/3 of the period of revolution. Subsequently, the

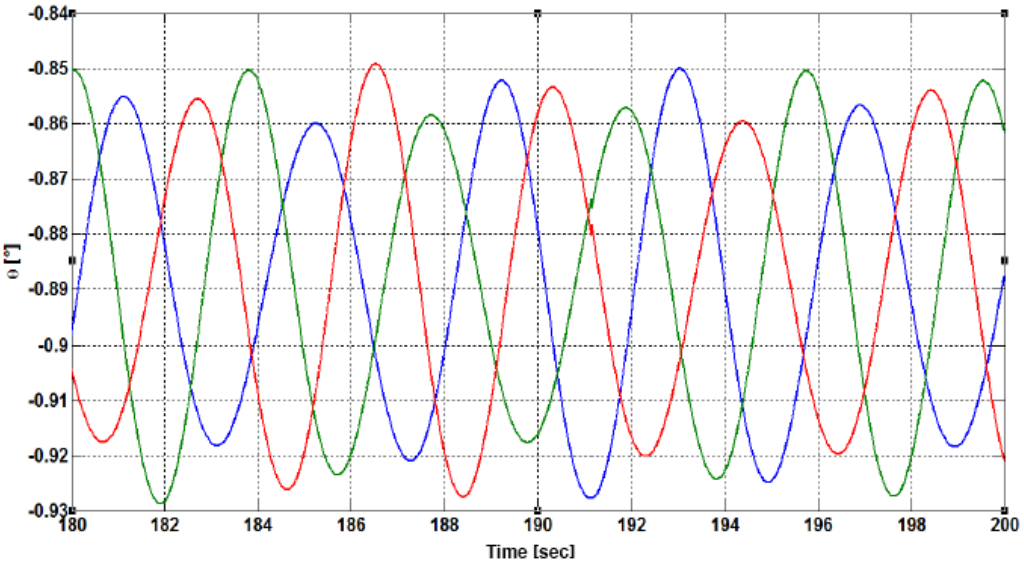

Figure 5.2: Open-Loop steady solution of pitch angle for the three blades.

effectiveness of the controller in a collective approach is assessed (it is means that all the blade controllers are activated at the same time).

Following equation (4.4) the input $u_j(k)$ is the collective torque forcing the pitch dynamics defined in equations (3.27). Moreover Q and is assumed to be an identity matrix as well as L but with a forward time shift operator equal to 70 samples. Furthermore, the proposed controller is coupled with a PD one and the gain values are reported in the first row of table (5.2). Starting from wind speed velocity $V_w = 11.4$ m/s the controller was asked to maintain the nominal angular velocity $\Omega_n = 1.266$ rad/s after an instantaneous increase of wind speed ($V_w = 15$ m/s). Figure (5.3) shows the results in terms of the angular velocity. Note that, after a 20 s-long transient, the angular velocity returns to its nominal value. Then, a purely periodic external distur-

Table 5.2: Controllers gains

Gains	P	I	D
Repetitive PD	-0.018	0	-0.01
Standard PID	-0.018	-0.00114	0

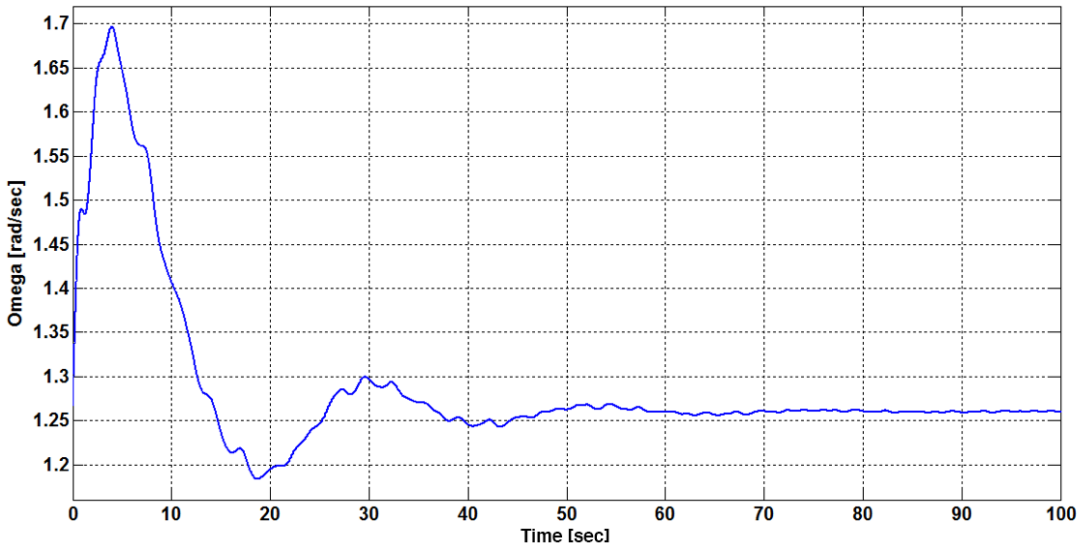

Figure 5.3: velocity when the PD-controller acts to reject Ω variation induced by an increase in wind speed.

bance (having period $\Psi = 2\pi$) on generator torque is introduced in order to stress the capabilities of the repetitive controller. The performance of the proposed controller is compared with that of a PI one alone (the gains of this controller are reported in the second row of table 5.2). Figures (5.4) and (5.5) show the outcome of the closed loop simulation, in terms of angular velocity and power output, respectively. In particular, the behavior of angular velocity without the control is depicted in blue, while the two control approaches are identified by green line (PI) and red line (repetitive-PD). It is evident that, while the mean values of both controlled cases match the requirement, only the repetitive controller is able to reject the periodic disturbance.

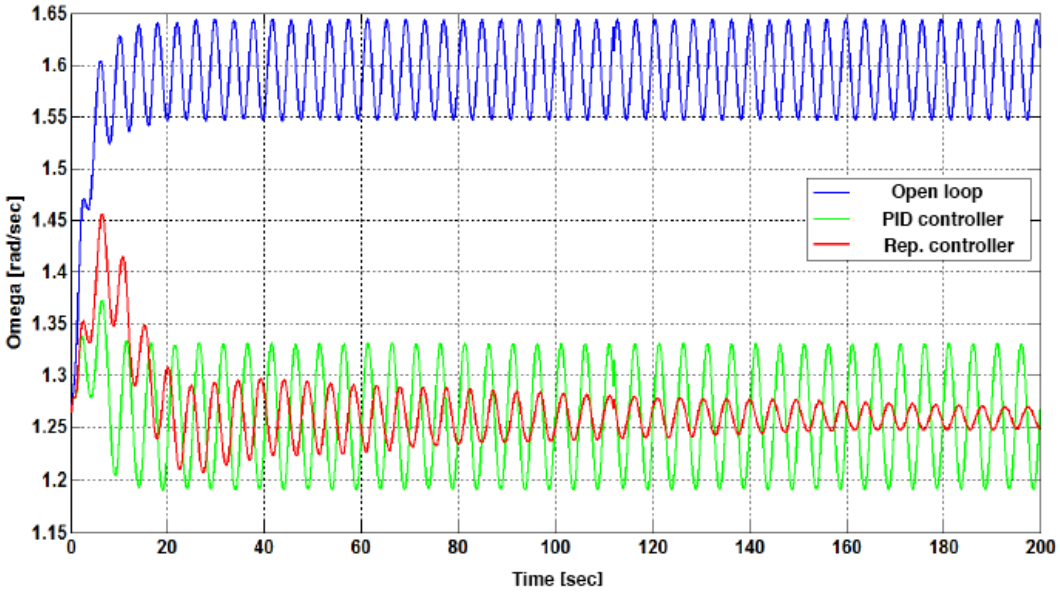

Figure 5.4: Angular velocity in presence of periodic torque disturbance.

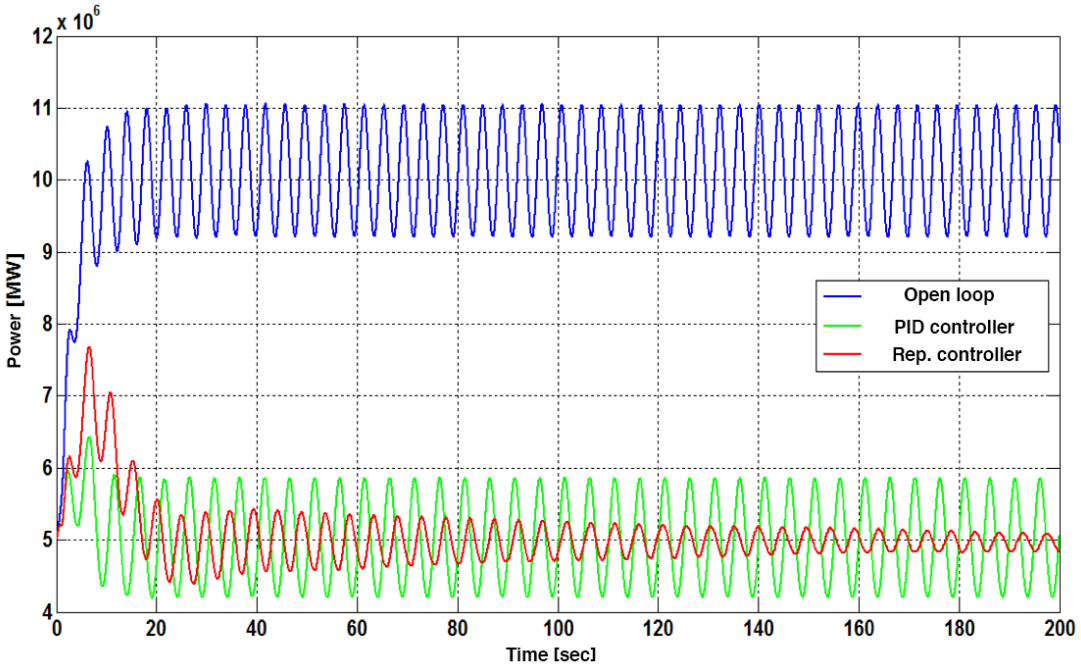

Figure 5.5: Power output in presence of torque disturbance.

To test the capability of the controller the non-uniform wind shear effect is considered (*e.g.*, due to terrain boundary layer), then periodic aero-elastic inputs and outputs arise. Broadly speaking, it is assumed that the wind speed is low at the Earth's surface and increases with the height. The wind shear is an important factor affecting both energy harvesting performance and aero-elastic response of the wind turbine. Optimal hub height, as well as turbine fatigue loading depend on it. Wind shear is influenced by the surface roughness of the Earth's surface and atmospheric stability.

Figure (5.6) shows the influence of α on the wind vertical variation, for $U(z_r) = 11.4$ m/s and $z_r = 90$ m. In this work, it has been assumed $\alpha = 0.17$, thus considering wind

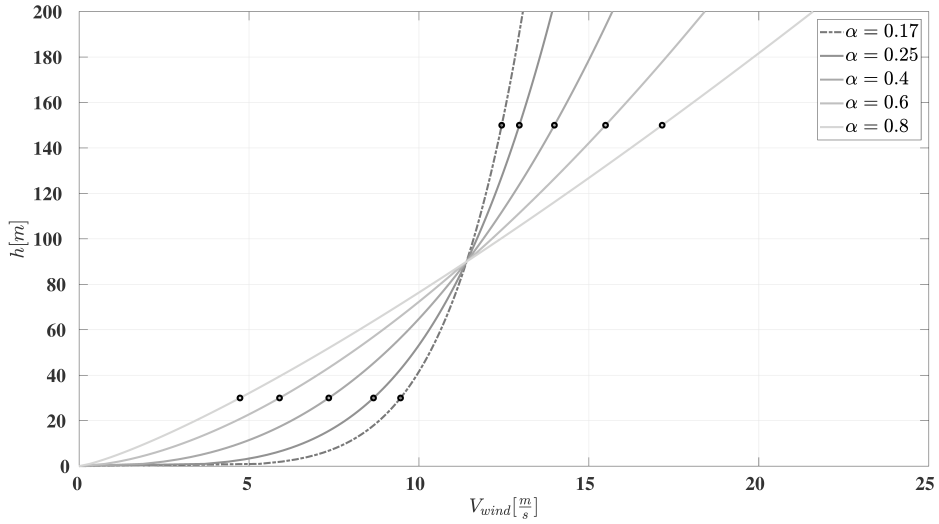

Figure 5.6: Different wind shear profiles.

speed variation from a minimum value of about 9 m/s to a maximum value of about 12 m/s. As already mentioned, such non-uniform wind distribution causes vibratory loads at the HAWT hub: in the following, individual pitch control based on repetitive control strategy is applied to alleviate such fatigue loads, while maintaining nominal rotational speed. First of all the open-loop configuration is analyzed, comparing the aero-elastic response with and without wind shear, starting from the same initial conditions.
Figure (5.7) shows that the wind shear causes a significant increase of flapping response

oscillations and associated hub loads (in the absence of wind shear, small-amplitude oscillations appear due to gravity effects). However, small oscillations appear also in the angular velocity response (not shown here) that, in principle, imply undesired oscillations of the output electric power. Next, the repetitive control is applied separately to

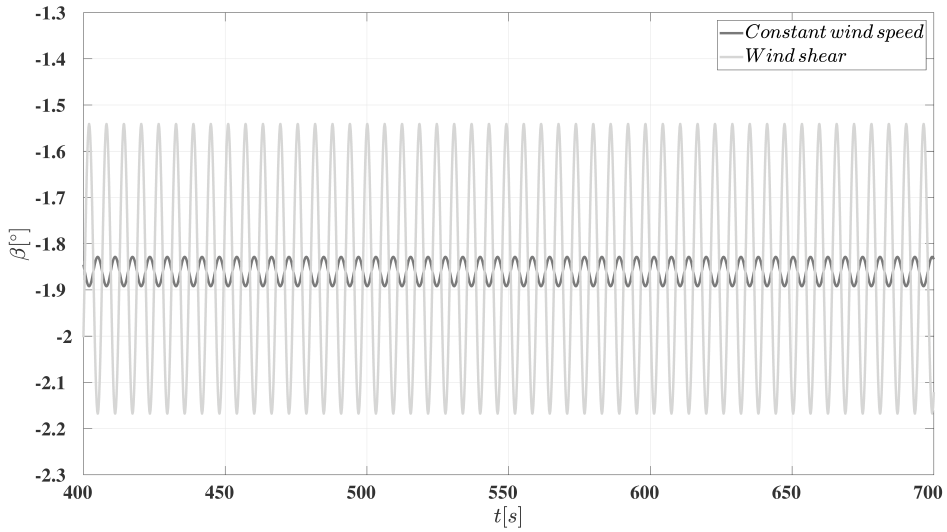

Figure 5.7: Increase of flapping oscillation amplitude due to wind shear.

both problems, namely angular velocity tracking and vibratory loads alleviation. First, the application of collective repetitive control, sketched in figure (5.8), to the nominal angular velocity tracking in presence of wind shear and hence periodic wind speed in the rotating frame is discussed.

Following equation (4.4) the input $u_j(k)$ is the collective torque forcing the pitch dynamics defined in equations (3.27). Moreover, Q is assumed to be an identity matrix and a heuristic approach is necessary for the determination of the L filter. In particular, considering L as a function of the gain parameter, G, and of the sample phase shift factor, δ, several tests are performed by varying δ for fixed G. The results show that, for the three values of G considered (namely, $G = 0.5, 1, 1.5$), the lowest tracking error is achieved for $\delta = 120$ samples, as shown in figures (5.9-5.11). Then, fixing this value, the gain parameter is changed. Figure (5.12) shows that the optimal control configuration

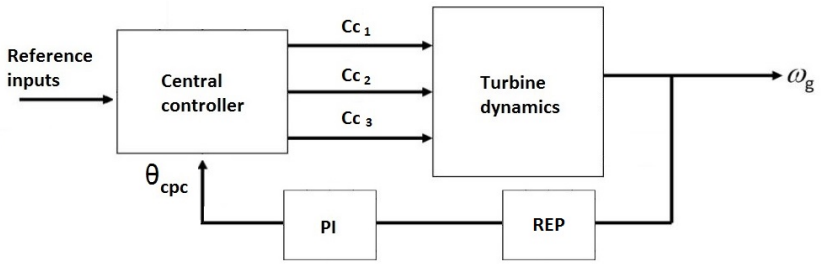

Figure 5.8: CPC angular velocity control scheme.

is achieved when $G = 1.5$.

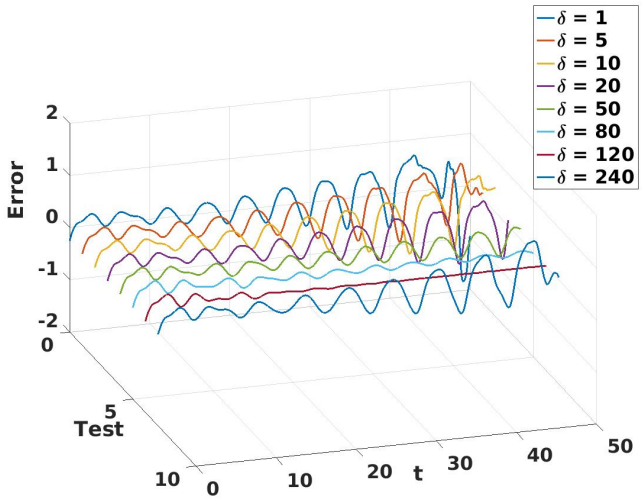

Figure 5.9: Tuning δ for G = 1.

To test the tuned control algorithm effectiveness, four different simulations with the collective pitch control approach, are performed with the inclusion of an external periodic disturbances on $U(z_r)$ with frequency equal to 1P, 2P, 3P,4P (the fundamental 1P coincides with the nominal value of the angular velocity). Figures (5.13-5.16) demonstrate that the periodic external disturbances affect the open-loop responses causing significant oscillations of the angular velocity. In addition, the comparison between the

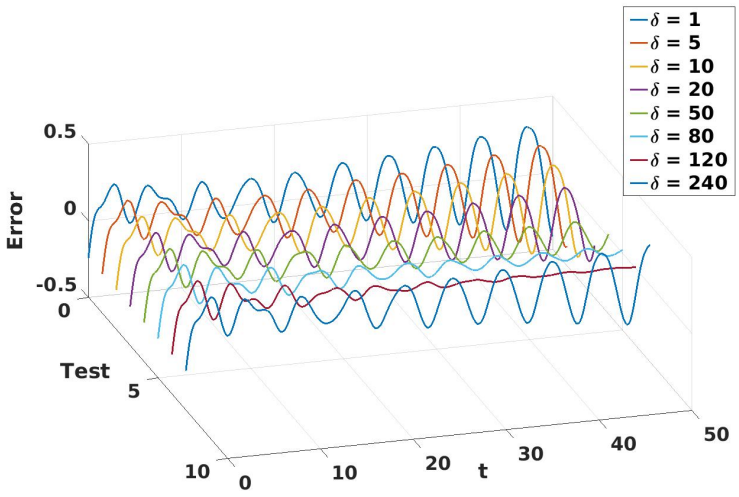

Figure 5.10: Tuning δ for G = 0.5.

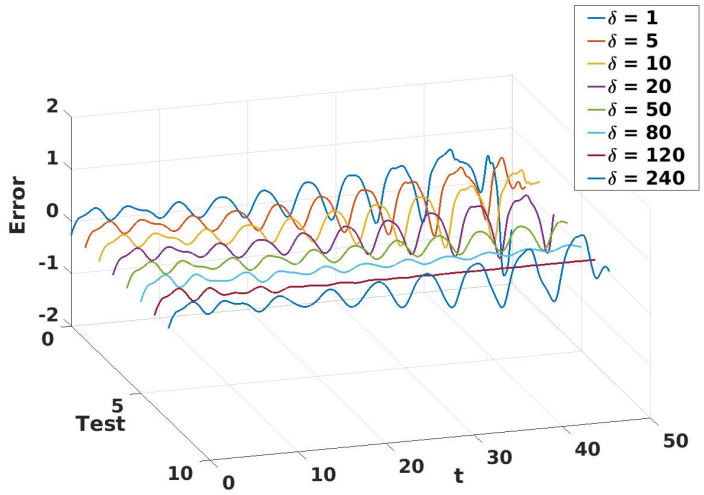

Figure 5.11: Tuning δ for G = 1.5.

results obtained by the proposed repetitive control approach and those from a classical PI approach reveal that the best tracking is obtained by the repetitive controller,

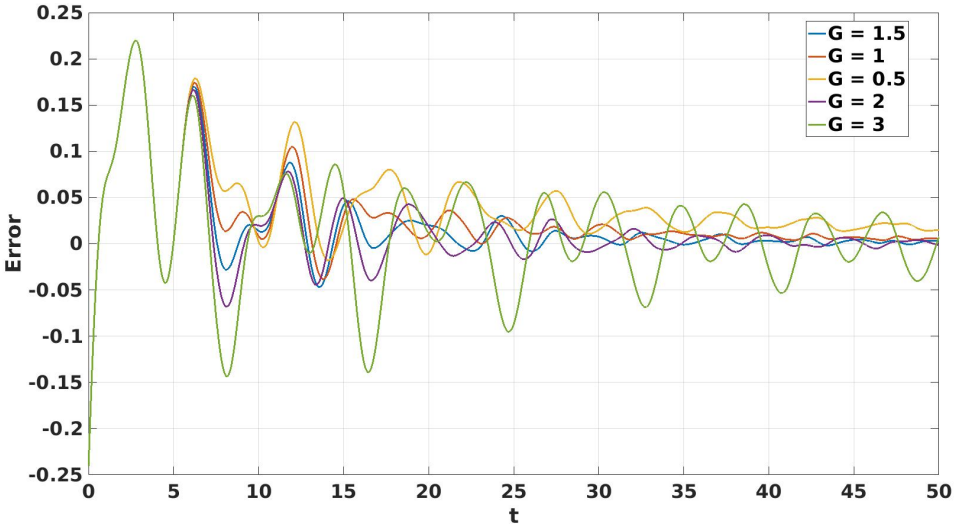

Figure 5.12: Tuning G for $\delta = 120$ samples.

which provides remarkable reduction of the angular velocity oscillations, with decreasing performance when increasing disturbance frequency.

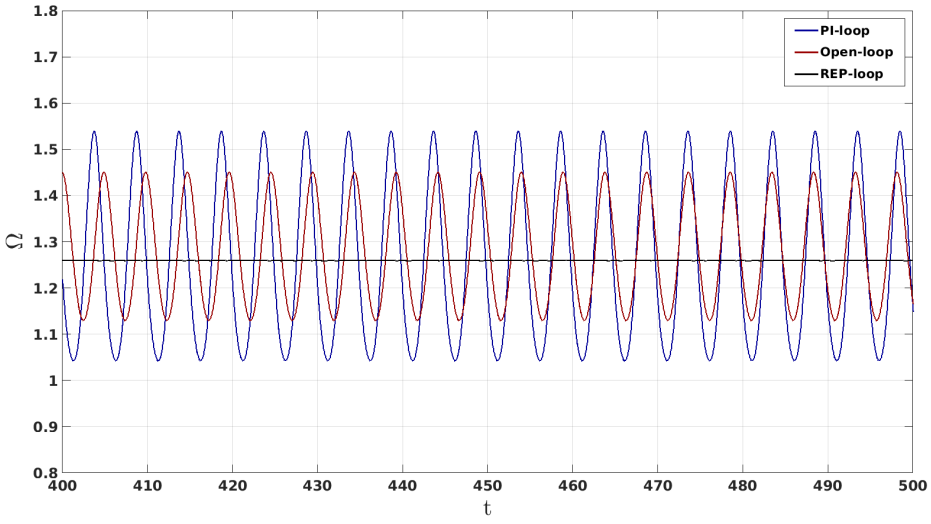

Figure 5.13: Effects of 1P external disturbance on open-loop and controlled responses.

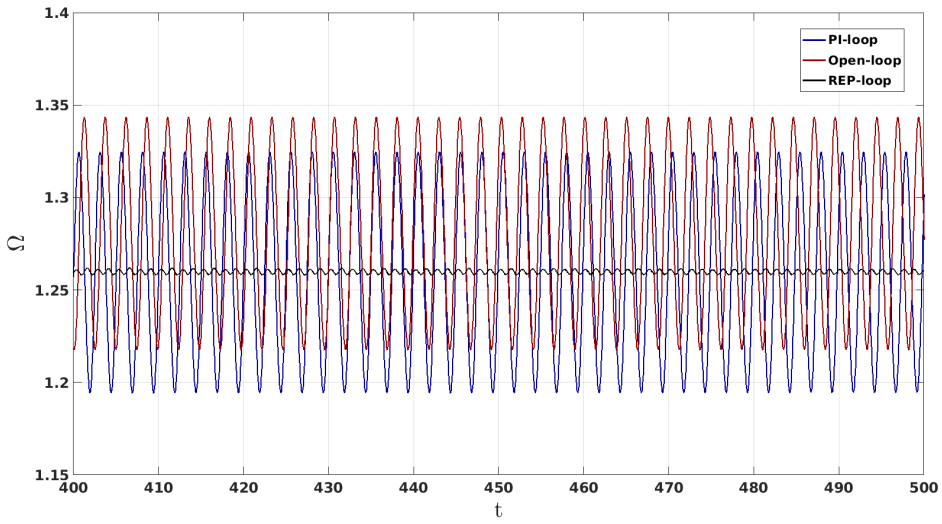

Figure 5.14: Effects of 2P external disturbance on open-loop and controlled responses.

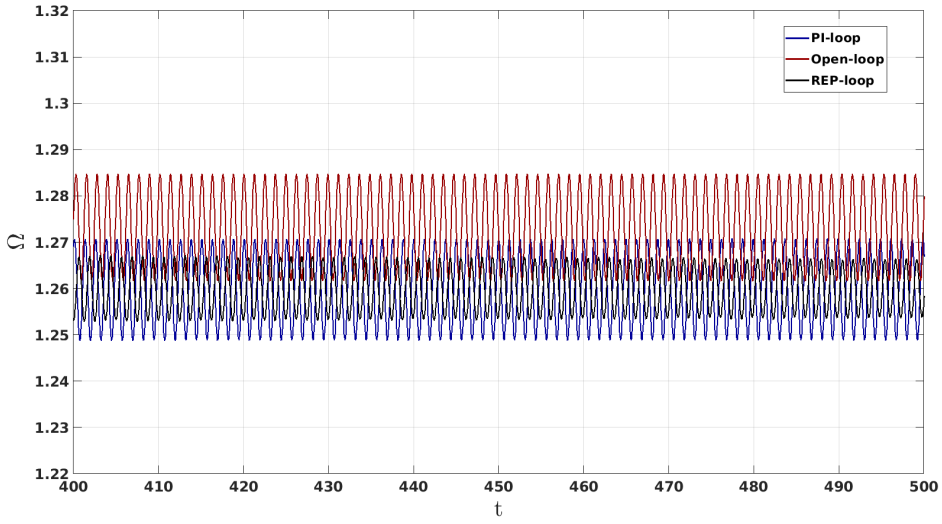

Figure 5.15: Effects of 3P external disturbance on open-loop and controlled responses.

Next, the Individual Pitch Repetitive Control (IPC), sketched in figure (5.17), is applied to the reduction of vibratory flap bending moment due to wind shear, figure

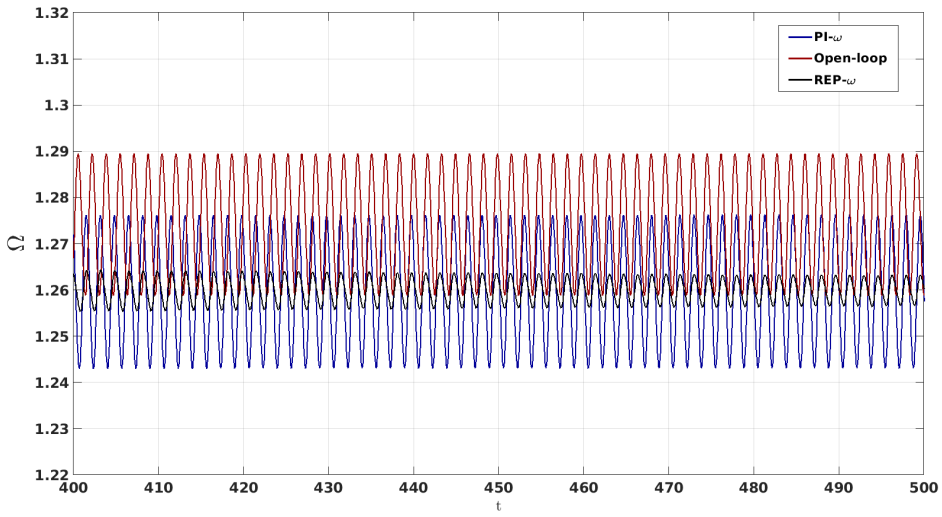

Figure 5.16: Effects of 4P external disturbance on open-loop and controlled responses.

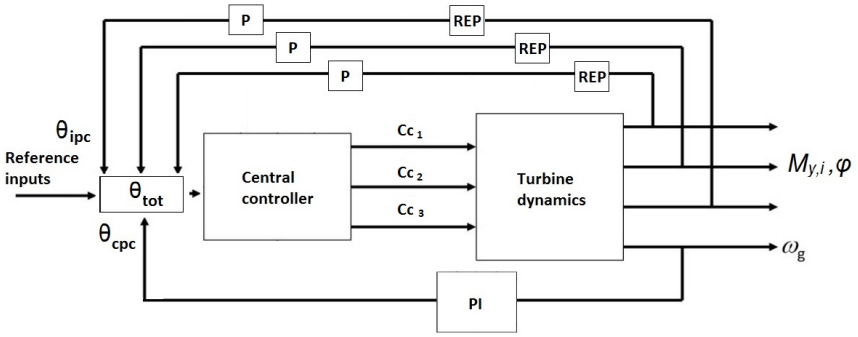

Figure 5.17: IPC flap motion control scheme.

(5.7) depicts the corresponding flap motion. Controlling this load, fatigue-life of blades and fixed structure components can be extended. A steady stable value for angular velocity is assured by application of a PI controller with proportional gain P=-0.018 and integral gain I = -0.0014. In figure (5.17) the angles θ_{ipc} are the portion of control input due to IPC, whereas θ_{cpc} represents the collective part. Final control signal θ_{tot} is the sum of IPC and CPC angles, so three different torques are obtained through a

central control which sums the two contributions (note that, in the IPC feedback loop, the gain P = -0.0005 is also present). Also in this case, a tuning procedure similar to that described for CPC repetitive is carried out for setting the repetitive parameters, see equation (4.4). As a result, the value $G = 1$ and the shift factor $\delta = 280°$ are identified. The error $e_j(k + 1)$ is considered equal to the difference with respect to the mean nominal flapping moment value obtained from a previous analysis. The performance of the proposed repetitive controller is shown in figures (5.18 - 5.21) where its outcomes are compared with those determined by application of both an angular velocity PI collective controller (PI_ω) and an individual PI flap bending moment controller (PI_ω-$PI_{M_{flap}}$). With application of the PI_ω controller , a steady state value of angular velocity is reached, see figure (5.20), whereas flap bending moment and flap degree of freedom present undesired periodic behaviors, blue curves in figures (5.18-5.19). The application of the PI_ω-$PI_{M_{flap}}$ controller not only provides reduced flapping moment and motion oscillations, of about -22% as indicated by the red curves in figures (5.18-5.19), but also it assures the achievement of the nominal angular velocity as it is reported in figure (5.20).

Instead, with the application of the repetitive IPC, the flapping moment and motion oscillations are strongly reduced, of about -94%, as indicated by the black curves in figures (5.18-5.19). Also in this case the rotor nominal angular speed is achieved, figure (5.20), demonstrating that no adverse interaction between PI_ω controller and IPC Repetitive controller arises. Furthermore, figure (5.21), depicts the FFT of the flap bending moment. Three peaks corresponding to the main harmonic components are shown. It is possible to observe that the 1P, 2P, 3P harmonic components (corresponding to 0.2 Hz, 0.4 Hz and 0.6 Hz) are reduced: 92% of reduction is achieved for the 1P component, while 63% of reduction is obtained for the 2P one.

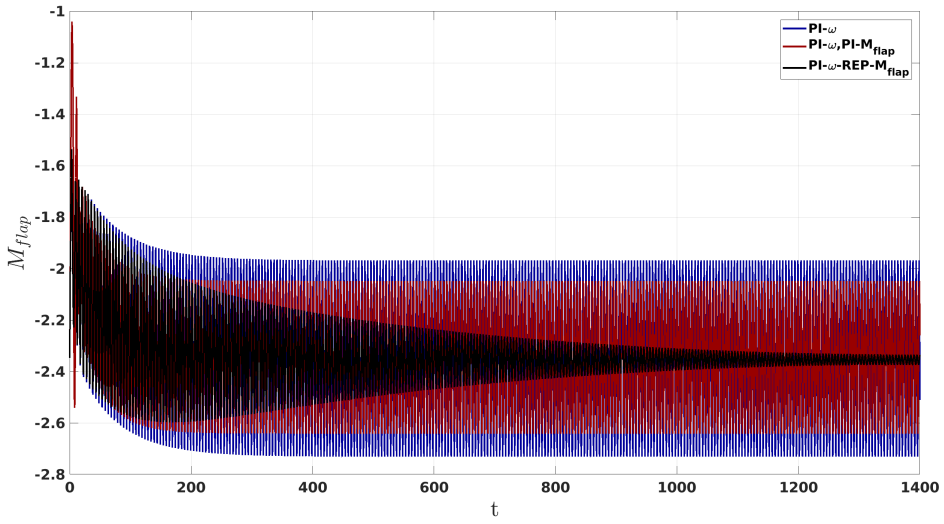

Figure 5.18: Bending moment for open-loop and controlled HAWT.

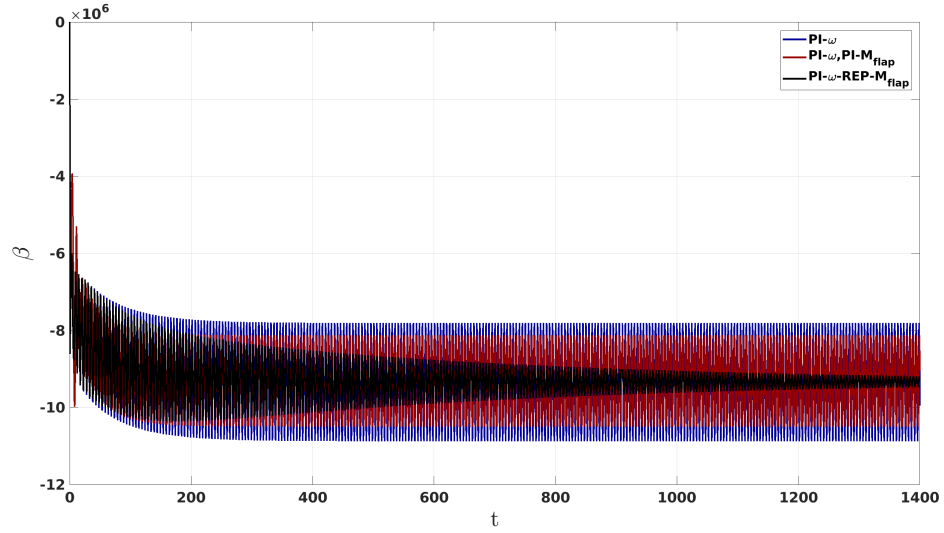

Figure 5.19: Flap angle for open-loop and controlled HAWT.

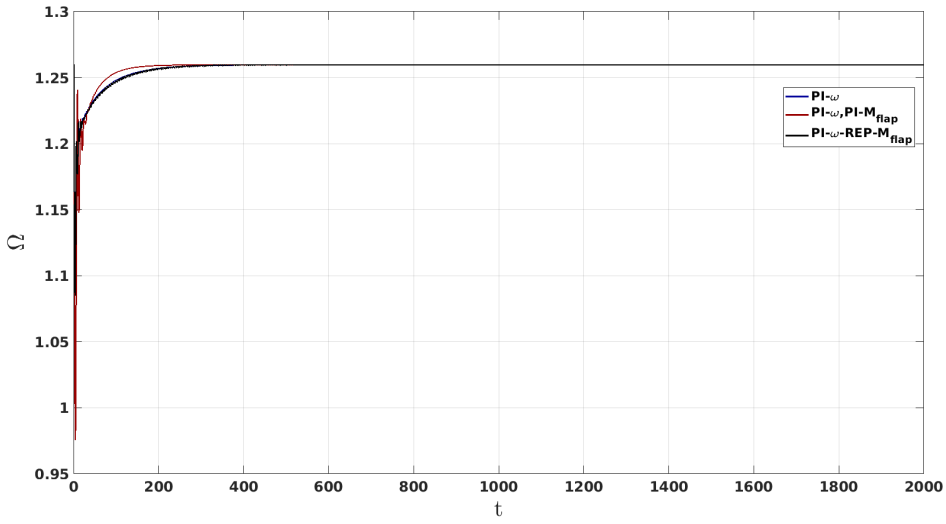

Figure 5.20: Angular velocity for open-loop and controlled HAWT.

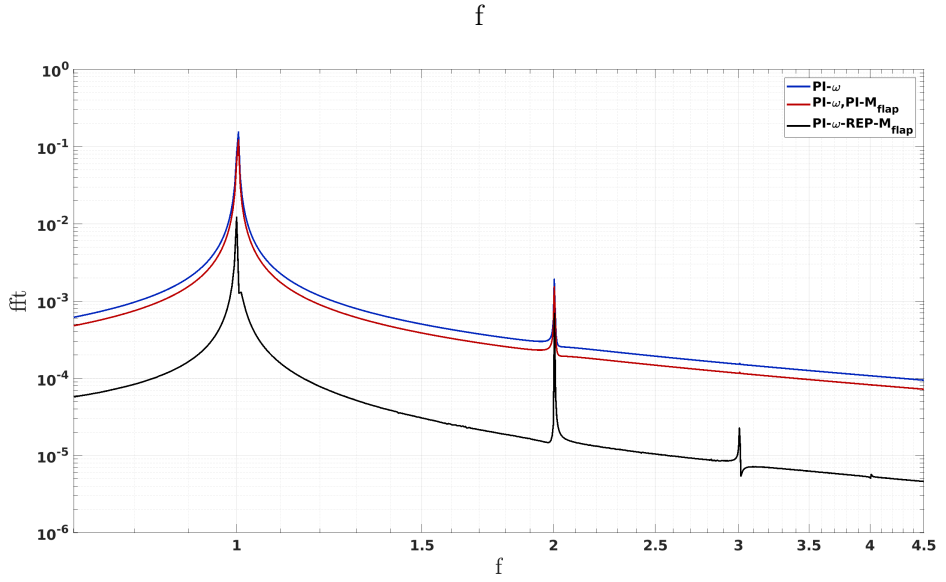

Figure 5.21: FFT of bending moment for open-loop and controlled HAWT.

5.2 Investigation on rotating and fixed blade loads and numerical results with the application of the Individual Pitch Control strategy

In this section objective and strategies for the wind turbines control are outlined in presence of both tower shadow and wind shear effects. In particular, the multi-harmonics control strategy is introduced. When the tower shadow effect is taken into account, each blade section experiences a different relative wind, that changes both local attack angle and dynamic pressure. Moving from the bottom to the top of the rotor disc, several changes in the aerodynamic loads can be observed: periodic flapping motion and increasing oscillations are experienced, with respect to the constant wind case, as shown in figure (5.22). In this section, a NP parallel individual pitch controllers for loads

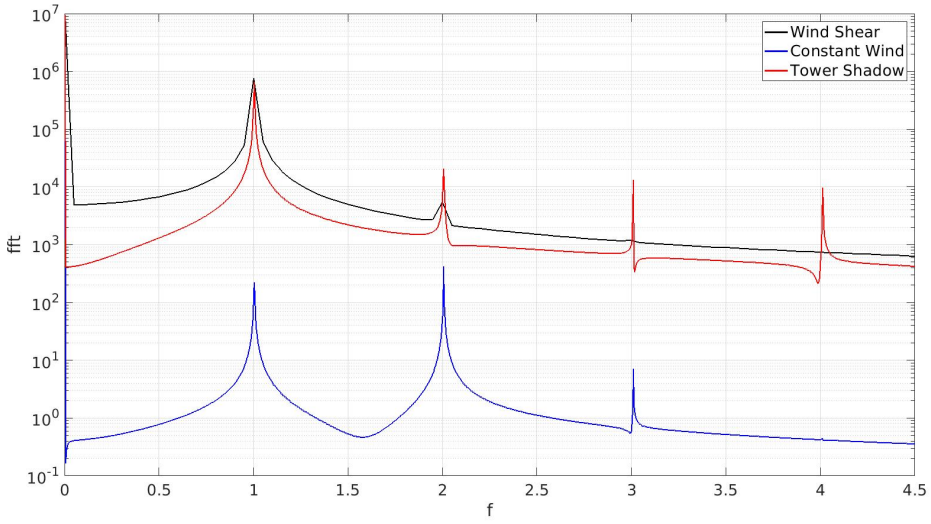

Figure 5.22: Tower Shadow's Fast Fourier Transformation on the flapping moment.

reduction is described. The goal of this IPC is to reduce the out-of-plane bending vibratory loads at the root of each blade ($M_{y,1}$,$M_{y,2}$,$M_{y,3}$), by adjusting the blade pitches (θ_1,θ_2,θ_3). The control strategy, sketched in figure (5.23), consists of the following steps:

i) Blade roots flapping moments, ($M_{y,i}$), are evaluated; ii) The Coleman's transformation up to the NP terms is applied to them, obtaining multi-harmonic loads vector

$\boldsymbol{M_c}$ as follow:

$$\boldsymbol{M_c} = \begin{Bmatrix} M_{avg} \\ M_{1P,tilt} \\ M_{1P,yaw} \\ \vdots \\ M_{NP,tilt} \\ M_{NP,yaw} \end{Bmatrix} = \frac{2}{3} \begin{bmatrix} \frac{1}{2} & \frac{1}{2} & \frac{1}{2} \\ \cos(\psi) & \cos(\psi + \frac{2\pi}{3}) & \cos(\psi + \frac{4\pi}{3}) \\ \sin(\psi) & \sin(\psi + \frac{2\pi}{3}) & \sin(\psi + \frac{4\pi}{3}) \\ \cos 2(\psi) & \cos 2(\psi + \frac{2\pi}{3}) & \cos 2(\psi + \frac{4\pi}{3}) \\ \sin 2(\psi) & \sin 2(\psi + \frac{2\pi}{3}) & \sin 2(\psi + \frac{4\pi}{3}) \\ \vdots & \vdots & \vdots \\ \cos N(\psi) & \cos N(\psi + \frac{2\pi}{3}) & \cos N(\psi + \frac{4\pi}{3}) \\ \sin N(\psi) & \sin N(\psi + \frac{2\pi}{3}) & \sin N(\psi + \frac{4\pi}{3}) \end{bmatrix} \begin{Bmatrix} M_{y,1} \\ M_{y,2} \\ M_{y,3} \end{Bmatrix} \quad (5.3)$$

In figure (5.23) the angles θ_{ipc} represent the portion of control input due to the IPC, whereas θ_{cpc} refers to the collective part. The final control signal is $\theta_{tot} = \theta_{ipc} + \theta_{cpc}$: three different torques are obtained through the combination of two contributions. Regarding the Coleman transformation method, low-pass second order butterworth filters that filters out the frequencies greater than 3P are designed. These ensure the independence of the control actions on the specific harmonic. Notice that, in the non-rotating reference frame, the considered signals depend on the Coleman transformation made.

A generic representation is reported below: The first term M_{avg} represents the average bending moment of the blade, M_{tilt},M_{yaw} are the tilt and yaw moments in the fixed reference frame. Regarding the transfer of loads:

- When the $1P$ Coleman transformation is applied, the $1P$ harmonic of the blade root moment signal, transposes into the $0P$ harmonic component in the fixed reference system.
- Higher harmonics will result in $(M * N_b - 1) - p$ and $(M * N_b + 1) - p$ components in the non-rotating reference system[1].

[1] N_b represents the number of blades and $M = (1, 2, ...)$

For instance 2P and 4P components in the rotating reference system result in 3P in the fixed frame. Summarizing, the control goal consists in using several IPC parallel loops targeting different harmonics through different Coleman transformations.

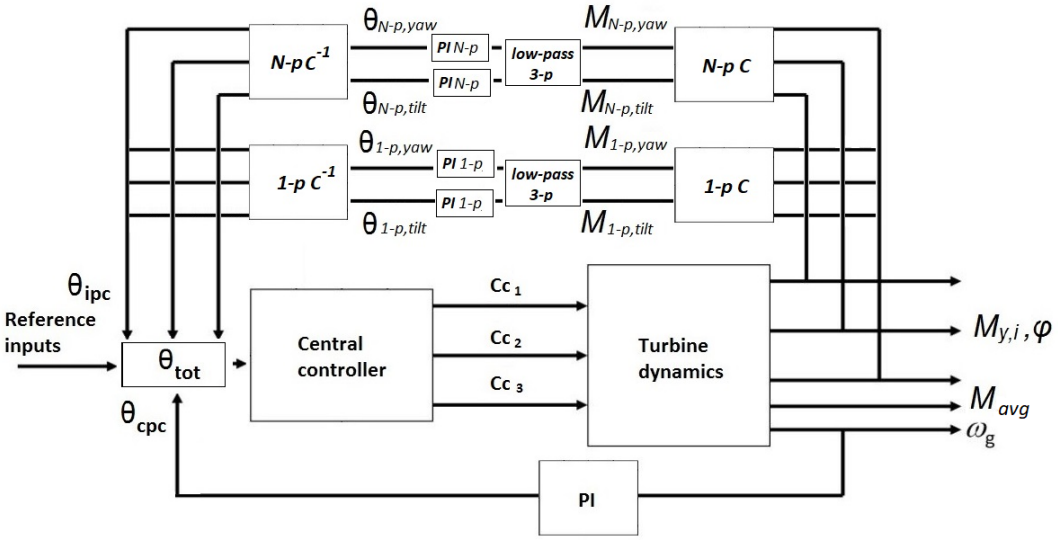

Figure 5.23: Multi-harmonic control scheme.

To validate the proposed approach several batch simulations are performed:

- Collective Pitch and IPC-1P;
- Collective Pitch and IPC-2P;
- Collective Pitch and IPC-3P;
- Collective Pitch and IPC-4P;
- Collective Pitch and IPC-(1,2,3,4)P.

Figures (5.24, 5.25) show the rotor power spectra when individual pitch control on 1P and 2P is applied in the fixed FOR (are reported the tilt and yaw components).

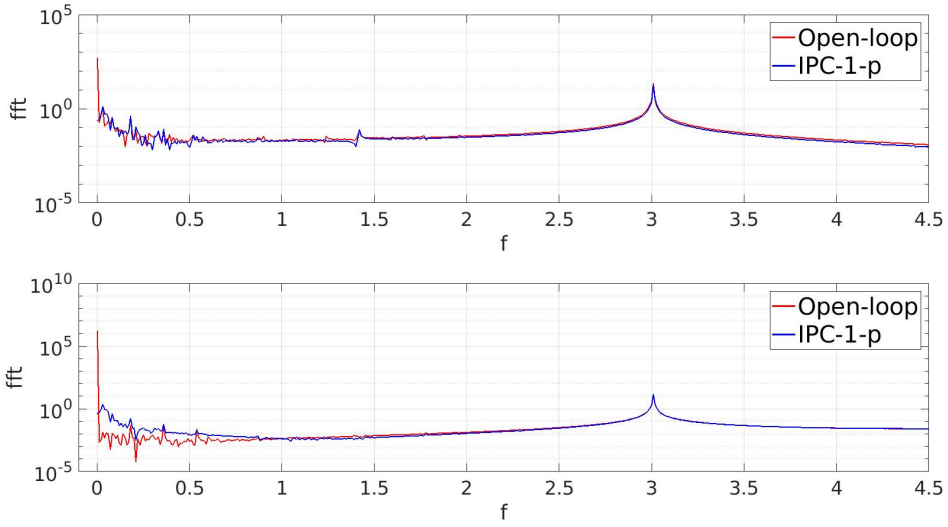

Figure 5.24: Effect on 1P flap tilt and yaw motions (blue lines) by Individual Pitch Control compared to the Open-loop case (red lines).

Two harmonic behaviors are reported: the red curve shows the Fast Fourier Transformation related to blade root flap moment in the open-loop configuration (harmonics from the first to the fourth are depicted), whereas the blue trend represents the individual 1P Coleman action. A complete reduction of the blade load at 1P, starting from a magnitude value of about 10^6, is obtained. Moreover, complete independence of the control action with respect to the harmonics, is achieved.

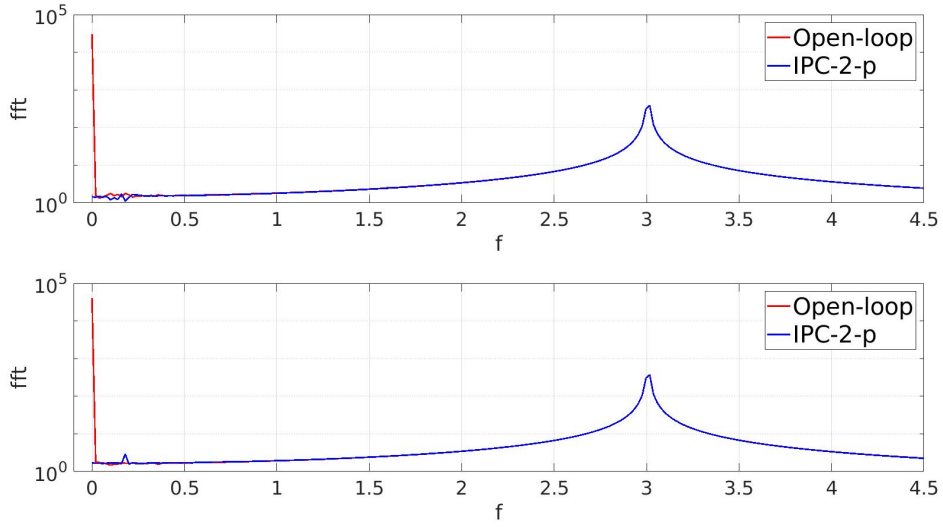

Figure 5.25: Effect on 2P flap tilt and yaw motions by Individual Pitch Control.

Furthermore figures (5.24, 5.24) show the effect of the PI control respect to tilt and yaw moments, where a $P_{tilt} = 0.001$, $I_{tilt} = 0.000014$, $P_{yaw} = 0.0002$, $I_{yaw} = 0.000014$ values are chosen as control gains. It should be noticed that, the 0P value decreases in both

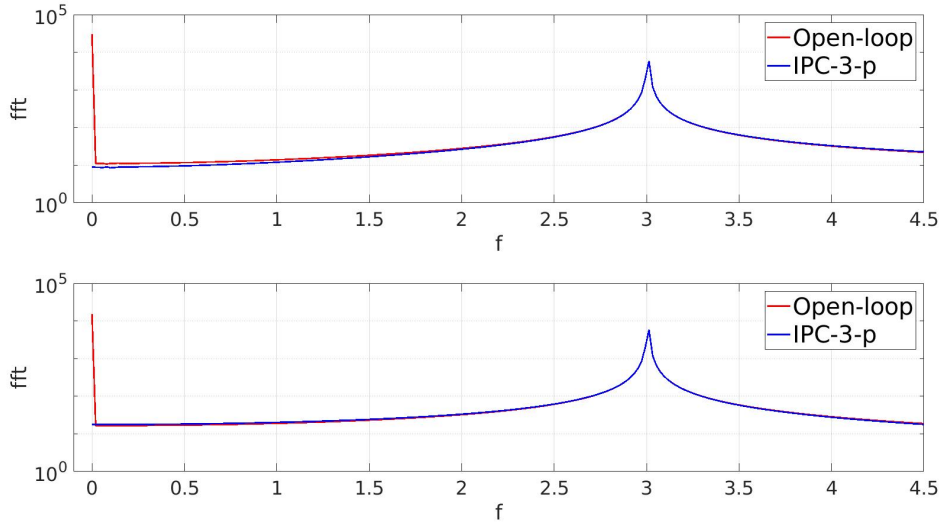

Figure 5.26: Effect on 3P flap tilt and yaw motions by Individual Pitch Control.

cases, strengthening the results related to flap motion 1P control. The same procedure

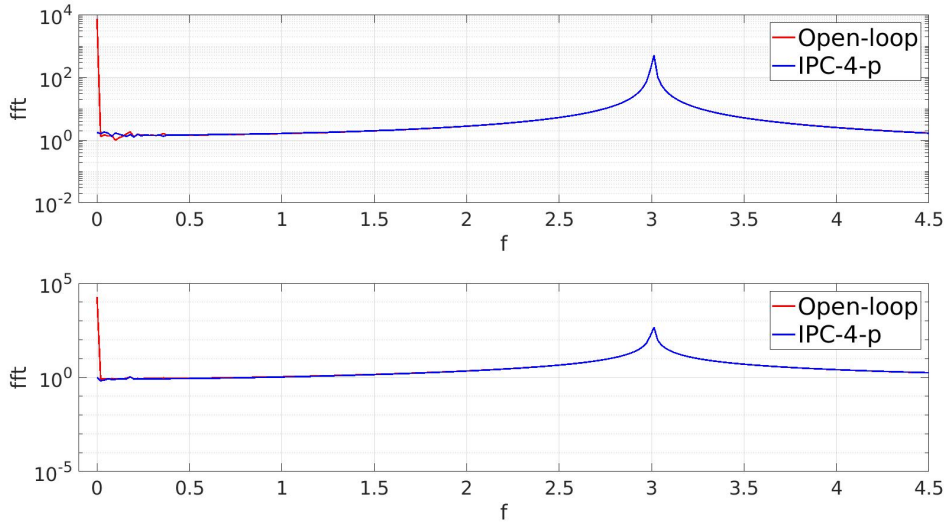

Figure 5.27: Effect on 4P flap tilt and yaw motions by Individual Pitch Control.

is applied to the 2P, 3P and 4P Coleman transformations. Figures (5.24-5.27) show the reduction of blade harmonic loads around 2P, 3P and 4P frequencies corresponding to the 0P reductions in the fixed reference system. These results is obtained with the following values of PI control gains:

- P_{tilt} = -0.01, I_{tilt} = -0.00014 (2P and 3P Coleman);
- P_{yaw} = -0.02, I_{yaw} = -0.00014 (2P and 3P Coleman);
- P_{tilt} = -0.01, I_{tilt} = -0.0008 (4P Coleman);
- P_{yaw} = -0.02, I_{yaw} = -0.00014 (4P Coleman).

Figure (5.32) shows the effect of parallel PI controls from the first to the fourth harmonics.The figure contains the FFT of the blade harmonic loads in the rotating FOR for both Open-loop (red line) and control (blue line) conditions.

The results show that as the Individual Pitch Control is applied on 1P, 2P and 4P frequencies in the fixed FOR, then the corresponding frequencies are eliminated in the rotating one. However the 3P frequency peak can not be completely damped (5.30) even if the corresponding 0P frequency is controlled in the fixed FOR (5.26). The reason is, see figure (5.23) and equation (2.8), because in this work there is not a control loop for

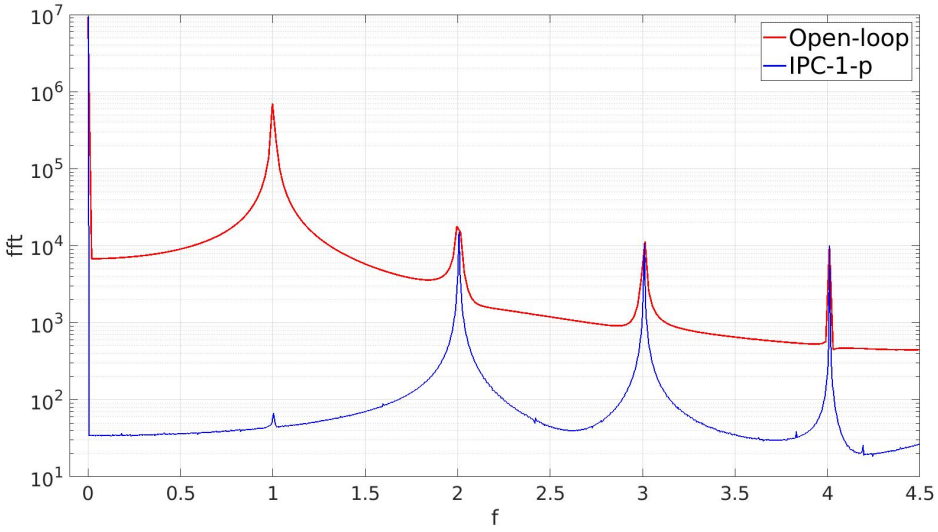

Figure 5.28: Effect on 1P harmonic of flap motion by Individual Pitch Control.

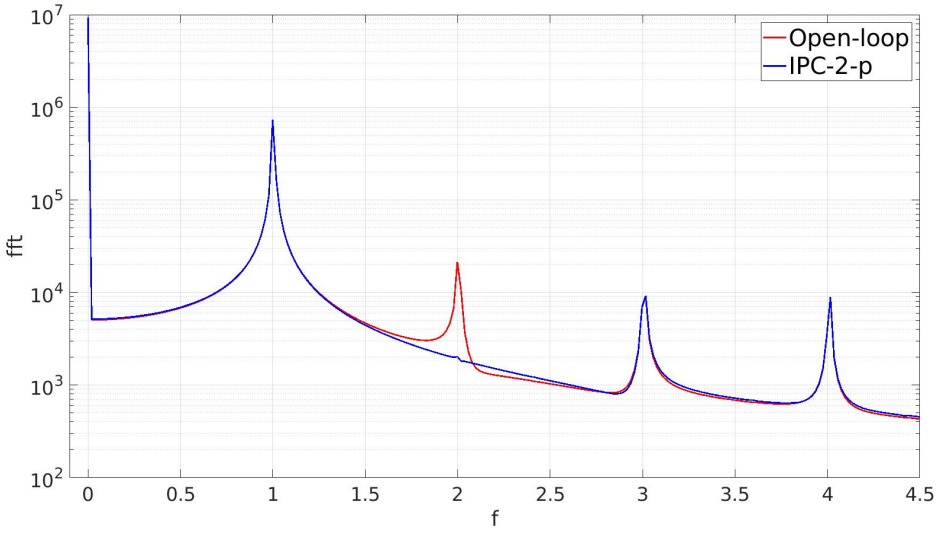

Figure 5.29: Effect on 2P harmonic of flap motion by Individual Pitch Control.

the average moment M_{avg} that is also affect to a portion of the 3P frequency. Moreover controlling M_{avg} with the proposed approach is not achievable due to the presence of higher harmonics that are multiple of the number of the blades (3P,6P...). It could applied a filter on the M_{avg} signal in the fixed reference system that filter out the frequencies greater than the 3P and it could used the proposed control to eliminated

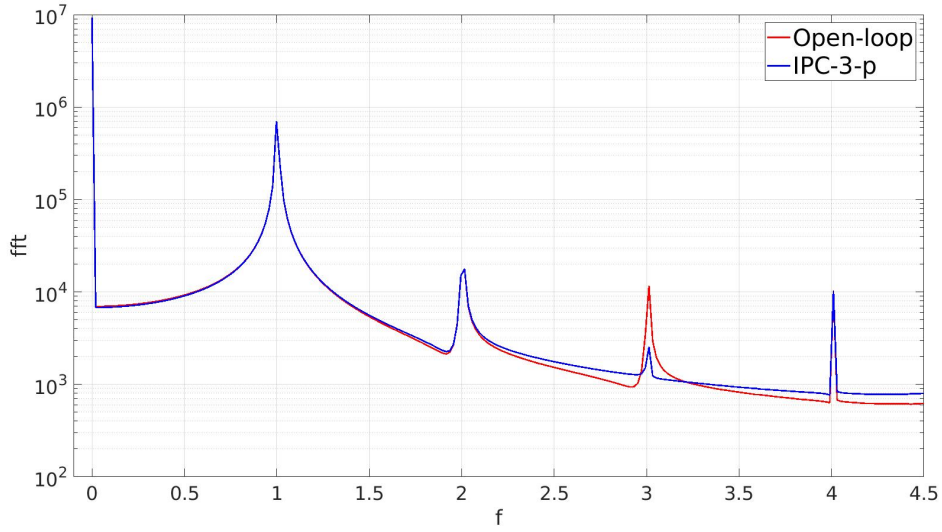

Figure 5.30: Effect on 3P harmonic of flap motion by Individual Pitch Control.

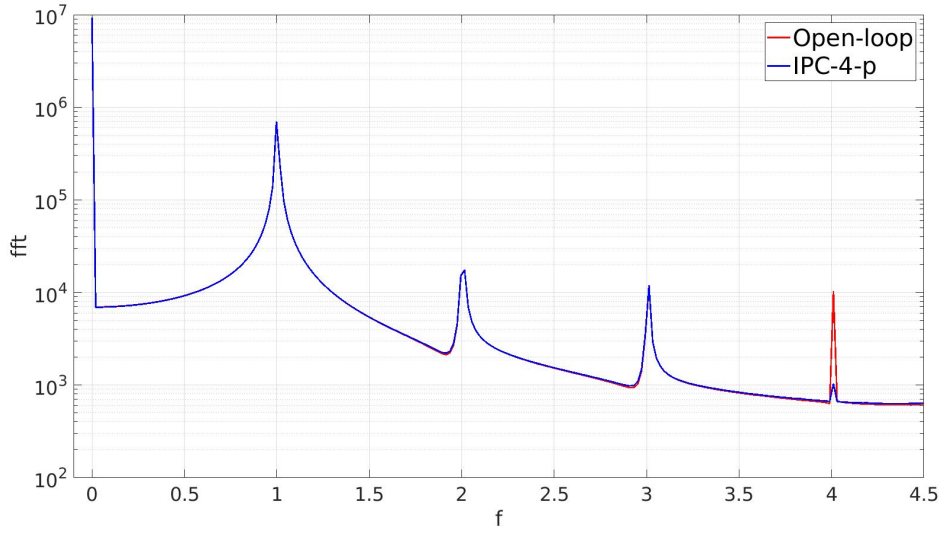

Figure 5.31: Effect on 4P harmonic of flap motion by Individual Pitch Control.

this component, but would remain anyway higher component that are not reported in figure (5.32).

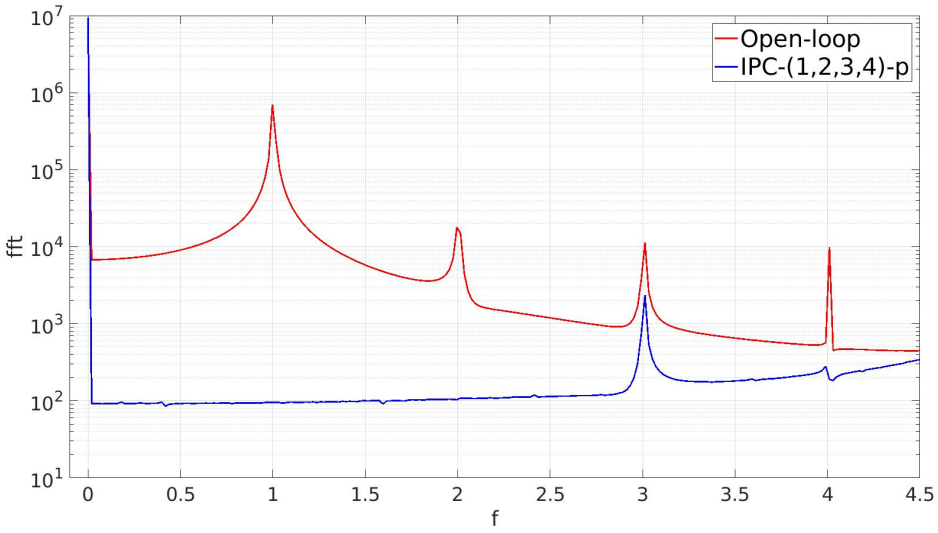

Figure 5.32: Effect on 1P, 2P, 3P and 4P harmonics of flap motion by Individual Pitch Control.

Chapter 6

Conclusions

In this work, a nonlinear differential aero-elastic model for three-bladed horizontal axis wind turbine is developed and applied for control purposes. The novelties of this work are both in the modelling and control.

With regard to the aero-elastic system, non-linearity that are neglected in other models are taken into account in structural and aerodynamic aspects, although the ordering schemes that simplify the equations are applied. Concerning the control approach, instead the classical tuning of general servo-controllers, such as PID or state feedback controllers, the repetitive control strategy is considered to handle with tracking reference command and/or rejecting periodic disturbances with a fixed period. Indeed, since its introduction to the control community, this technique has distinguished itself by its high precision, simple implementation and little performance dependency on system parameters.

The model is obtained through the Euler Lagrange formulation, whereas the aerodynamic loads are obtained using a quasi-steady strip theory. The model includes a detail representation of tower shadow and wind shear modules which are often approximated or neglected in existing models. Both, wind shear and tower shadow, cause considerable fluctuations in the aerodynamic loads of wind turbine parts such that periodic components result in turbine angular velocity, flap bending moment and flap displacement. Therefore, strategies for mitigating these fluctuations are developed in both non-rotating and rotating reference systems. A Repetitive control theory is introduced

and a "spatial" repetitive-PD controller, acting on collective pitch algorithm, is also proposed for the rejection of a periodic disturbance and of the periodicity characteristic of wind turbines. The results show that, contrary to a simple PI controller, the spatial repetitive-PD controller has the capability to reject both kind of disturbances. In addition, a repetitive individual pitch controller has been applied for vibratory flapping moment induced by wind shear, combined with a PI collective control for angular velocity. For both problems, the proposed repetitive controller has demonstrated to be very successful, remarkably more effective than classical PI controller: it is capable of rejecting the periodic perturbations introduced, while tracking the nominal angular velocity. All the harmonic components of the flapping moment have been reduced by the application of the repetitive individual pitch controller. Furthermore, tower shadow effect is considered, such that harmonic components related to the flapping bending moment increase with respect to constant wind case and wind shear one. A simple PI control design has been derived using a multi-blade transformation (Coleman transformation) for the individual pitch control combined with a PI collective control for angular velocity. The proposed design control is applied to a harmonic content till to the 4P. For all cases considered, the proposed multi-harmonic individual control has demonstrated to be very successful, reducing all the harmonic components of the flapping moment. However, by applying the 3P Coleman transformation a complete 3P frequency cancellation is not reached even if the 0P component of tilt and yaw moments is controlled.

Future works should include the improvement of aero-elastic model with: i) the inclusion of the dynamic stall; ii) the modeling of lag motion of the blades, which plays a crucial role in aero-elastic stability; iii) the capability to model rotors with unbalanced blades (e.g. due to mechanical or structural problems during life cycle). Furthermore, a crucial effect that should be taken into account for on-shore wind turbine is the Soil-Structure Interaction (SSI) that is affected by different parameters including turbine size, foundation type (spread foundation, mono pile, pile group with cap and anchored spread foundation), and soil properties. From a practical point of view, the proposed controller needs the use of sensors for both load monitoring on the blades and inflow measurements. Structural sensors can be highly accurate but only respond to loads after they occur. Inflow sensor detects changes sooner, but is sensitive to errors in

the models that relate aerodynamic variables to loads. The wind turbine environment produces challenging operating conditions for load sensors. Access and maintenance are difficult and the sensors may be exposed to precipitation, ice, dirt, insects and lightning. Therefore, the development of robust sensor technologies for wind turbines is needed in order to improve their performances.

Bibliography

[1] D. Hodges and R. ORMISTON, "Stability of elastic bending and torsion of uniform cantilevered rotor blades in hover," in *14th Structures, Structural Dynamics, and Materials Conference*, p. 405, 1973.

[2] S. Feinberg, "Wind turbine prices fall to their lowest in recent years," *Bloomberg New Energy Finance Press Release*, vol. 7, p. 2011, 2011.

[3] K. Smith, G. Randall, D. Malcolm, N. Kelley, and B. Smith, "Evaluation of wind shear patterns at midwest wind energy facilities," in *American Wind Energy Association (AWEA) WINDPOWER 2002 Conference*, Citeseer, 2002.

[4] S. Rehman and N. M. Al-Abbadi, "Wind shear coefficients and their effect on energy production," *Energy Conversion and Management*, vol. 46, no. 15-16, pp. 2578–2591, 2005.

[5] S. Rehman and N. M. Al-Abbadi, "Wind shear coefficient, turbulence intensity and wind power potential assessment for dhulom, saudi arabia," *Renewable Energy*, vol. 33, no. 12, pp. 2653–2660, 2008.

[6] X. Shen, X. Zhu, and Z. Du, "Wind turbine aerodynamics and loads control in wind shear flow," *Energy*, vol. 36, no. 3, pp. 1424–1434, 2011.

[7] Z. Yang, Y. Li, and J. E. Seem, "Individual pitch control for wind turbine load reduction including wake interaction," in *American Control Conference (ACC), 2011*, pp. 5207–5212, IEEE, 2011.

[8] J. F. Manwell, J. G. McGowan, and A. L. Rogers, *Wind energy explained: theory, design and application*. John Wiley & Sons, 2010.

[9] F. D. Bianchi, H. De Battista, and R. J. Mantz, *Wind turbine control systems: principles, modelling and gain scheduling design*. Springer Science & Business Media, 2006.

[10] D. A. Spera, "Wind turbine technology," 1994.

[11] J. H. Laks, L. Y. Pao, and A. D. Wright, "Control of wind turbines: Past, present, and future," in *American Control Conference, 2009. ACC'09.*, pp. 2096–2103, IEEE, 2009.

[12] J. V. Ringwood and S. Simani, "Overview of modelling and control strategies for wind turbines and wave energy devices: Comparisons and contrasts," *Annual Reviews in Control*, vol. 40, pp. 27–49, 2015.

[13] E. Bossanyi, "Individual blade pitch control for load reduction," *Wind energy*, vol. 6, no. 2, pp. 119–128, 2003.

[14] T. J. Larsen, H. A. Madsen, and K. Thomsen, "Active load reduction using individual pitch, based on local blade flow measurements," *Wind Energy*, vol. 8, no. 1, pp. 67–80, 2005.

[15] T. Olsen, E. Lang, A. Hansen, M. Cheney, G. Quandt, J. VandenBosche, and T. Meyer, "Low wind speed turbine project conceptual design study: Advanced independent pitch control; july 30, 2002–july 31, 2004 (revised)," tech. rep., National Renewable Energy Lab., Golden, CO (US), 2004.

[16] M. Hand, A. Wright, L. Fingersh, and M. Harris, "Advanced wind turbine controllers attenuate loads when upwind velocity measurements are inputs," in *44th AIAA Aerospace Sciences Meeting and Exhibit*, p. 603, 2006.

[17] M. M. Hand, *Mitigation of wind turbine/vortex interaction using disturbance accommodating control*. National Renewable Energy Laboratory Boulder, CO, 2003.

[18] K. A. Stol, "Disturbance tracking and blade load control of wind turbines in variable-speed operation," in *ASME 2003 Wind Energy Symposium*, pp. 317–323, American Society of Mechanical Engineers, 2003.

[19] A. D. Wright, *Modern control design for flexible wind turbines*. National Renewable Energy Laboratory Golden, CO, 2004.

[20] A. D. Wright and L. Fingersh, "Advanced control design for wind turbines; part i: control design, implementation, and initial tests," tech. rep., National Renewable Energy Laboratory (NREL), Golden, CO., 2008.

[21] J. Mullen and J. B. Hoagg, "Wind turbine torque control for unsteady wind speeds using approximate-angular-acceleration feedback," in *Decision and Control (CDC), 2013 IEEE 52nd Annual Conference on*, pp. 397–402, IEEE, 2013.

[22] V. Rezaei and K. E. Johnson, "Robust fault tolerant pitch control of wind turbines," in *Decision and Control (CDC), 2013 IEEE 52nd Annual Conference on*, pp. 391–396, IEEE, 2013.

[23] D. Schlipf, D. J. Schlipf, and M. Kühn, "Nonlinear model predictive control of wind turbines using lidar," *Wind Energy*, vol. 16, no. 7, pp. 1107–1129, 2013.

[24] S. Gros, "An economic nmpc formulation for wind turbine control," in *Decision and Control (CDC), 2013 IEEE 52nd Annual Conference on*, pp. 1001–1006, IEEE, 2013.

[25] J. Friis, E. Nielsen, J. Bonding, F. D. Adegas, J. Stoustrup, and P. F. Odgaard, "Repetitive model predictive approach to individual pitch control of wind turbines," in *Decision and Control and European Control Conference (CDC-ECC), 2011 50th IEEE Conference on*, pp. 3664–3670, IEEE, 2011.

[26] H. Hosseini and M. Kalantar, "Repetitive control scheme for an ecs to improve power quality of grid connected wind farms using svm," in *Smart Grids (ICSG), 2012 2nd Iranian Conference on*, pp. 1–7, IEEE, 2012.

[27] I. Houtzager, J.-W. van Wingerden, and M. Verhaegen, "Rejection of periodic wind disturbances on a smart rotor test section using lifted repetitive control," *IEEE Transactions on Control Systems Technology*, vol. 21, no. 2, pp. 347–359, 2013.

[28] R. Fratini, R. Santini, J. Serafini, M. Gennaretti, and S. Panzieri, "A spatial repetitive controller applied to an aeroelastic model for wind turbines," *World Academy*

of Science, Engineering and Technology, International Journal of Mechanical, Aerospace, Industrial, Mechatronic and Manufacturing Engineering, vol. 10, no. 9, pp. 1615–1623, 2016.

[29] J. Manwell *et al.*, "Wind energy explained, chisester," 2002.

[30] G. Lloyd and G. Hamburg, "Guideline for the certification of wind turbines," *July 1st*, 2010.

[31] B. J. Jonkman, "Turbsim user's guide: Version 1.50," 2009.

[32] E. L. Petersen, N. G. Mortensen, L. Landberg, J. Højstrup, and H. P. Frank, "Wind power meteorology. part i: Climate and turbulence," *Wind Energy: An International Journal for Progress and Applications in Wind Power Conversion Technology*, vol. 1, no. S1, pp. 25–45, 1998.

[33] R. L. Bielawa, *Rotary wing structural dynamics and aeroelasticity*. American Institute of Aeronautics and Astronautics, 2006.

[34] P. Sørensen, A. D. Hansen, and P. A. C. Rosas, "Wind models for simulation of power fluctuations from wind farms," *Journal of wind engineering and industrial aerodynamics*, vol. 90, no. 12-15, pp. 1381–1402, 2002.

[35] S. A. Huyer, D. Simms, and M. C. Robinson, "Unsteady aerodynamics associated with a horizontal-axis wind turbine," *AIAA journal*, vol. 34, no. 7, pp. 1410–1419, 1996.

[36] M. Robinson, D. R. Galbraith, Shipley, and M. Miller, "Unsteady aerodynamics of wind turbines," in *33rd Aerospace Sciences Meeting and Exhibit*, p. 526, 1995.

[37] W. Johnson, *Helicopter theory*. Courier Corporation, 2012.

[38] P. J. Carpenter and B. Fridovich, "Effect of a rapid blade-pitch increase on the thrust and induced-velocity response of a full-scale helicopter rotor," 1953.

[39] J. G. Leishman, "Challenges in modelling the unsteady aerodynamics of wind turbines," *Wind Energy: An International Journal for Progress and Applications in Wind Power Conversion Technology*, vol. 5, no. 2-3, pp. 85–132, 2002.

[40] J. M. Greenberg, "Airfoil in sinusoidal motion in a pulsating stream," 1947.

[41] T. Theodorsen, "General theory of aerodynamic instability and the mechanism of flutter," 1949.

[42] S. Crews, K. H. Hohenemser, and R. A. Ormiston, "An unsteady wake model for a hingeless rotor," *Journal of Aircraft*, vol. 10, no. 12, pp. 758–760, 1973.

[43] R. A. Ormiston, "Technical notes: Application of simplified inflow models to rotorcraft dynamic analysis," *Journal of the American Helicopter Society*, vol. 21, no. 3, pp. 34–37, 1976.

[44] D. A. Peters, "Hingeless rotor frequency response with unsteady inflow," 1974.

[45] H. Curtiss Jr, "Stability and control modelling, 12th european rotorcraft forum," *Garmisch-Partenkirchen, Germany*, 1986.

[46] D. M. Pitt, "Rotor dynamic inflow derivatives and time constants from various inflow models.," tech. rep., ARMY TROOP SUPPORT AND AVIATION MATERIEL READINESS COMMAND ST LOUIS MO, 1980.

[47] A. Hansen and C. Butterfield, "Aerodynamics of horizontal-axis wind turbines," *Annual Review of Fluid Mechanics*, vol. 25, no. 1, pp. 115–149, 1993.

[48] W. Bierbooms, G. van Bussel, and L. Vermeer, "Experimental and 1heoretical investigations of unsteady aerodynamic flow about a wind turbine,"

[49] T.-Y. Doh and J. R. Ryoo, "Robust repetitive controller design and its application on the track-following control system in optical disk drives," in *Decision and Control and European Control Conference (CDC-ECC), 2011 50th IEEE Conference on*, pp. 1644–1649, IEEE, 2011.

[50] L. Cuiyan, Z. Dongchun, and Z. Xianyi, "Theory and applications of the repetitive control," in *SICE 2004 Annual Conference*, vol. 1, pp. 27–34, IEEE, 2004.

[51] J. Friis, E. Nielsen, J. Bonding, F. Adegas, J. Stoustrup, and P. Odgaard, "Repetitive model predictive approach to individual pitch control of wind turbines," in

Decision and Control and European Control Conference (CDC-ECC), 2011 50th IEEE Conference on, Dec 2011.

[52] H. Hosseini and M. Kalantar, "Repetitive control scheme for an ecs to improve power quality of grid connected wind farms using svm," in *Smart Grids (ICSG), 2012 2nd Iranian Conference on*, May 2012.

[53] I. Houtzager, J. W. van Wingerden, and M. Verhaegen, "Rejection of periodic wind disturbances on a smart rotor test section using lifted repetitive control," *IEEE Transactions on Control Systems Technology*, vol. 21, pp. 347–359, March 2013.

[54] S. Hara, Y. Yamamoto, T. Omata, and M. Nakano, "Repetitive control system: a new type servo system for periodic exogenous signals," *IEEE Transactions on Automatic Control*, vol. 33, pp. 659–668, Jul 1988.

[55] M. Poloni and G. Ulivi, "Iterative trajectory tracking for flexible arms with approximate models," in *Advanced Robotics, 1991. 'Robots in Unstructured Environments', 91 ICAR., Fifth International Conference on*, June 1991.

[56] A. Carozzi, A. Fioretti, M. Poloni, F. Nicolo, and G. Ulivi, "Implementation of a tracking learning controller for an industrial manipulator," in *Control Applications, 1993., Second IEEE Conference on*, Sep 1993.

[57] S. Panzieri and G. Ulivi, "Disturbance rejection of iterative learning control applied to trajectory tracking for a flexible manipulator," in *European Control Conf. (ECC 1995)*, (Roma, Italy), September 1995.

[58] P. Lucibello, S. Panzieri, and F. Pascucci, "Suboptimal output regulation of robotic manipulators by iterative learning," in *11th Int. Conf. on Advanced Robotics*, 2003. ILC.

[59] Y.-H. Yang and C.-L. Chen, "Spatially periodic disturbance rejection using spatial-based output feedback adaptive backstepping repetitive control," 2008.

[60] C.-L. Chen, G.-C. Chiu, and J. Allebach, "Robust spatial-sampling controller design for banding reduction in electrophotographic process," *Journal of Imaging Science and Technology*, vol. 50, no. 6, pp. 530–536, 2006.

[61] B. Mahawan and Z.-H. Luo, "Repetitive control of tracking systems with time-varying periodic references," *International Journal of Control*, vol. 73, no. 1, pp. 1–10, 2000.

[62] M. Nakano, J.-H. She, Y. Mastuo, and T. Hino, "Elimination of position-dependent disturbances in constant-speed-rotation control systems," *Control Engineering Practice*, vol. 4, no. 9, pp. 1241–1248, 1996.

[63] E. A. Bossanyi, "Further load reductions with individual pitch control," *Wind Energy: An International Journal for Progress and Applications in Wind Power Conversion Technology*, vol. 8, no. 4, pp. 481–485, 2005.

[64] T. K. Barlas and G. A. van Kuik, "Review of state of the art in smart rotor control research for wind turbines," *Progress in Aerospace Sciences*, vol. 46, no. 1, pp. 1–27, 2010.

[65] J. Jonkman, S. Butterfield, W. Musial, and G. Scott, "Definition of a 5-mw reference wind turbine for offshore system development," tech. rep., National Renewable Energy Lab.(NREL), Golden, CO (United States), 2009.

[66] J. M. Jonkman, M. L. Buhl Jr, *et al.*, "Fast userâĂŹs guide," *National Renewable Energy Laboratory, Golden, CO, Technical Report No. NREL/EL-500-38230*, 2005.

Appendix A

Examples of transfers between rotating frame and fixed frame of reference

This appendix contains analytical derivations of two load transfers between the rotating and fixed frame of reference. We restrict the transformation to the tilting moment. The tilting moment is dependent of the flap-wise blade root moments as shown in the following equation.

$$M_{tilt} = \frac{2}{3} \sum_{i=1}^{3} M_{y,i} \cos(\psi_i) \tag{A.1}$$

Where M_{tilt} is the tilt component of the flap-wise moment in the 1P transformed system, $M_{y,i}$ is the flapping moment related to the blade $i = 1, 2, 3$ and ψ_i is the angular position of the blade i. For three bladed turbine the angular position related to a generic blade is:

$$\psi_i = \psi + \frac{2\pi(i-1)}{3}.$$

A.1 1P Coleman transformation of the 1P-2P load components present in the blade root moment

When the signal has only the 2P component which is

$$M_{y,i} = \cos(2\psi_i) \tag{A.2}$$

by the application of (A.1), the following equation for the total tilting moment can be obtained:

$$M_{tilt} = \frac{2}{3}\left[\cos(2\psi)\cos(\psi) + \cos 2(\psi + \frac{2\pi}{3})\cos(\psi + \frac{2\pi}{3}) + \cos 2(\psi + \frac{4\pi}{3})\cos(\psi + \frac{4\pi}{3})\right]. \tag{A.3}$$

By using the trigonometric rule $\cos(A)\cos(B) = \frac{1}{2}[\cos(A-B) + \cos(A+B)]$:

$$M_{tilt} = \frac{2}{3}\left[\frac{1}{2}\left(\cos(\psi)+\cos(3\psi)+\cos(\psi+\frac{2\pi}{3})+\cos(3\psi)+\cos(\psi+\frac{4\pi}{3})+\cos(3\psi)\right)\right] \tag{A.4}$$

and $\cos(A+B) = \cos(A)\cos(B) - \sin(A)\sin(B)$

$$M_{tilt} = \cos(3\psi)+\frac{1}{3}\left[\cos(\psi)+\cos(\psi)\cos(\frac{2\pi}{3})-\sin(\psi)\sin(\frac{2\pi}{3})+\cos(\psi)\cos(\frac{4\pi}{3})-\sin(\psi)\sin(\frac{4\pi}{3})\right] \tag{A.5}$$

with

$$\begin{aligned} &-\sin(\psi)\sin(\frac{2\pi}{3}) - \sin(\psi)\sin(\frac{4\pi}{3}) = -\frac{\sqrt{3}}{2} + \frac{\sqrt{3}}{2} = 0 \\ &\cos(\frac{2\pi}{3}) = \cos(\frac{4\pi}{3}) = -\frac{1}{2} \end{aligned} \tag{A.6}$$

it is obtained:

$$M_{tilt} = \cos(3\psi) + \frac{1}{3}\left[\cos(\psi) - \frac{1}{2}\cos(\psi) - \frac{1}{2}\cos(\psi)\right] = \cos(3\psi). \tag{A.7}$$

This means that any 2P loads present in a signal (in this case in the blade root flapping moment) will results in 3P loads in the fixed FOR.

Furthermore when a 1P Coleman transformation is used for 1P load component present in a signal that is

$$M_{y,i} = \cos(\psi_i) \tag{A.8}$$

the resulting tilt moment is

$$M_{tilt} = \frac{2}{3}\left[\cos^2(\psi) + \cos^2(\psi + \frac{2\pi}{3}) + \cos^2(\psi + \frac{4\pi}{3})\right]. \tag{A.9}$$

Thus by assuming the trigonometric rule $\cos(A+B) = \cos(A)\cos(B) - \sin(A)\sin(B)$

$$\begin{aligned}\cos^2(\psi + \frac{2\pi}{3}) &= \frac{1}{4}\cos^2(\psi) + \frac{\sqrt{3}}{4}\sin(\psi)\cos(\psi) + \frac{3}{4}\sin^2(\psi)\\ \cos^2(\psi + \frac{4\pi}{3}) &= \frac{1}{4}\cos^2(\psi) - \frac{\sqrt{3}}{4}\sin(\psi)\cos(\psi) + \frac{3}{4}\sin^2(\psi)\end{aligned} \tag{A.10}$$

and the resulting tilt moment is:

$$M_{tilt} = \frac{2}{3}\left[\frac{3}{2}\cos^2(\psi) + \frac{3}{2}\sin^2(\psi)\right] = 1 \tag{A.11}$$

Summarizing, any 1P load in the rotating FOR will results in a 0P component in the fixed FOR , also the 2P signal component in the rotating FOR Will results in 3P component.